Estimation of Fatigue Life of Welded Joint Using Vibration-Fatigue Computational Model

By

Eniyavan Subramanian

A thesis submitted to
the Faculty of Graduate Studies
in partial fulfilment of
the requirements for the degree of
Master of Science

Department of Mechanical and Manufacturing Engineering
Faculty of Engineering
University of Manitoba
Winnipeg, Manitoba

December 2015

Abstract

Heavy vehicle structures are made from welded carbon steel frames. During operation these frames are subjected to random dynamic loads, which induce fatigue at the welded joints. A Finite Element based process for calculating fatigue life of welded joint under single excitation random loading is proposed in this study. The proposed method combines Equivalent Equilibrium Structural Stress (E^2S^2) method for weld fatigue and PSD based vibration fatigue technique for handling random loads. Fatigue life of a welded T-joint is analysed using the proposed method in frequency domain and validated against a transient dynamic analysis. The main advantage of the proposed method is the analysis run time is reduced almost 12 times compared to transient analysis.

Effect of geometric changes on weld fatigue life is studied. It is found the tube thickness increase at lower thickness ranges significantly increases the fatigue life compared to higher thickness ranges.

Acknowledgments

Foremost, I would like to express my deepest gratitude to my advisor Dr.Yunhua Luo for the patience, motivation and immense knowledge. I would also like to express my sincere gratitude for his support, during the most challenging period of my life.

I am also grateful to my colleagues and supervisors at New Flyer Industries for supporting me throughout this thesis.

Finally I would like to express my gratitude to my wife Nanthini Balasubramaniam for the unconditional love, patience and support throughout the entire program.

Dedication

Dedicated to our beloved daughter

Mythre Eniyavan

For ever in our hearts

“How very softly you tiptoed into our world.

Almost silently. Only for a moment you stayed.

But what an imprint your tiny footprints

Have left upon our hearts.”

Contents

List of Tables

List of Figures

List of Copyrighted Material

Fig 2.4 was cited from Equilibrium-equivalent structural stress approach to fatigue analysis of a rectangular hollow joint. Permission was obtained on 23rd March 2015.

Fig 2.9 was cited from Equilibrium-equivalent structural stress approach to fatigue analysis of a rectangular hollow joint. Permission was obtained on 23rd March 2015

Fig 3.4 was cited from Finite element based fatigue calculations. Permission was obtained on 10th September 2015

Fig 3.13 was cited from Finite element based fatigue calculations. Permission was obtained on 10th September 2015

List of Abbreviations

3D	Three Dimensional
APTA	American Public Transportation Association
ASME	American Society of Mechanical Engineers
ASTME	American Society of Tool and Manufacturing Engineers
BM	Base Metal
CAD	Computer Aided Design
CNG	Compressed Natural Gas
CPU	Central Processing Unit
CSV	Comma Separated Values
DFT	Discrete Fourier Transform
E^2S^2	Equilibrium Equivalent Structural Stress
FEA	Finite Element Analysis
FEM	Finite Element Method
FFT	Fast Fourier Transform
GMAW	Gas Metal Arc Welding
GTAW	Gas Tungsten Arc Welding
HAZ	Heat Affected Zone
IFFT	Inverse Fast Fourier Transform
IIW	International Institute of Welding
JSME	Japan Society of Mechanical Engineers
LBW	Laser Beam Welding

LEFM	Linear Elastic Fracture Mechanics
MDOF	Multi Degrees Of Freedom
PDF	Probability Density Function
PSD	Power Spectral Density
RMS	Root Mean Square
SAE	Society of Automotive Engineers
SMAW	Shielded Metal Arc Welding
S-N	Stress-Life
VBA	Visual Basic for Application

List of Symbols

γ	Irregularity factor
σ_b	Bending stress
σ_m	Membrane stress
σ_s	Structural stress
σ_x	Stress along X-direction
τ_{xy}	Shear stress
$\{\phi\}$	Modal vector
ω	Angular frequency
a_n, b_n	Coefficient of Fourier transform
b	Slope of fatigue curve
f(t)	Force signal in time Domain
f_y	Line force along y
m_n	n^{th} spectral moments
m_x	Line moment along x
$x(\omega)$	Signal in frequency domain
x(t)	Signal in time domain
{y(t)}	Generalised displacement vector

C	Damping of the system
D	Fatigue damage
E[P]	Expected number of peaks
E[0]	Expected zero crossing
$F(\omega)$	Force signal in frequency domain
F_y	Nodal force along y
$H(\omega)$	Transfer function
I(r)	Load correction factor
K	Stiffness of the system
M	Mass of the system
M_x	Nodal moment along x
N	Fatigue life
N(S)	Stress histogram
P(S)	Probability density function
$R(\tau)$	Auto correlation function
$S(\omega)$	PSD signal
S_s	Equilibrium-Equivalent Structural Stress

Chapter 1

Introduction

1.1 Background

Bus structures are mostly built with tubular welded construction to reduce cost. Fatigue failure of welded joints is one of the most significant structural problems faced by bus manufacturers.

According to American Public Transportation Association (APTA) guidelines [1] the structural members of the bus has to withstand against fatigue failures for 500,000 miles or 12 years life whichever comes first. Otherwise the bus manufacturer is responsible for the warranty cost. So when a new bus is developed the structure has to be proven to last this lifetime.

In order to prove that a new bus structure will last this life, currently a full-scale accelerated fatigue testing is conducted on a prototype bus. New Flyer Industries uses a third party testing group to conduct this testing.

To conduct this accelerated fatigue test, first a road operating test is conducted on a prototype bus [2] . The objective of the road operating test is to measure the time history ac-

celeration of the axles caused due to road excitations during the normal operating conditions. In order to accelerate the testing process, the acceleration data is scaled so that the fatigue damage caused due to 500,000 miles is achieved within much shorter period. Using the compressed acceleration data the prototype bus is excited using a four-post shaker and fatigue life of the bus structure will be validated.

To enable easy installation during bus manufacturing, functional systems are pre-assembled into sub-frames called racks. Various racks are designed specifically to carry systems like Compressed Natural Gas (CNG) tanks, hybrid battery packs, cooling modules, etc. Racks are mostly constructed using plates and tubes welded together. Depending on the vehicle configuration like Diesel bus, CNG bus, hybrid bus, etc. different systems are added to the vehicle. During the full vehicle accelerated test, only the heaviest configuration is tested. In order to validate other racks that were not part of the full vehicle test, a sub-model shaker table test is conducted.

Rack to be tested was installed on a smaller shaker table and excited using compressed acceleration data. Frequent inspections were conducted during the course of the test. If structural failure is detected, depending upon the severity of the failure, the test was stopped and a solution was developed quickly. The main drawback of this test is that it is very expensive. Since, only a limited number of strain gauges can be installed on the tested structure, investigating the cause of failure and developing a fix becomes challenging. To validate the fix, the entire test has to be extended so that the fix is validated for the requirement of 500,000 miles.

Systems are changing often and racks have to be developed to accommodate the changes. Due to the longer lead times associated in procuring the materials and building the proto-

type parts and the cost involved, it is neither effective nor efficient to run multiple physical tests to validate the newer rack designs. The racks cannot be overbuilt, since fuel economy is becoming a critical requirement for modern busses. A more efficient method is required to quickly validate the rack design.

Finite element analysis (FEA) is a powerful tool that has been applied in industries to simulate real world structural problems. Finite element analysis can be adopted in the rack design process to save cost and time. However, there are two major challenges to be overcome in order to adopt finite element analysis to predict fatigue life of the rack.

1.1.1 Prediction of fatigue life at welded joint

Most of the fatigue failure in the welded structures occurs closer to welded joints. The main reason for this, according to Wolfgang Fricke [3], is that the welding process strongly affects the material properties due to heating, cooling and addition of filler material, resulting in in-homogenous material near the welds. Welding process also adds pores, inclusions and undercuts which are randomly distributed. The irregular shape of a weld leads to high stress concentration and the geometry of the weld varies depending on the welder and equipment used.

To predict fatigue life of welds using the conventional Fracture Mechanics, notch stress is required. But weld shape is not known so notch stress cannot be computed. To overcome this difficulty there are various methods like nominal stress method [4, 5], Structural stress method [6, 7, 8, 9, 10, 11, 12], notch stress method [13, 14, 15] and linear elastic fracture mechanics approach [16, 17, 18]were developed over the years. Several organizations like British Standards Eurocode 3 [4, 5]and International Institute of Welding

(IIW) [19] are making efforts to develop more reliable methods and to establish corresponding industrial codes.

1.1.2 Computational time

During road operation the bus structure is subjected to random vibrations caused by rugged road profile, frequent braking and cornering. Conducting a transient dynamic analysis on a structure, over the whole test period would be very time consuming or nearly impossible, as the time step required in solving this problem is very small in order to capture all the peak responses.

1.2 Objectives

The objective of this research is to develop a computational procedure based on the Finite Element Method (FEM) to predict the fatigue life of welded rack assembly subjected to a single excitation random dynamic loading.

Chapter 2

Fatigue Life Evaluation of Welds

Although great progresses have been made in many traditional manufacturing techniques, welding is still one of the most commonly used methods for joining metals. It is used and has been adopted in a wide range of industries such as aerospace, automobiles, transportation, machinery and ship building. For example, a great template for welding formation can be articulated within the constructs for a bus structure which is assembled mainly using rectangular hollow tubes with plates fused together. However, these structures are subjected to fatigue loading. This is crucial since most of the structural failures in a bus structure are caused due to fatigue of welds [20, 21, 22]. Fatigue of welded joints is very complex as it is determined by at least three groups of factors, 1) material properties, 2) vibration frequency, and 3) magnitude of loading. Essentially, the welded joint is one of the weakest regions in a structure. Yet, the life of the entire structure is dependent on the fatigue of the welded joints. This chapter will discuss the causes of fatigue at welded joints, the difficulties in predicting fatigue life and the current approach in overcoming these difficulties and estimating fatigue life for welded joints.

2.1 Review of Gas-Metal Arc Welding Process

Fusion welding is the process of connecting two pieces of metal using heat. There are various fusion welding processes used in practice like shielded metal arc welding (SMAW), gas tungsten arc welding (GTAW), laser beam welding (LBW) and gas metal arc welding (GMAW). Among them GMAW is the most commonly used method for welding bus structures. This is because it is the most economical welding method for joining both thin and moderately thick sheets.

In GMAW welding an electric arc is struck between the work piece and the electrode. This electric arc melts the electrode and parts of the work piece. The molten electrode combines with the molten work piece when allowed to cool they form a permanent joint. In this process the electrode can be continuously fed which makes it easier to weld without multiple starts and stops. Shield gas is fed through the nozzle to prevent the molten metal from reacting with gasses like oxygen and nitrogen present in the atmosphere.

The proper selection of welding gasses limits non-metallic inclusions resulting in tougher joints. Any small changes in welding parameters affect the weld shape and can create flaws to the joints. Qualification procedures can be placed between production runs which will establish faith in the process and limit the flaws in the welded joints.

2.2 Causes for low fatigue life in welded joints

Most fatigue failures in welded structure occur closer to welds because they are generally the weakest points of a structure. There are various factors that contribute to the low fatigue strength. Welding involves heating and cooling of materials in a localised region re-

sulting in the material property around these regions becoming in-homogenous. The geometry of the weld creates high stress concentration which also is a major contributor to fatigue life reduction. In addition to the above tensile residual stress at the welded joint, which is a by-product of welding process also reduces the fatigue life considerably.

2.2.1 Metallurgy of welded joints

There are three distinct regions around the welds caused by the varying temperatures experienced by the material. They are the Weld, the Heat Affected Zone (HAZ) and the unaffected Base Metal (BM). When steel is used as the work piece the temperature at welds exceed its melting point (1370^{o}C) but the temperature at the BM is below 600^{o}C, leaving the material property unaffected.

The HAZ is located between the Weld and the BM. Depending on the temperature experienced in different region of the Heat Affected Zone (HAZ), the property of metal is varied. This variation in material property is explained using the Iron-Carbide diagram, Fig 2.1, created based on literature [23, 24]

As shown in the figure, temperatures adjacent to the welds are closer to melting point of steel. This region is called the solid liquid transition zone and contains delta ferrite and liquid metal.

The next region is called the grain growth zone. During welding the temperature in this region will reach above recrystallization temperatures but below the melting point of steel, transforming the material to coarse grain austenite.

The next region is the re-crystallization zone where the temperature reaches closer to the re-crystallization but above temperature A1. At temperature A1 material which consists

of ferrite and austenite mixture starts to completely transform into austenite. Materials in this zone are transformed to fine grain austenite.

The last region in the HAZ will be subjected to temperatures between A1 and A2 and will just begin to transform into austenite and ferrite mixture. A2 is the temperature at which the pure ferrite gets transformed into austenite and ferrite mixture.

The fatigue curve of the base material and that of the filler material cannot be used for predicting the fatigue life of a joint because the properties of the welds are not homogeneous near the weld.

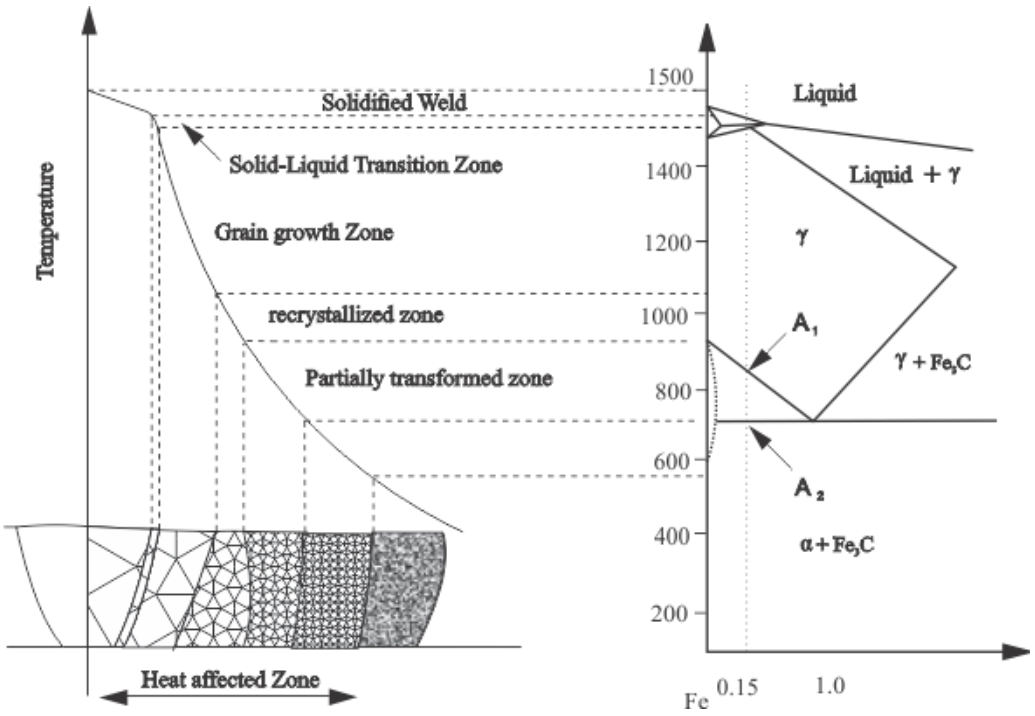

Fig.2.1 Sub-zones of HAZ shown on Fe-Fe_3C diagram

2.2.2 Geometry of Weld

The fatigue life of a welded joint is greatly affected by its geometry, which is dependent on the type of process used, the environment and the quality of workmanship, among other factors. The shape of the weld creates two types of stress concentrations, one at the toe of the weld and the other the root of the weld as shown in Fig 2.2, are the two locations fatigue cracks are most likely to occur [8, 25]. The radius at the weld toe and the flank angle of the weld are the two significant parameters which affect the welded joints. Radaj et al [8] has summarized the toe radius and flank angle for different weld geometries generated using different processes, thicknesses, electrode coatings and methods. The radius varied from .01 mm to 3 mm, the flank angle varied from 15-80°. Due to these large variations in data, it is difficult to establish a general geometric stress concentration factor.

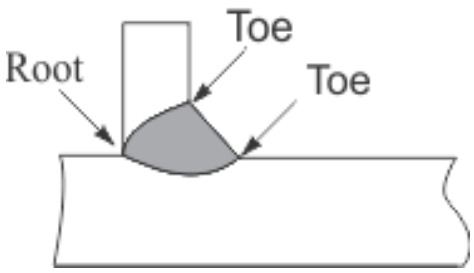

Fig. 2.2 Weld toe and root

T. L. Teng et al [26] conducted experiments to understand the effects of weld geometry on fatigue life. He found a correlation between the weld toe radius and fatigue life and that if the radius at the weld toe is reduced, the fatigue life lowers considerably. He also summarised the effect of flank angle on fatigue life and concluded that if the flank angle is increased, fatigue life is reduced.

This suggests that fatigue life is very sensitive to geometry of weld. Without proper geometric definition it is difficult to accurately predict fatigue life, which thus has posed a bigger challenge in the fatigue life prediction.

2.2.3 Residual stress

Although welding is a method that has been in practice for centuries, it has not been perfected and can cause unfavourable by-products such as residual stresses introduced at the joints. Residual stress can be tensile or compressive in nature. Tensile residual stress in a joint can increase the crack growth rate, reducing the fatigue capability of a joint. Compressive stress can reduce the crack growth rate [27, 28]and improve the fatigue capability of a joint. It is difficult to estimate the amount of residual stress in a joint. Non-destructive testing like X-ray detraction is used to estimate the amount of residual stress, but it is a costly process.

T. L. Teng et al [26] conducted experiments to find the effect of residual stress on fatigue life and confirmed that the tensile residual stress will reduce the fatigue life of the joints. Residual stress is an unknown factor that has to be accounted for during fatigue analysis.

2.3 Computational methods for estimating weld fatigue life

Fatigue life of a welded joint is dependent on the notch stress at the weld toe. However predicting the nonlinear stress at the weld toe is highly impractical due to the statistical

nature of weld geometry. Many organisations like British standard Eurocode3 [4, 5], International Institute of Welding (IIW) [19], American Society of Mechanical Engineers (ASME) [29], European Commission [30], Battelle institute [10], Volvo car corporation [31], Ford [11], MAN bus international [32], Lappeenranta University of Technology [33], Fraunhofer Institut [34], Trinity College Dublin [35] and Nagoya University [36, 37] have spent their resources in finding a way to overcome this difficulty. This section will review four methods commonly used as standards and guidelines developed by these organisations.

2.3.1 Nominal stress method

In this method the nominal stress in the region closer to the weld, which excludes the stress concentration caused by weld geometry and construction detail is used for computing fatigue life. International organisation such as Eurocode3 [4, 5], International Institute of Welding (IIW) [33] have published codes based on nominal stress. To develop the codes, standard welded joint types that are commonly used were manufactured in different sizes, welded using different methods and in different environmental conditions and tested under different loading conditions. Based on these tests, fatigue curves (S-N) were developed using the nominal stress and the number of cycles it took for failure. All these curves are consolidated into one graph and each curve is given a category number as illustrated in Fig 2.3.

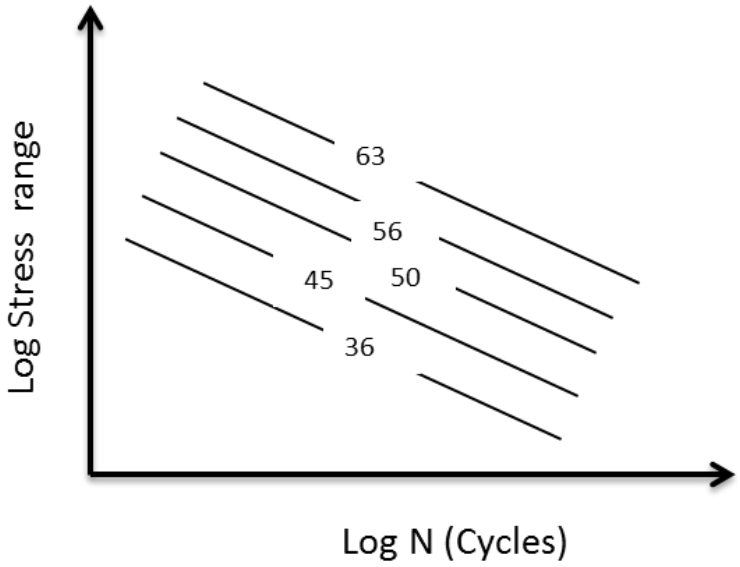

Fig. 2.3 S-N curve based on nominal stress method

Fatigue curves are developed from testing welded specimen, the effect of material inhomogeneity, geometry, stress concentration and residual stress are included in the fatigue curve. A table with the category number along with joint type, size range and loading mode is published in the standard [4] . If the fatigue life of a welded joint has to be validated during the design phase, the nominal stress closer to the weld is evaluated. Based on the detail, size and loading mode the joint category number is selected from the table. Fatigue of the joint is computed from the S-N curve based on the nominal stress and category number.

This method is simple to use and reasonably reliable as long as it fits one of the geometries in the table. Applying nominal stress method for fatigue evaluation of bus structure becomes impossible because the bus structure consists of numerous joint types, most of which do not fall in one of the standard categories listed.

2.3.2 Structural hot spot stress method

Crack initiation and propagation is governed by the stress close to the weld [18]. Stress at the weld toe can be decomposed to membrane stress $\sigma_{m,}$, bending stress σ_b and a nonlinear peak stress σ_{nlp} due to notch as shown in Fig 2.4. It is impossible to compute the non-linear peak stress accurately. This method is based on using only the membrane and bending stress component for fatigue life computation, and the non-linear notch stress is eliminated from the computation process. The sum of the membrane and bending stress at the weld toe is called hot spot stress or structural stress. The stress concentration due to the micro detail of the weld notch is excluded from the computation process and is included in the S-N curve. However the macro effect caused by the construction detail (such as the t-joint, stiffener at the joint) is included into the stress computation process. This method is mainly applicable for cracks originating from the weld toe. The cracks originating from weld root can be avoided by better manufacturing process.

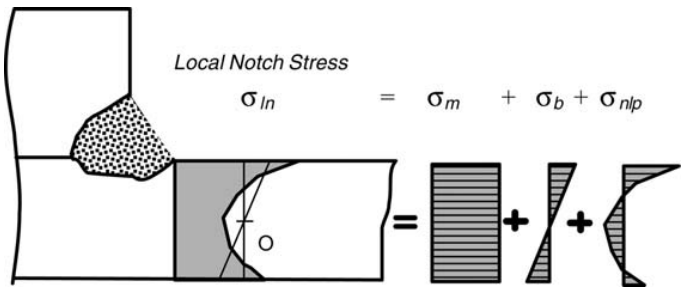

Fig. 2.4 Decomposition of stress at weld toe [10]

During the 1960's the fatigue life estimated from strain measured at 2mm from weld toe yielded better results [3]. The stress was still affected by notch which caused scatter in the results. Over a period of time this method was refined and new techniques were developed. Although several methods are published in the literature [38, 33, 31, 36, 30],

two methods are most commonly used in the industry, the surface extrapolation technique [33] and the equilibrium-equivalent structural stress approach [38] .

2.3.2.1 Surface Extrapolation Technique

The surface extrapolation technique measures stress at two locations from the weld toe. First one is measured at a distance of 0.4 times (0.4t) the thickness of the plate and the other one from a distance equal to the thickness of the plate. Structural stress is obtained by extrapolating the two measured stress to the weld toe as shown in Fig 2.5 [33]. This technique removes the non-linear peak stress but includes all other local effects. Linear extrapolation is used if stress is obtained from two points and quadratic extrapolation is used if stress is measured from three points.

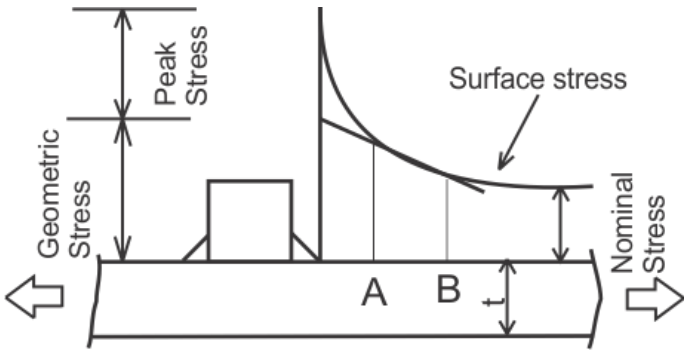

Fig. 2.5 Geometric or Hot spot stress extrapolation technique

The extrapolated stress is called hot spot stress. According to IIW [33] hotspots are classified as type ‘a’ or type ‘b’. When the weld is along the surface of the plate it is called a type ‘a’ hotspot. Stress in type ‘a’ hotspots is highly dependent on the thickness of the plate. When the weld is along the edge it is called a type ‘b’ hotspot as shown in the Fig

2.6. Stresses in type ‘b’ hotspots are not dependent on the thickness of the plate, resulting in differing handling of each type of hotspot.

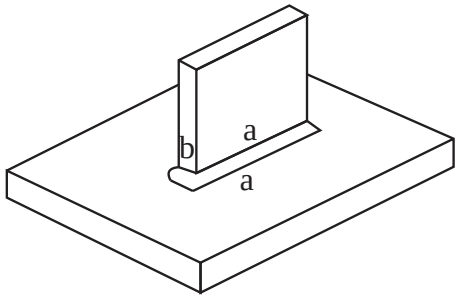

Fig. 2.6 Type ‘a’ and type ‘b’ hotspots

For type ‘a’ hotspots strains are measured at 0.4t and 1.0t from the weld toe for extrapolation to obtain hot spot stress, where t is the thickness of the plates attached. For type ‘b’ it is recommended to measure strains at 4mm, 8mm and 12 mm from the weld toe.

International Institute of Welding (IIW) [33] and Euro code [4] have published S-N curves based on hotspot stress. IIW has published 9 fatigue curves grouped based on loading type and geometry. Similarly, Euro code has published six fatigue curves based on similar categories. In both of the codes standard number of fatigue curves is significantly lower compared to the nominal stress method.

Savaidis et al [32] has used the extrapolation technique to validate the fatigue life of MAN bus structure. The substructure of the bus was analyzed using FEA based on stress extrapolation and the results were compared with physical test samples. The probability of survival was found to be within International Institute of Welding (IIW) recommendations for hotspot stress.

T. Partanen and E.Niemi [7] summarized the tests done at Lappeenranta University of Technology between 1980 and 1994. Tests were carried out on over 100 steel specimens up to 10mm in thickness and with butt and fillet welds. Both constant amplitude and variable amplitude loads were applied to the test specimens and they found that the extrapolated hotspot stress technique yielded consistent results.

Although this method is recommended by international organizations, the selection of proper fatigue curves becomes challenging, since bus structure consist of numerous joint types and complex loading modes which might not fit one of the details published in the standards. Therefore, this method is well suited for bridge and building construction where predefined joints are used more frequently, but for automotive applications a more generalised method is required.

2.3.2.2 Equilibrium-equivalent structural stress method

The equilibrium-equivalent structural stress method first proposed by P. Dong et al [38] is a mesh insensitive method for computing structural stresses. Stress distribution in a plate is considered to be linearly distributed through the depth, with the mid-plane acting as a neutral point. As shown in the Fig 2.7 a plane A-A runs through the weld toe and another plane B-B is at a distance of δ from the A-A. According to structural mechanics stress resultants along plane A-A and plane B-B will be in equilibrium.

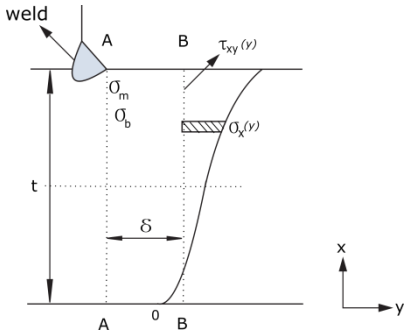

Fig. 2.7 Equilibrium-equivalent structural stress method

σ_m and σ_b are respectively the membrane and bending stress along plane A-A which exclude the non-linear stress due to weld notch. $\sigma_x(y)$ is the stress distribution along B-B in x direction and $\tau_{xy}(y)$ is the shear stress distribution along plane B-B. By imposing equilibrium along planes A-A and B-B and summation of force along x and moment about point o will yield Eqs. (2.1) and (2.2) [38].

$$\sigma_m = \frac{1}{t}\int_0^t \sigma_x(y).dy \tag{2.1}$$

$$\sigma_m \frac{t^2}{2} + \sigma_b \frac{t^2}{6} = \int_0^t \sigma_x(y).y.dy + \delta \int_0^t \tau_{xy}(y).dy \tag{2.2}$$

From the above equation we can see as δ decreases the shear stress becomes insignificant. Using stress distribution $\sigma_x(y)$ obtained from FEA structural stress can be calculated. Dong et al [9] evaluated several structures based on the structural stress obtained using this technique and master S-N curve from ASME code and found the results to be promising. This method is adopted for this thesis and discussed in more detail in the next section.

2.3.3 Effective notch stress approach

The radius of the weld at the weld toe and root play a significant role in notch stress distribution. As the radius reduces the notch becomes sharper and stress increases sharply. Radaj et al [14] proposed a method based on the Nueber's hypothesis [39], and suggested using a fictitious radius at the toe and root to compute the notch stress. He found that for a welded structure with ductile steel using a 1mm radius yielded good results for infinite fatigue life.

Frickle et al [13] reviewed a notch stress method by Seeger et al [40]. In this method a 1-mm radius as shown in Fig 2.8 was used. It was considered as a mean of the radius, not as a fictitious value. A large number of specimens were tested and S-N curve was developed based on the calculated notch stresses. It was found the S-N curves of the parent material and the welds were close.

The biggest advantage for using this method is that it can be used for fatigue life prediction of both toe cracking and root cracking. However, Radaj et al [14] stated that this method is new and requires more testing before its implementation into industrial application. This method requires model welds in FEA and convergence studies, which is both time consuming and costly.

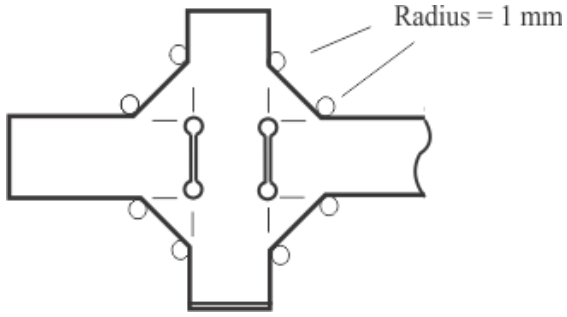

Fig. 2.8 Notch stress method

2.3.4 Linear elastic fracture mechanics approach-

Welds contain numerous micro cracks as a result of welding process and the majority of the fatigue life is spent on increasing the crack length. Martinsson et al [16] reviewed a weld fatigue evaluation method based on the Linear Elastic Fracture Mechanics (LEFM) approach. In this method an initial crack length is assumed and crack propagation is estimated using analytical or FEA based methods. Three-dimensional (3D) crack propagation based on FEA procedures are used for the analysis. Welds were modeled using 1 mm as a notch radius similar to notch stress approach.

The main advantage of this method is that the S-N curve is not required since failure is based on critical crack length. This method is ideal for analysing large structures, especially in understanding how failure in one location will affect the load redistribution in other locations. This method can be adopted to solve a wide range of welded structures, but is computationally intense and time consuming.

2.4 Implementation of Finite Element Method to predict fatigue life of welded joints

Historically fatigue life of welded structures is predicted based on strain gauge measurements and simple analytical calculations. For a complex structure the geometric domain is complex and the boundary conditions are not simple, so developing an analytical solution is not feasible. However numerical solution based on the Finite Element Method (FEM) has gained significant importance due to the advancements in computational methods. Today FEM is used to solve a wide variety of problems like structural, thermal,

fluid dynamics, and electromagnetism. In the Finite Element Method complex geometric domains are divided into subdomains and the elements are used to represent the original problem domain.

Any complex structure can be modeled using Finite Element Method as long as the geometry is clearly defined. As discussed earlier the major problem with welded joints is that the geometry of the welds cannot be clearly defined. Finite Element Method can be used to compute stresses like structural stress and nominal stress used for predicting fatigue life. Among all the computation methods discussed earlier, the structural stress method is computationally less expensive and is gaining significance. Structural stress method is adopted for this thesis and will be explained in more detail.

The Equilibrium Equivalent Structural Stress method (E^2S^2) is a recently developed method for computing the fatigue life of welded joints using FEA by Dong et al [38, 10]. E^2S^2 uses a stress index to compute the fatigue life of a welded joint based on structural stress. Computation of structural stress based on equilibrium between two planes has been explained in Section 2.3.2.2. This section will focus on the finite element implementation of this method.

Procedure for modelling welded joints is explained in detail in literature [10] , either solid or shell elements can be used to model the joints. If solid elements are used to represent the welded joints 20 node hexahedral elements is recommended for the plates and 15 node wedge elements for representing the welds. 20-node hexahedral element is recommended because even with one layer along the thickness it can capture the bending behaviour closely. From FEA results the normal and shear stress distribution, $\sigma_x(y)$ and

$\tau_{xy}(y)$ shown in Fig 2.7 can be obtained. Using Eqs. (2.1) and (2.2) provided in the previous section structural stress can be calculated.

A more efficient method for computing structural stress was developed using the four node linear shell elements [10] , which is simple to mesh and computationally less expensive. The results from both solid elements and shell elements compare very closely [10, 9].

Both welds and plates are modelled using shell element, with the thickness of the weld equal to the plate thickness/ $\sqrt{2}$. Using shell elements, nodal force and moments can be directly extracted along the weld toe. These nodal forces and moments are in global co-ordinate system. First a local co-ordinate system is created on each node along the weld. The co-ordinate system is oriented, such that y-axis is normal to the weld line and x-axis is parallel to weld line as illustrated in Fig 2.9 [10]. The nodal forces and moments in global co-ordinates are transformed to these in the local co-ordinates to obtain the normal force F_y perpendicular to the weld and the moment M_x parallel to the weld.

Structural stress is calculated using these forces and moments. Stress is a continuous function but the forces and moments are discrete values at nodes. First they are converted to a distributed values referred to as line force and line moments in E^2S^2 method [10]. In order to calculate line force f_y and line moments m_x work equivalent argument is used. Work done by the nodal force is equal to the work done by the line force along the weld [10]. Using this principal Eqs. (2.5) to (2.8) [10, 9] were developed to calculate the line forces and line moments.

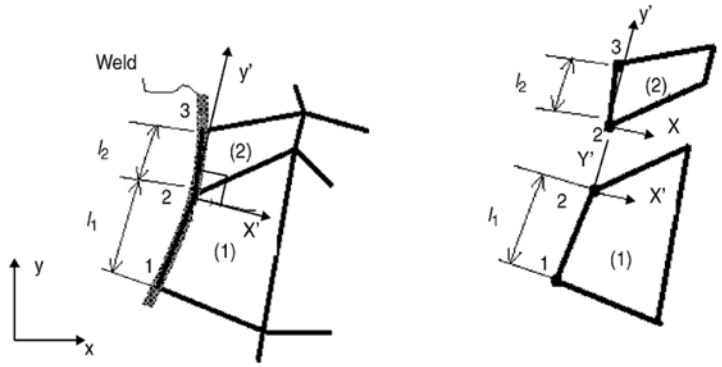

Fig. 2.9 Structural stress from shell elements [10]

$$\sum F_{yi} + \int_0^l f_y\,(x)\,dx = 0 \tag{2.3}$$

$$\sum F_{yi}\,x_i + \int_0^l f_y\,(x)x\,dx = 0 \tag{2.4}$$

$$f_{y1} = \frac{2}{l}\left(2F_{y1} - F_{y2}\right) \tag{2.5}$$

$$f_{y2} = \frac{2}{l}\left(2F_{y2} - F_{y1}\right) \tag{2.6}$$

$$m_{x1} = \frac{2}{l}\left(2M_{x1} - M_{x2}\right) \tag{2.7}$$

$$m_{x2} = \frac{2}{l}\left(2M_{x2} - M_{x1}\right) \tag{2.8}$$

Where F_{y1} , F_{y2} are the nodal forces at Node-1 and Node-2 respectively and M_{x1}, M_{x2} are the nodal moments at Node-1 and Node-2 respectively. Similarly f_{y1} ,f_{y2} are the calculated line forces at Node-1 and Node-2 respectively and m_{x1}, m_{x1} are the calculated line moments at Node-1 and Node-2 respectively. Element length at the weld toe is denoted by l.

Once line forces and line moments are calculated structural stress can be directly calculated using the following relationship.

$$\sigma_s = \sigma_m + \sigma_b = \frac{f_y}{t} + \frac{6m_x}{t^2} \tag{2.9}$$

Where σ_s , σ_m and σ_b are the structural, membrane and bending stress respectively. When welds contain numerous elements, line forces and line moments lead to a system of simultaneous equations. Dong et al [9] converted this system of equation into a matrix form given below. Using this matrix line forces and line moments can be calculated very quickly.

$$\begin{Bmatrix} F_1 \\ F_2 \\ F_3 \\ \vdots \\ \vdots \\ F_n \end{Bmatrix} = \begin{bmatrix} \frac{l_1}{3} & \frac{l_1}{6} & 0 & 0 & \cdots & 0 \\ \frac{l_1}{6} & \frac{(l_1+l_2)}{3} & \frac{l_2}{6} & 0 & \cdots & 0 \\ 0 & \frac{l_2}{6} & \frac{(l_2+l_3)}{3} & \frac{l_3}{6} & 0 & 0 \\ 0 & 0 & \ddots & \ddots & \ddots & 0 \\ \vdots & \ddots & \ddots & \ddots & \frac{(l_{n-2}+l_{n-1})}{3} & \frac{l_{n-1}}{6} \\ 0 & \cdots & \cdots & 0 & \frac{l_{n-1}}{6} & \frac{l_{n-1}}{3} \end{bmatrix} \begin{Bmatrix} f_1 \\ f_2 \\ f_3 \\ \vdots \\ \vdots \\ f_n \end{Bmatrix} \tag{2.10}$$

In order to account for different thickness and loading modes a correction factor is introduced to the stress index S_s. This corrected stress index is called equilibrium –equivalent structural stress, which is calculated by using Eqs. (2.11), (2.12) and (2.13) [9].

$$S_s = \frac{\sigma_s}{t^{\frac{2-m}{2m}} I(r)^{\frac{1}{m}}} \tag{2.11}$$

Where t is the thickness of the plates joined, m is 3.6 which is the slope of the crack growth curve and I(r) is the load correction factor

$$I(r)^{\frac{1}{m}} = .0011\,r^6 + 0.0767\,r^5 - .0988\,r^4 + 0.0946\,r^3 + 0.0221\,r^2 + .014\,r + 1.2223 \quad (2.12)$$

$$r = \frac{\sigma_b}{\sigma_m + \sigma_b} \quad (2.13)$$

A master S-N curve [9] was developed based on testing samples with different joint types, loading modes, and different thickness to use with the E^2S^2 method. Over 1000 test samples were used to characterize this test master S-N curve, Eqs. (2.14) [9] is used to define the fatigue S-N curve.

$$\Delta S_s = C\,.\,N^b \quad (2.14)$$

Where N is the number of cycles to failure, b and C are fatigue constants published in the literature [9] for the different statistical parameter listed in Table 2.1.

Statistical basis	C	h
Mean	19 930.2	
+ 2σ	28 626.5	
− 2σ	13 875.8	− 0.32
+ 3σ	31 796.1	
− 3σ	12 492.6	

Table 2.1 Fatigue constants

In Feb 2003 SAE (Society of Automotive Engineers) [10] published a weld fatigue challenge to the researchers and its members. The challenge was to predict the fatigue of a T-joint made from welding two rectangular hollow tubes. A load of 4000 lbs fully reversed

loads has to be applied to the joints and the number of cycles to failure has to be predicted. Kyuba and Dong [10] made their predictions based on E^2S^2 and won the challenge. Mean life obtained by testing was around 75,000 cycles, estimated mean life by E^2S^2 method was around 74,000 cycles.

M.H. Kim et al [12] conducted fatigue assessments on welded joints used in ship structures using E^2S^2 method. The results were found to be comparative with the physical test conducted on the samples.

Dong et al [11] at Ford used E^2S^2 method to compute the fatigue life of the rear axle, sub frame and body mount of cars. Results were compared with the physical vehicle road test schedules, and were found to be in very good co-relation. Ford has developed an in-house tool based on E^2S^2 method.

The E^2S^2 method is straight forward and involves only one fatigue curve. All thickness and load corrections are added to the stress index to account for variations. Automotive industries have started to adapt this method. Based on the discussions in this section E^2S^2 method is ideal for this application and is adopted for this thesis.

2.5 Test models from literature

In order to effectively use this method in this thesis certain part of the E^2S^2 calculation procedure is automated using MS-Excel-VBA. Once the nodal force and moments are obtained from FEA the automated procedure does all the transformation and calculates the E^2S^2 stress. The procedure is illustrated using the flowchart in Fig 2.10.

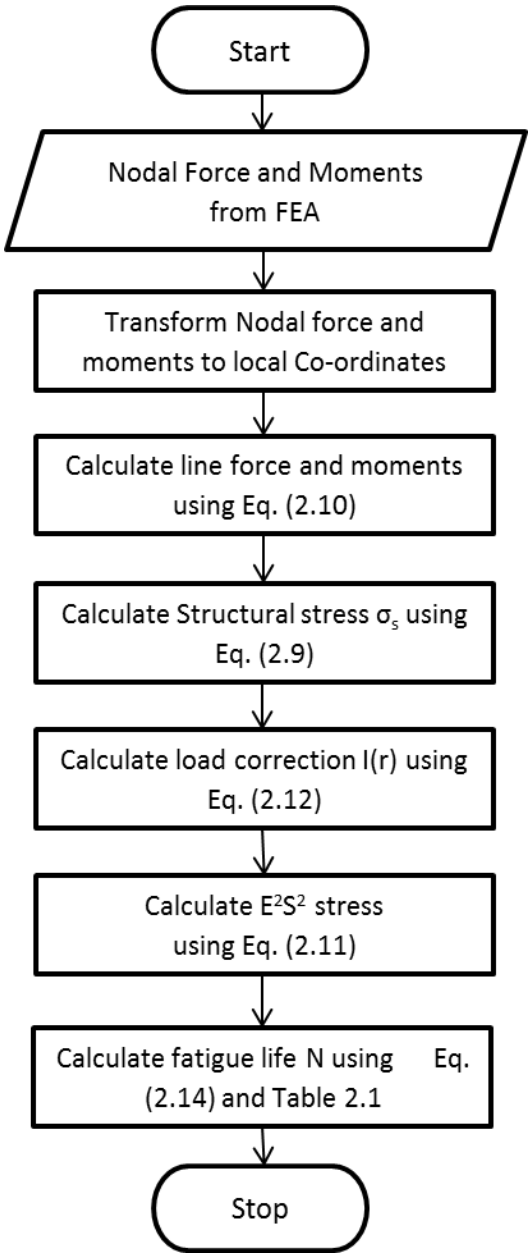

Fig. 2.10 Flow chart of the E^2S^2 method

To understand the procedure and to validate the automated procedures two models from the literature by Dong et al [10, 6] was recreated and verified.

The first model [6] consists of a plate welded to an I-beam section as shown in the Fig 2.11. Finite Element Model of this structure was modelled using Hypermesh [41] pre-

processing software using the guidelines discussed in Section 2.4. Four node shell element is used for this model. The dimensions and material properties were adopted from literature [6]. The calculated structural stress along the welds is shown in the graph Fig 2.12. The calculated results compare very closely with the results from literature [6].

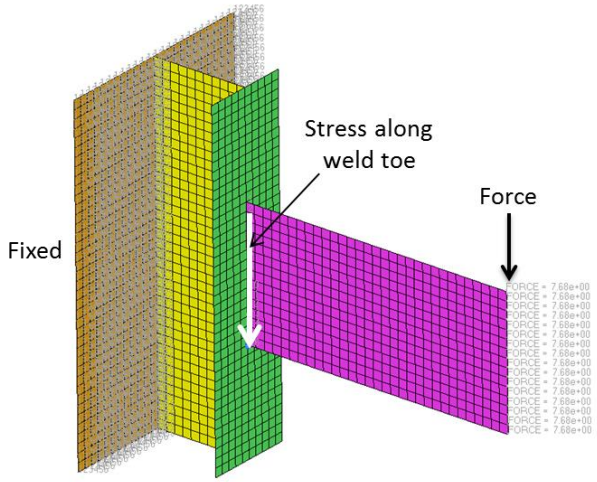

Fig. 2.11 Finite Element Model of I-Beam and the weld

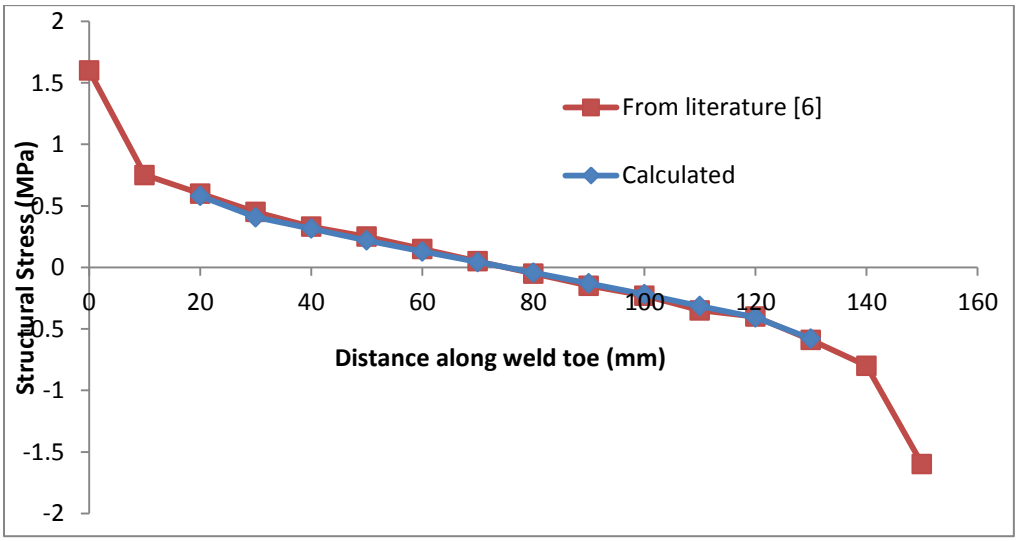

Fig. 2.12 Structural stress along weld toe for I-beam

The first model has a simpler geometry and does not involve complex transformations. In order to validate the automated procedure against more complex geometry, another model from literature [10] was selected for validation. The second model is a tubular T-joint as shown in Fig 2.13. Please refer to literature [10] for dimensions and material properties. Using the same technique applied to previous model, FE model was constructed and analysed. Structural stress calculated along the weld toe is plotted against the results from literature [10] , results compare closely. Corner fillet radius of the rectangular tubes has not been provided in the literature, for this analysis it was assumed to be twice the tube thickness. That might be the reason for a slight deviation in stress levels closer to the peak stress.

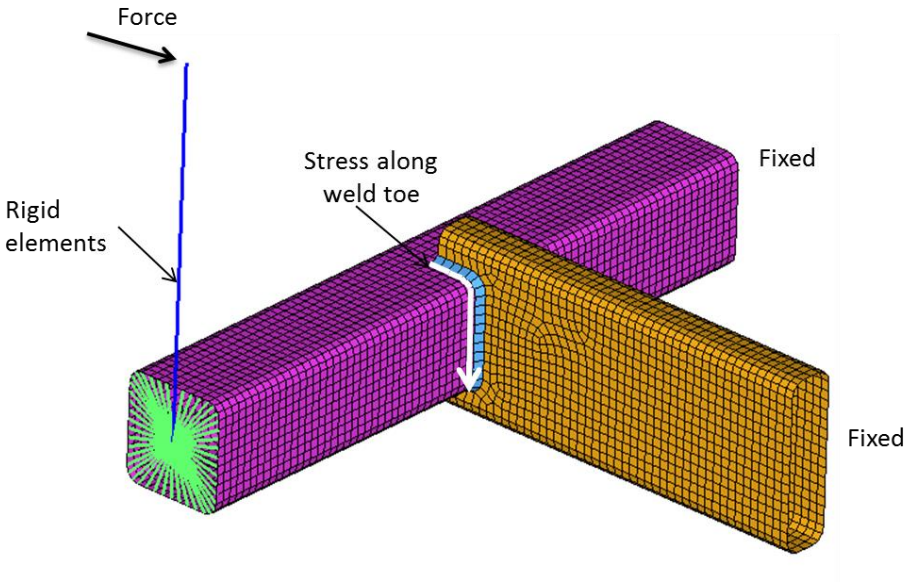

Fig. 2.13 Finite Element Model of Tubular T-joint

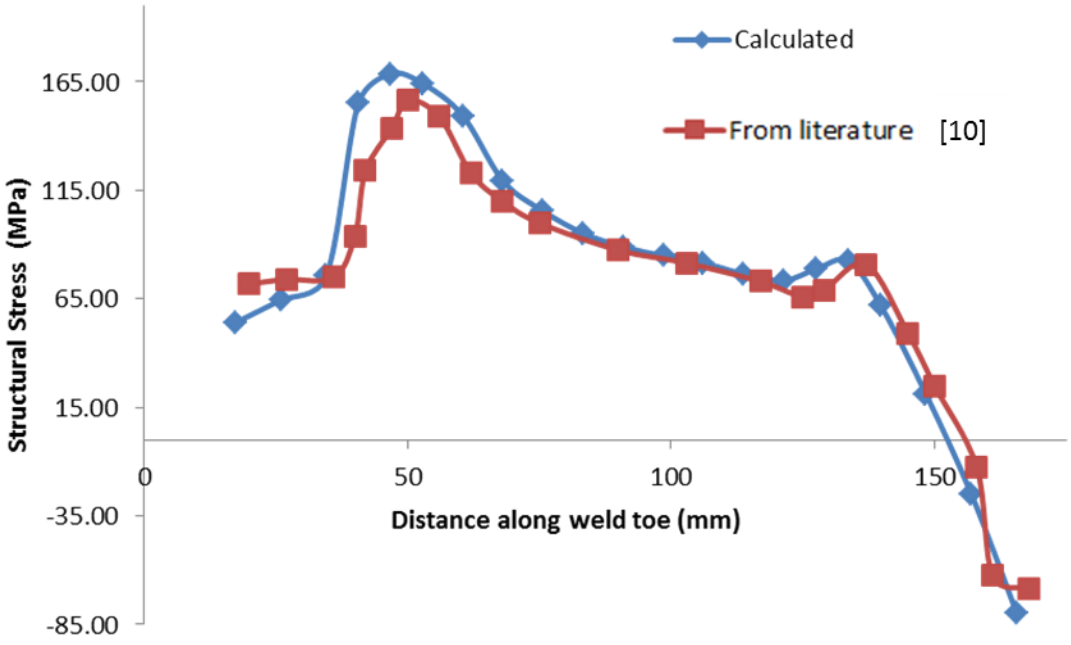

Fig. 2.14 Structural stress along weld toe for the Tubular T-joint

Chapter 3

Fatigue life evaluation under random loading

3.1 Introduction

In Chapter 2, weld fatigue was addressed quite extensively. In this chapter fatigue life evaluation under random loading will be addressed. To begin, dynamic loadings on structures are broadly classified into deterministic and random loads. If the characteristics of a load can be explicitly defined as function of time then it is termed as deterministic load. For example loads developed due to rotating equipments are deterministic in nature. However most of the loads in the real world such as excitation of the automobile structure due to irregular roads, wind loads on buildings cannot be defined as a function of time, they are called random loads.

Since the random loads are unpredictable, estimating the behaviour of a structure to such loads becomes challenging. Even though random loads are unpredictable they may exhibit some form of statistical regularity and can be characterised statistically. This chapter first elaborates methods to characterise random signals, then focuses on how to obtain response of structures subjected to random loading.

3.2 Signal Processing

Loads on structures can be characterised as continuous signal in the time domain. If a signal is as simple as a sine wave its characteristics such as amplitude, frequency can be easily defined. However for complicated signals their characteristics cannot be obtained directly. Various signal processing techniques are available to transform the complicated signals, so that some meaningful conclusions can be derived. This section will review signal processing methods specifically used to characterise random signals.

3.2.1 Signal in frequency domain

Any periodic signal can be represented using a series of harmonic functions with different amplitude, frequency and phase. Fourier series [42] is a mathematical tool which helps in breaking the periodic function x(t) into series of sine and cosine wave forms. Analytical form of Fourier series is represented using Eq. (3.1) [42].

$$x(t) = \frac{a_0}{2} + \sum_{n=1}^{\infty} (a_n \cos \mathrm{n}\omega\mathrm{t} + b_n \sin \mathrm{n}\omega\mathrm{t}) \qquad (3.1)$$

Where co-efficient a_0 represents the mean of the signal, a_n and b_n are the amplitudes of the sine and cosine waves at various frequencies ω. The co-efficient are calculated using Eqs. (3.2) and (3.3)

$$a_n = \frac{2}{\tau}\int_0^{\tau} x(t)\ \cos n\omega t\, dt \tag{3.2}$$

$$b_n = \frac{2}{\tau}\int_0^{\tau} x(t)\ \sin n\omega t\, dt \tag{3.3}$$

Once the periodic signal is represented in Fourier series the signal in time domain can be transformed into frequency domain by using Fourier transform. If x(t) is the signal in time domain it can be transformed into frequency domain by using Eq. 3.4 [42].

$$X(\omega) = \int_{\infty}^{-\infty} x(t)e^{-i2\pi\omega t}\, dt \tag{3.4}$$

X(ω) is a function in frequency domain which is a complex function. Modulus of X(ω) gives amplitude of the signal at different frequencies. Similarly, argument of X(ω) gives phase information of the signal [43].

In the above Fourier series equation, x(t) has to be defined as a continuous function in order to compute its transform. When a signal is gathered during testing or operation they are measured in discrete form at certain time interval. Fitting an analytical function would be tedious or in many cases not possible. Discrete Fourier Transform (DFT) was developed in late 1900s, instead of analytical function it uses discrete signals directly to compute the Fourier transform. There are various FFT algorithms available but Cooley-Turkey algorithm [44] is most popularly used. This algorithm is found to be more ideal

for computer implementation. Using FFT a discrete signal in time domain can be transformed into frequency domain. Similarly a signal in frequency domain can be converted back to time signal using Inverse Fast Fourier Transform (IFFT). The FFT and IFFT can be computed using Eqs. 3.5 and 3.6 [44] respectively.

$$\mathrm{X}(\omega_n) = \frac{T_p}{\mathrm{N}} \sum_k x(t_k)\, \mathrm{e}^{\mathrm{i}\left(\frac{2\pi n}{N}\right)\mathrm{k}} \tag{3.5}$$

$$x(t_k) = \frac{1}{T_p} \sum_n \mathrm{X}(\omega_n)\, \mathrm{e}^{\mathrm{i}\left(\frac{2\pi k}{N}\right)\mathrm{n}} \tag{3.6}$$

Where T_p is the time period of the signal $x(t_k)$, N is the number of data points.

3.2.2 Autocorrelation Function

For the development of random vibration theory autocorrelation function is one of the important statistical terms. Auto correlation for a random time function x(t) is defined as the mean of product of x(t) and x(t+τ) where τ is the separation time [45, 46].

$$R(\tau) = E[x(t)x(t+\tau)] = \lim_{T\to\infty} \frac{1}{T} \int_0^T x(t)x(t+\tau)dt \tag{3.7}$$

If the signal is a stationary random process the mean and standard deviation is independent of time t. In such cases the autocorrelation function is independent of time t, it only depends on separation time τ. Autocorrelation function is illustrated using Fig 3.2. A signal x(t) is shifted by time τ to form x(t+τ) then x(t) is multiplied by x(t+ τ) to form the second curve. Integrating the second curve gives the autocorrelation func-

tion R(τ). For various values of separation time τ autocorrelation R(τ) function can be developed.

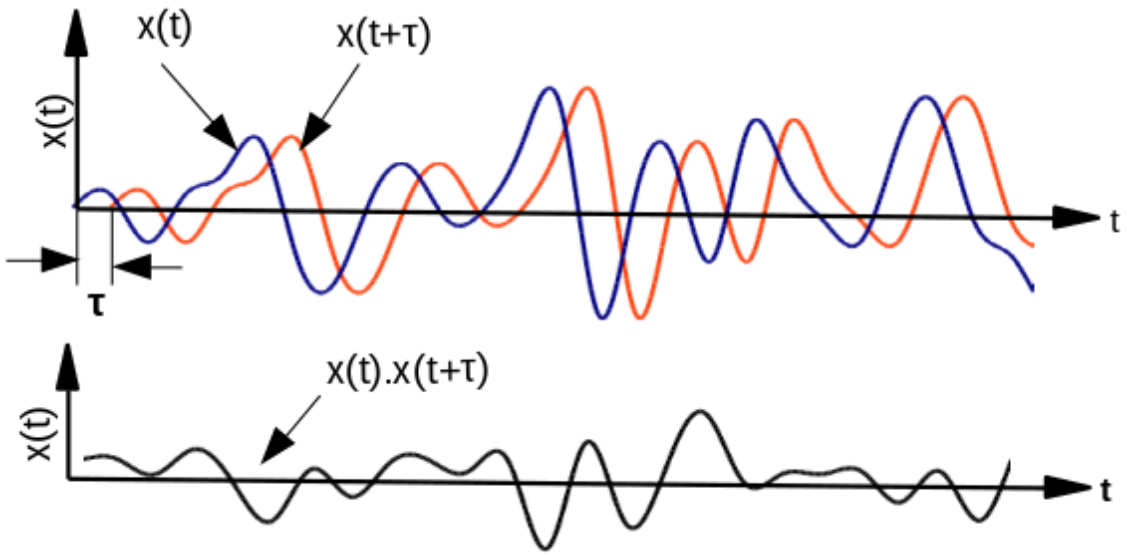

Fig 3.1 Product of mean of signals with time shift

3.2.3 Power spectral density

Power Spectral Density (PSD) is another very important statistical form of representing a signal. PSD is the mean square of the signal at a given frequency [47]. It is another frequency domain representation of a signal. For most of the engineering problems the amplitude of the signal is one of the most important parameters. In PSD all the amplitude information is conserved but the phase information is ignored. To represent the signal in PSD the input signal is assumed random and stationary [48].

A graph can be plotted with PSD along Y-axis and frequency along X-axis as shown in Fig 3.3. By definition the area of the strip shown at a given frequency is the mean square of the signal at that frequency.

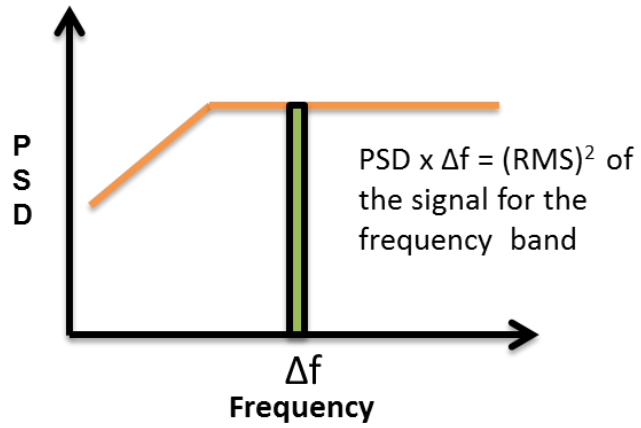

Fig 3.2 Power spectral density and amplitude

Using this definition amplitude of the signal for a given frequency can be recalculated from the PSD curve using Eq. (3.10) [49].

RMS of a sine wave = Amplitude /√2 (3.8)

Mean square of the sine wave = (Amplitude /√2)^2

= Area of the PSD curve (3.9)

Amplitude = √ (2 X Area of the PSD curve) (3.10)

Units of PSD is (base unit)^2 / Hz. For example, for stress PSD the unit is (N/m^2)^2/Hz, for acceleration PSD the unit is (m/s^2)^2/Hz.

PSD can be calculated from a signal in time domain using the three techniques, Fast Fourier Transform, autocorrelation function and band pass filter method. Fast Fourier Transform technique is used in this thesis, the other two techniques discussed here for understanding the PSD signal better.

3.2.3.1 Fast Fourier Transform

PSD $S(\omega)$ can be calculated by squaring the modulus of FFT and divided by the twice the time period (T) of the signal. Eq. (3.11) [43] is used calculate the PSD $S(\omega)$ using FFT.

$$S(\omega) = \frac{1}{2T} |FFT|^2 \tag{3.11}$$

To calculate PSD, the stationary input random signal is transformed into frequency domain using FFT. The modulus of the transform which refers to amplitude of the signal is squared to derive the PSD values.

This method is most commonly used, since FFT calculations can be easily computed using digital computers. Most of the commercial data processing software's use FFT for calculating PSD. In this research Ncode Designlife [50] software is used for transforming the signal from time series to PSD and vice versa. Ncode Designlife uses FFT technique for the transformation process.

3.2.3.2 Autocorrelation function

Autocorrelation function can be used to calculate PSD of the signal. It has been proven that Fourier transform of autocorrelation function $R(\tau)$ gives power spectral density function $S(\omega)$ [42, 45, 47]as shown in Eq. (3.12) [42].

$$S(\omega) = \frac{1}{2\pi} \int_{-\infty}^{\infty} R(\tau) e^{-i\omega t} d\tau \tag{3.12}$$

3.2.3.3 Band Pass filter method

Band pass filter method is a less commonly used method for calculating PSD function of a signal. It is mainly used for understanding the PSD concept. In this method the input

signal is filtered using a frequency filters with different band widths. Then RMS of the signal is calculated for each band widths. PSD for each bandwidth is obtained by squaring the RMS value and dividing by its band width [51]. Using different bandwidth a continuous PSD function can be developed. Fig 3.4 illustrates the band pass filter procedure.

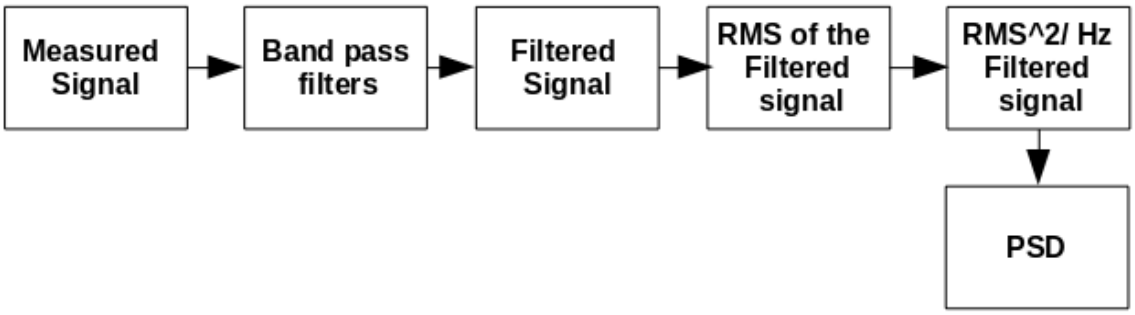

Fig 3.3 Process flow of band pass filter method

3.2.4 Categories of PSD

There are four main categories of PSD signals which are widely observed in engineering application, namely Sine wave, Narrowband process, Wideband process and White noise. It is important to categorise the signal, since each signal requires different fatigues strategies which are discussed later in this section.

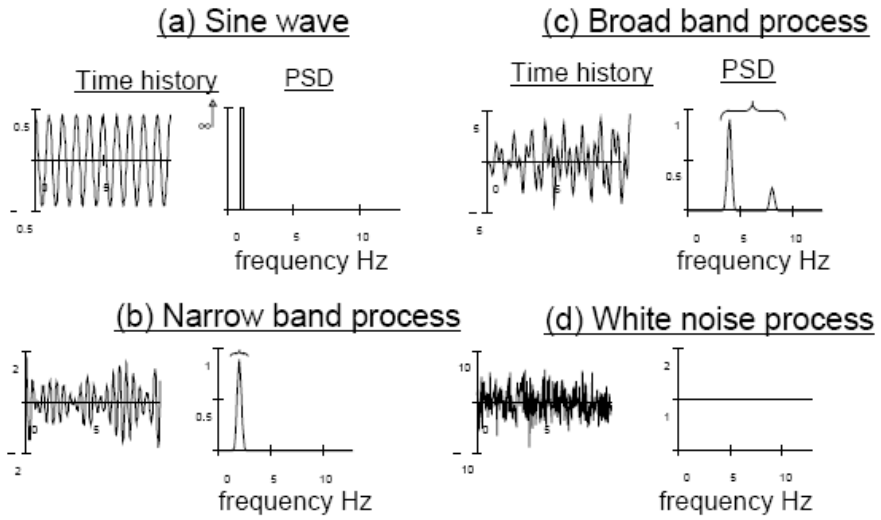

Fig 3.4 Categories of PSD signals [48]

PSD of sine wave is used just for understanding purposes only since the sine wave is not a random signal. PSD of a sine wave as shown in Fig 3.5(a) will be narrow curve tending towards infinity at the frequency of the sine wave. But in real life any signal will have a definite time period T. If the definite time period of the sine wave is known, based on Eq. 3.11 PSD will have a definite value instead of infinity.

In narrowband process the signal might consist of numerous sinusoidal waves with frequencies focused on very narrow band as shown in Fig 3.5(b).

In broadband process the signal consists of numerous sinusoidal waves with frequencies dispersed at wider frequency band as shown in Fig 3.5(c).

White noise signal consist of sine waves with constant amplitude in all the frequencies as shown in Fig 3.5(d).

3.2.5 Characterization of a random signal

A random signal can only characterised using statistical parameters. Expected number of peaks E[P] and expected zero crossing E[0] are two most significant parameters that are required for fatigue life computation. A section of sample random signal is shown in the Fig 3.6. The signal cuts the zero line two times during upward movement, the expected upward zero crossing for the signal E[0] = 2. Similarly, the number of upward peaks in the signal is four; therefore, the expected peak for the signal E[P] = 4.

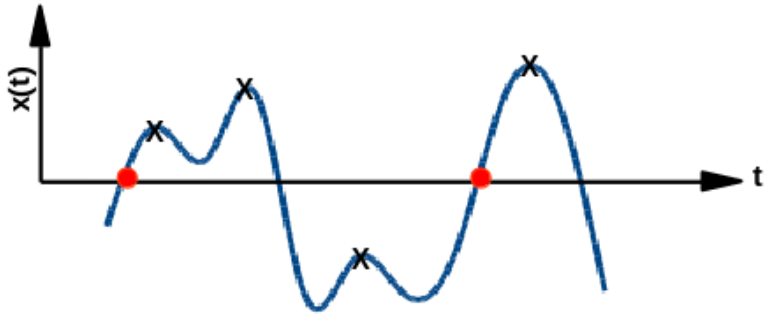

Fig 3.5 Spectral peak and zero crossing

Irregularity factor γ is calculated based on E[0] and E[P] using Eq. (3.13) [43].

$$\gamma = \frac{E[0]}{E[P]} \tag{3.13}$$

If the irregularity factor γ is closer to 1 the signal is a narrow band signal. If the irregularity factor is closer to 0 then the signal is a wide band signal [43]. Thus, a random signal in time domain can be characterised.

In order to characterise a PSD signal another important statistical term called spectral moments is used. The n^{th} spectral moment of a PSD signal is the summation of the area of a strip in the PSD curve (Fig 3.7) multiplied by the corresponding frequency raised to

the power of n. Eqs. 3.14 [43] is used for calculating various n^{th} moments m_n. Generally first five moments are required for fatigue life computations.

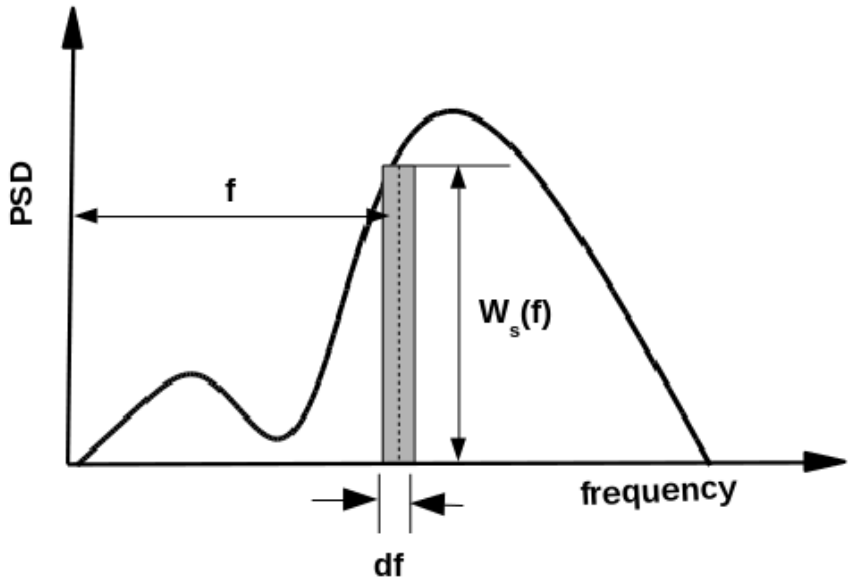

Fig 3.6 Spectral moment

$$m_n = \int_0^\infty f^n \, W(f) df = \sum f_s^n \, W_s(f) \, \delta f \tag{3.14}$$

Expected upward zero crossing E[0] and expected peak E[P] can be calculated from the spectral moments using Eqs. (3.15) and (3.16) [43].

$$E[0] = \sqrt{\frac{m_2}{m_0}} \tag{3.15}$$

$$E[P] = \sqrt{\frac{m_4}{m_2}} \tag{3.16}$$

From the above irregularity factor γ can be directly computed from the spectral moments using Eq. (3.17) [43].

$$\gamma = \sqrt{\frac{m_2^2}{m_0 m_4}} \tag{3.17}$$

3.3 Transfer Function

Transfer function in vibration is a complex function which relates input to the output. Transfer function is the fundamental characteristics of the system. Simple relationship, relating input force F(ω) to response displacement X(ω) using transfer function H(ω) is shown in Eq. (3.18).

$$X(\omega) = H(\omega)F(\omega) \tag{3.18}$$

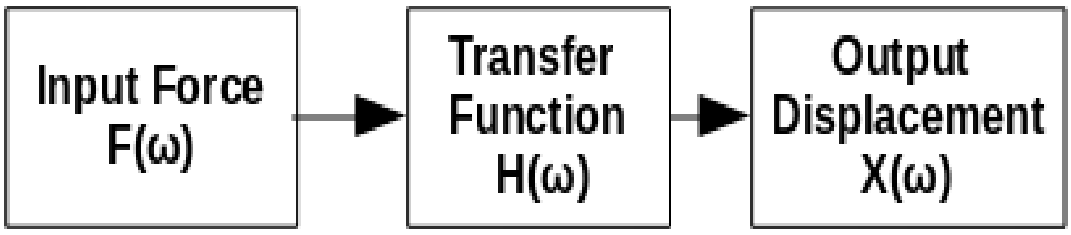

Fig 3.7 Transfer function

In PSD based structural analysis transfer function is the key element. In this section transfer function for single degree of freedom systems and multi degree of freedom systems are reviewed in detail.

3.3.1 Transfer function for single degree of freedom

For single degree of freedom system with mass M, damping C and stiffness K the equations of motion is given by Eq. (3.19).

$$M\ddot{x}(t) + C\dot{x}(t) + Kx(t) = f(t) \tag{3.19}$$

Where f(t) is the external force applied to the system and x(t) is the displacement of the system.

If f(t) can be expressed as an harmonic function in time, the response displacement x(t) can also be represented as an harmonic function [49]. They are expressed in exponential form using Eqs. (3.20) and (3.21).

$$f(t) = F\, e^{i\omega t} \tag{3.20}$$

$$x(t) = X\, e^{i\omega t} \tag{3.21}$$

Where F is the magnitude of the excitation force and X is the magnitude of the response displacement. The first two derivatives of displacement will yield velocity and acceleration as shown in Eqs. (3.22) and (3.23).

$$\dot{x}(t) = i\omega X\, e^{i\omega t} \tag{3.22}$$

$$\ddot{x}(t) = -\omega^2 X\, e^{i\omega t} \tag{3.23}$$

Substituting the velocity and acceleration into the equation of motion (3.19) yields

$$-M\omega^2 X\, e^{i\omega t} + C\, i\omega X\, e^{i\omega t} + KX\, e^{i\omega t} = F\, e^{i\omega t} \tag{3.24}$$

Rearranging Eq. (3.24) gives response displacement in terms of transfer function.

$$X(\omega) = H(\omega)F(\omega) \tag{3.25}$$

$$H(\omega) = \frac{1}{-M\omega^2 + C\, i\omega + K} \tag{3.26}$$

Similarly PSD response can be calculated using the same transfer function. To obtain the relationship Eq. (3.25)'s modulus is squared both sides and divided by twice the time period T of the signal as shown in Eq. (3.27).

$$\frac{1}{2T}|X(\omega)|^2 = \frac{1}{2T}\,|H(\omega)|^2 |F(\omega)\ |^2 \tag{3.27}$$

Applying the definition of PSD to Eq. (3.27) gives the relationship (3.28) [49], which relates input force PSD $S_f(\omega)$ to response displacement PSD $S_x(\omega)$ using transfer function $H(\omega)$.

$$S_x(\omega) = |H(\omega)|^2 \; S_f(\omega) \tag{3.28}$$

3.3.2 Transfer function for multi degree of freedom (MDOF) system using modal superposition technique

Modal superposition technique is one of the most efficient methods for solving MDOF linear structural dynamics problems [52]. The technique is discussed more detailed in this section.

3.3.2.1 Modal analysis

Modal analysis is the process of determining the inherent dynamic characteristic of the system like natural frequencies and mode shapes [53]. A structure will in principle contain infinite number of degrees of freedoms and infinite natural frequencies. At each natural frequency the structure tends to vibrate in a specific form, they are called mode shapes. The natural frequencies and mode shapes depend on the mass, damping, stiffness and the boundary condition of the structure. They are totally independent of the applied loading. The natural frequencies and the mode shapes are very important in dynamic analysis of structures. When a structure gets excited closer to its natural frequency they tend to resonate, resulting in very large response amplitude.

Modal analysis is the base for modal superposition technique. Numerical method based modal analysis is discussed here. Any continuous structure with infinite degrees of free-

dom can be discretized into n degrees of freedom using FEM (Finite Element Method). Consider a structure with mass matrix [M], Stiffness matrix [K] and with no damping subjected to free vibration. The equation of motion of the system is given by Eq. (3.29).

$$[M]\ddot{x}(t) + [K]x(t) = 0 \tag{3.29}$$

The non-trivial solution of Eq. (3.29) will be of the form

$$x(t) = \{\phi\}\sin(\omega t) \tag{3.30}$$

Where ϕ_i is the amplitude of i^{th} degree of freedom. Substituting in Eq. (3.29) it will become a simple algebraic Eq. (3.31) [53].

$$([K] - \omega^2[M])\{\phi\} = 0 \tag{3.31}$$

The Eq. (3.31) becomes an eigen value problem. Solving it will yield the eigen value ω^2 and eigen vector $\{\phi\}$. Root of the eigen value ω is the natural frequency of the system, eigen vector $\{\phi\}$ is the mode shape of the system.

3.3.2.2 Harmonic response using modal superposition technique

When a multi degree of freedom system is subjected to a harmonic force f(t), the equation of motion is given by Eq. 3.32.

$$[M]\{\ddot{x}(t)\} + [C]\{\dot{x}(t)\} + [K]\{x(t)\} = \{f(t)\} \tag{3.32}$$

Where [C] is the damping matrix of the system. In modal superposition technique the key step is to transform the displacement vector x(t) to the generalised co-ordinates. The transformation is given using Eq. (3.33), where the displacement is represented as a summation of product of mode shape $\{\phi\}$ and its corresponding scalar multiplier y called modal co-ordinates. The transformation is illustrated using Fig 3.9 with the first three modes

$$x(t) = \{\phi_1\}y_1(t) + \{\phi_2\}y_2(t) + \{\phi_3\}y_3(t) + \cdots \{\phi_n\}y_n\ (t) \quad (3.33)$$

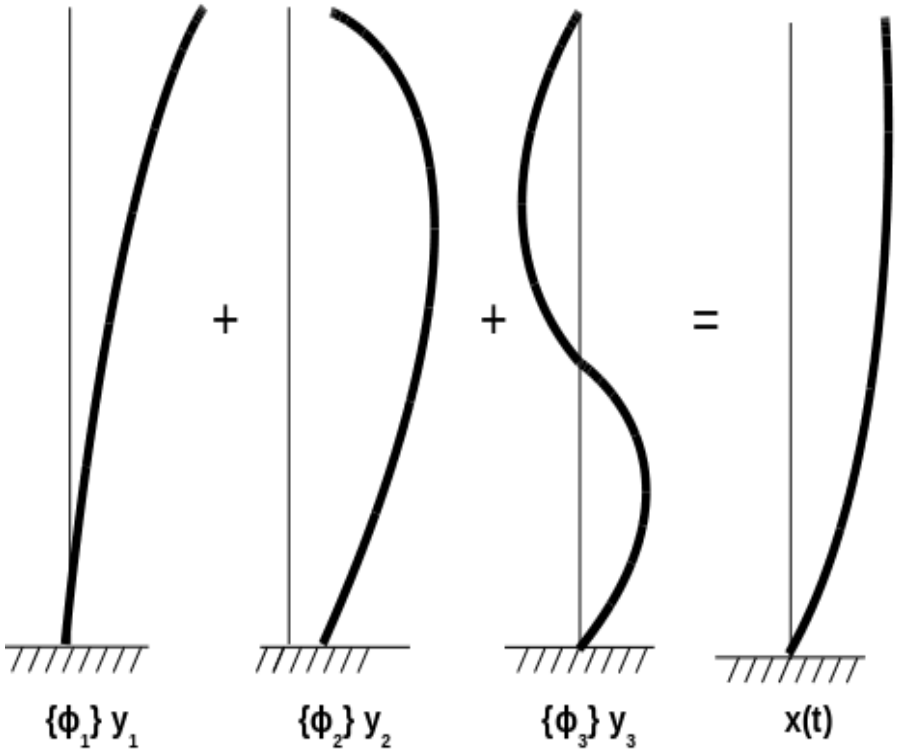

Fig 3.8 Modal superposition technique

Where $\{\phi_1\}, \{\phi_2\}$ and $\{\phi_3\}$ are the first, second and third modal vector and y_1,y_2 and y_3 are the respective modal co-ordinates.

The above equation can be re-written as

$$x(t) = [\phi]\,\{y(t)\} \quad (3.34)$$

Where $[\phi]$ and $\{y(t)\}$ are given in Eqs. (3.35) and (3.36) respectively.

$$[\phi] = [\{\phi_1\}\,\{\phi_2\}\{\phi_3\} \ldots \{\phi_n\}] \quad (3.35)$$

$$\{y(t)\} = [y_1, y_2, \ldots y_n]^T \quad (3.36)$$

When a structure is excited at a frequency closer to a resonant frequency, the corresponding mode shape might dominate the deflection shape at that frequency. The value of cor-

responding scalar multiplier y tend be higher compared to the scalar multiplier of other modes. This is explained in detail in Section 4.3.1.

To continue with modal superposition technique, the equation of motion 3.32 is modified by applying displacement transformation Eq. (3.34).

$$[M][\phi]\{\ddot{y}(t)\} + [C][\phi]\{\dot{y}(t)\} + [K][\phi]\{y(t)\} = \{f(t)\} \quad (3.37)$$

Pre multiplying Eq. 3.37 with $[\phi]^T$ and applying the orthogonal property the above equation can be reduced to a set of uncoupled equations given in Eq. (3.38), where the classical damping is used.

$$M_n\{\ddot{y}(t)\} + C_n\{\dot{y}(t)\} + K_n\{y(t)\} = F_n \quad (3.38)$$

Where

$$M_n = [\phi]^T[M][\phi] \quad (3.39)$$

$$K_n = [\phi]^T[K][\phi] \quad (3.40)$$

$$C_n = [\phi]^T[C][\phi] \quad (3.41)$$

$$F_n = [\phi]^T\{f(t)\} \quad (3.42)$$

Eq. (3.38) is similar to Eq. (3.24), so transfer function for the uncoupled system can be developed as shown in Eq. (3.43).

$$Y_n(\omega) = H(\omega)F_n(\omega) \quad (3.43)$$

Using the transfer function PSD response can be calculated using the same method discussed in section 3.3.1.

3.4 Fatigue analysis in time domain

Fatigue analysis is traditionally performed in time domain, the process is illustrated using Fig 3.10. Response of a structure can be calculated using a static analysis or by mode based transient dynamic analysis. If the operating frequency does not cause resonance in the structure and the inertial effects can be neglected static analysis can be conducted using unit load. Stress obtained from the analysis can be multiplied with the load time history to obtain stress response time history.

Mode based transient dynamic analysis can be used otherwise, to capture all the resonant effects. The major drawback with the transient dynamic analysis is the time step required for the analysis will be very small, which will lead to very long run time. In many cases the analysis is not feasible.

Based on the stress levels experienced in components there are two analysis methods commonly used, namely high cycle fatigue and low cycle fatigue. High cycle fatigue is characterised by stress within the elastic region, which results in higher number of fatigue cycles. On the other hand low cycle fatigue is characterised by stress in the plastic region causing permanent deformations and lower fatigue cycles. Most of the components in automobiles are subjected to high cycle fatigue and it is adopted for this thesis.

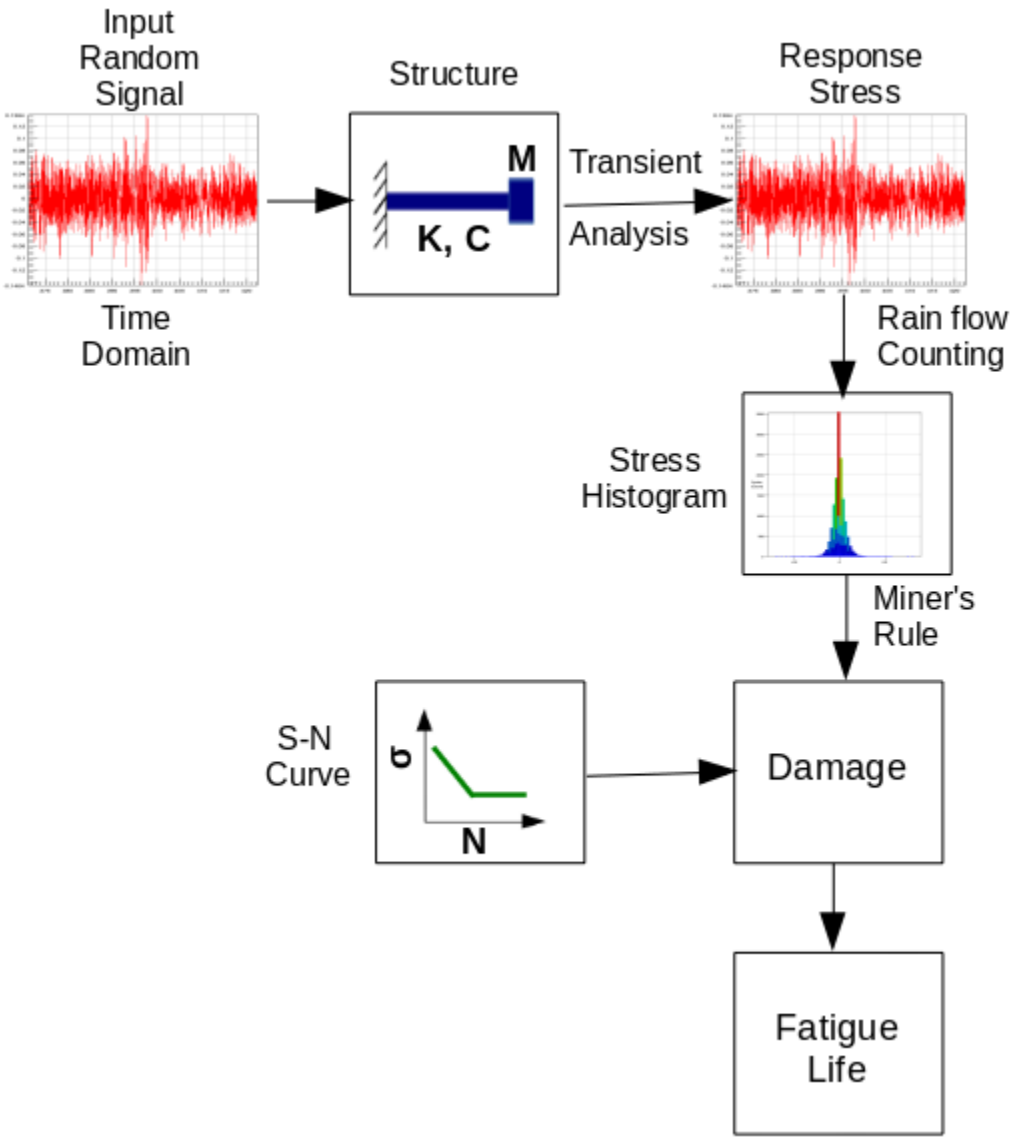

Fig 3.9 Fatigue analysis in time domain

3.4.1 Stress life (S-N) curve

Fatigue properties of material are given using S-N curves. To develop S-N curve material specimens are subjected to cyclic stress and the number of cycles it takes to failure is noted. The test is repeated at different cyclic stress levels and the corresponding number of cycles to failure is noted. A graph can be plotted with stress along y-axis and number of cycles to failure along x-axis, the plot is called an S-N curve. Generally they are plotted on a log-log scale as shown in Fig 3.11.

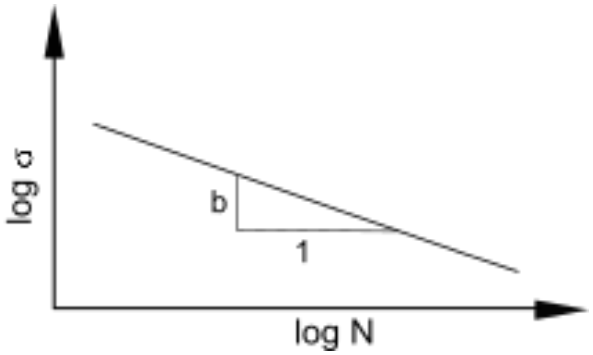

Fig 3.10 S-N Curve

An equation can be defined to fit the curve and it is generally of the form given in Eq. (3.44).

$$\sigma = \ C \ . \ N^{b} \qquad (3.44)$$

Where C is the fatigue constant and b is the slope of the curve. The constants C and b are published in the literature for different materials [54]. For weld fatigue using structural stress method, the constants are given in Table 2.1 [9]. Various standards like ASTM E 739-1980 [55] and JSME S002-1981 [56] have published recommendation on how to conduct fatigue tests to obtain S-N curves.

3.4.2 Cumulative damage -Miner's rule

For simple constant amplitude cyclic loading such as the ones experienced in rotating equipment computing the fatigue life is straight forward. Based on the response stress amplitude fatigue life can be directly computed using S-N curve. But if the loading contains multiple amplitudes like the one shown in Fig 3.12, cumulative damage method is used for computing fatigue life. When a component is subjected to cyclic load certain amount of damage is accumulated for each cycle based on its amplitude. Summation of damage caused by individual cycles gives the total damage accumulated. This method for computing damage is called the Palmer-Miner linear damage rule [25].

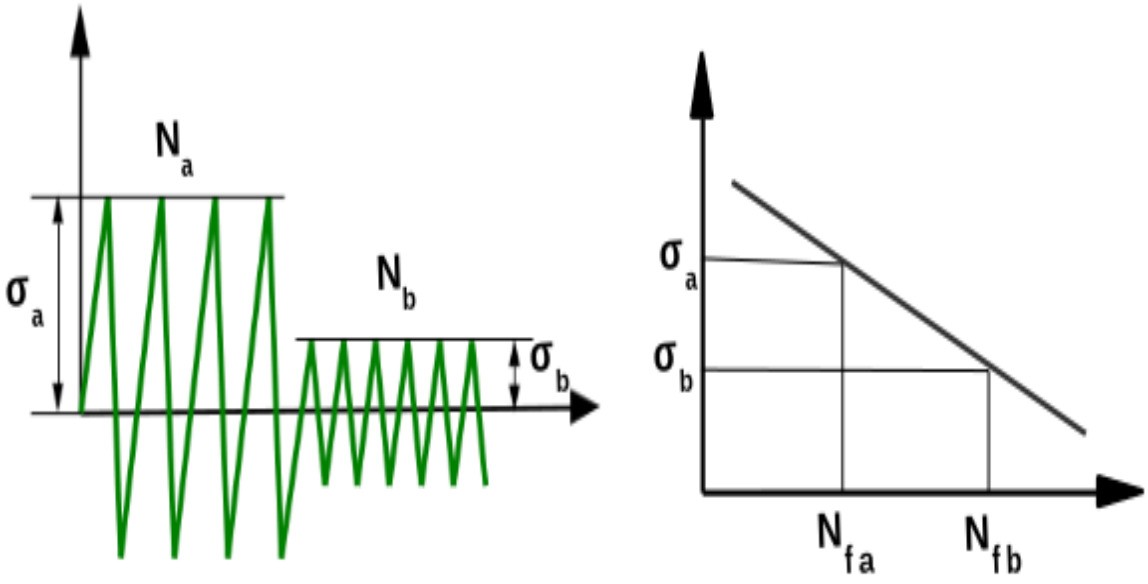

Fig 3.11 Cumulative Damage

Consider a loading with two stress amplitudes σ_a and σ_b as shown in Fig 3.12 .Stress amplitude σ_a has N_a number of reversals and σ_b has N_b number of reversals. From S-N curve for stress amplitude σ_a number of cycles to failure N_{fa} can be computed, similarly

N_{fb} for σ_b can be calculated. Individual damages D_a, D_b for σ_a and σ_b are calculated as follows,

$$D_a = \frac{N_a}{N_{fa}} \tag{3.45}$$

$$D_b = \frac{N_b}{N_{fb}} \tag{3.46}$$

$$Total\ Dmage\ D = D_a + D_b \tag{3.47}$$

Palmer's damage rule states that when the total damage reaches value close to 1 the component fails [57].

3.4.3 Rain flow cycle counting

In order to use Miner's rule to evaluate damage, fully reversed stress cycles has to be separated from more complex loadings. Like the ones experienced in real world, identifying the individual cycles becomes challenging. To overcome this difficulty various cycle counting methods are developed like level crossing method, peak valley counting, range counting, Markov counting and rainflow cycle counting. Among them rainflow counting method [58] is more accurate and is commonly used in the industry. This algorithm was developed by Japanese researchers Matsuiski and Endo [59]. In this method, first the stress time history signal is rotated 90̊ and water is assumed to flow from the top of the signal, the path of the water flow is used for cycle counting. The following rules where developed for cycle counting.

1. Each rain flow begins at the beginning of the time series and inside of every peak and valley.

2. Rain flow initiated at the peak drops until it reaches the opposite peaks more positive (or valley more negative) than from a peak it started.
3. Rain flow stops when it meets rain flow from above.
4. Rain flow must terminate at the end of the signal.

Rain flow counting algorithm for complex stress time history signals was explained graphically [59]. It would be quite tedious to do the count cycles graphically, so numerical based methods were developed to count the cycles directly from the discrete signals. ASTM E 1049-85 [60] has published a numerical algorithm for rainflow cycle counting and widely used in the industry.

To summarise the fatigue process in time domain, first response of a structure is obtained by either FEA or by testing. The complicated stress response is broken down into simple variable amplitude cycles and a histogram of stress is developed using rainflow counting technique. By using Miner's rule and S-N curve total damage is calculated, which gives fatigue life directly.

3.5 Fatigue analysis in frequency domain

The process of calculating fatigue life in frequency domain is explained using a process flow chart shown in Fig 3.12. In this method first the input load signal in time domain is transformed to a PSD signal in frequency domain. Using linear transfer function the response stress PSD is calculated. This response stress PSD is converted to a stress histogram N(S) using various statistical techniques. Four of the most commonly used techniques are explained in this section.

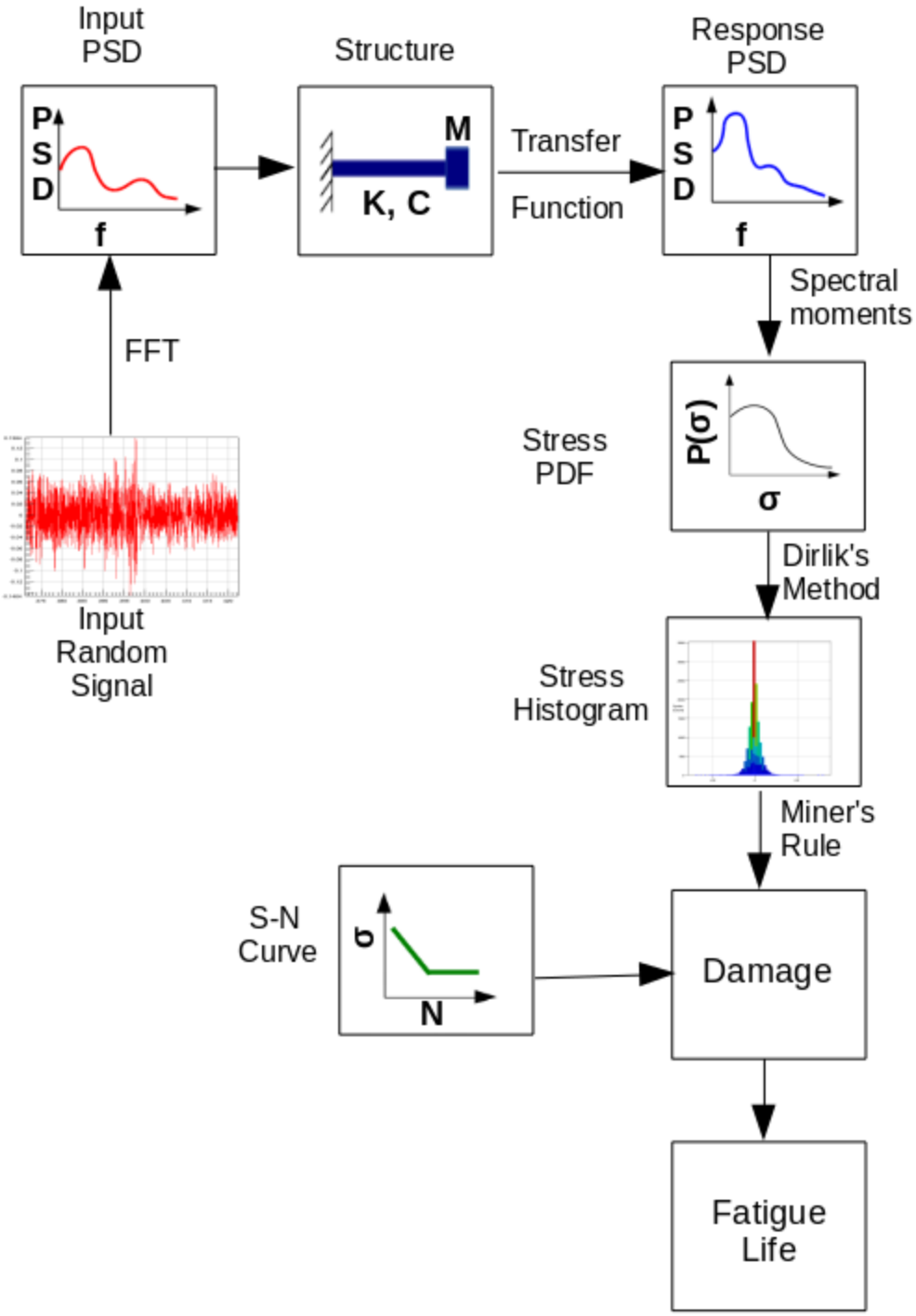

Fig 3.12 Fatigue analysis in frequency domain

3.5.1 Narrow band approach

Fatigue life estimation using Narrow band approach was first proposed by Bendat et al [61] in 1964 using probability density function, P(S), of the stress. In his method stress histogram is calculated using Eq. (3.48) [61].

$$N(S) = E[P].T.P(S) \tag{3.48}$$

Where T is the time period of the signal and E[P] is the expected peaks calculated using Eq. (3.16).

Bendat et al assumed for every peak in the time signal there is trough of similar magnitude and the stress amplitude follows Rayleigh's distribution. Changing the probability density function (PDF) to Rayleigh's distribution in Eq. (3.48) it becomes Eq. (3.49) where m_0 is the zeroth spectral moment calculated using Eq. 3.14.

$$N(S) = E[P]\,.\,T.\ \left[\frac{S}{4m_0}e^{\frac{-S^2}{8m_0}}\right] \tag{3.49}$$

When this narrow band solution was applied to the wide band process the solution was found to be too conservative [49]. This is mainly due to the assumption that every peak has a trough with equal magnitude. Consider the two signals shown in Fig. 3.14 [43]. The first one is a narrow band signal with two sine waves at very close frequencies. The second signal is a broad band signal with two sine waves at far apart frequencies. If the cycle count is done using the assumption every peak has trough, the resultant for the both the signal is shown in the third figure in green. It is almost matching the narrow band signal, but it gives too many cycles for a wide band process. Results from this method will yield very conservative results for wide band process.

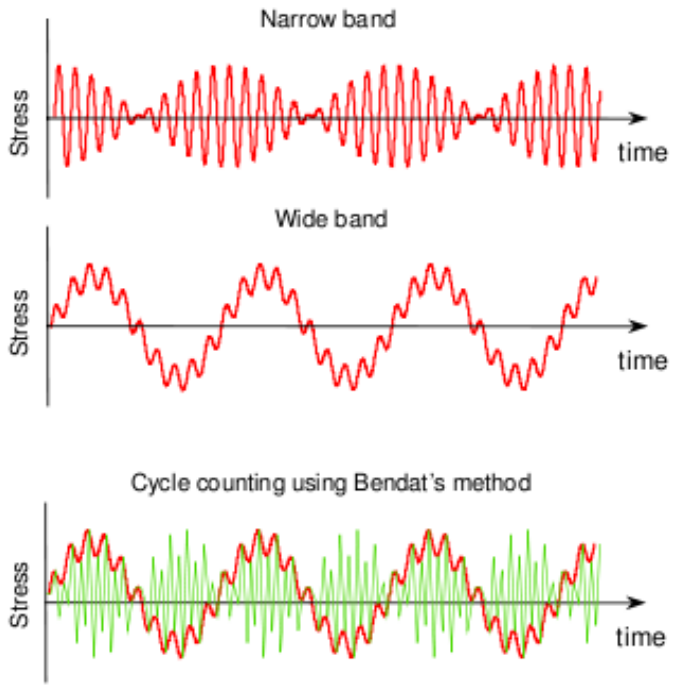

Fig 3.13 Narrow band method [48]

To improve this narrow band process many methods were developed. Tuna [62], Caudhury and Dover, Wirsching [63] and Hancock [64] developed various correction factors to reduce this conservatism. These methods were based on the PSD response signal back to time signal using IFFT. They were developed mainly for offshore platforms. These methods improved the narrowband process but still way conservative and couldn't be applied for all applications.

3.5.2 Broad band approach (Steinberg)

Steinberg et al [65] proposed a method for broad band process. He assumed the PDF of stresses follow Gaussian distribution. This method is based on discrete multiples of RMS value, the stress histogram is given by Eq. (3.49) [65].

$$E[D] = E[P] \,.\, T. \begin{vmatrix} .683 \text{ x } 2RMS \\ +\, .271 \text{ x } 4RMS \\ +\, .043 \text{ x } 6RMS \end{vmatrix} \qquad 3.49$$

3.5.3 Lalanne approach

Lalanne [66] improved the narrow band approach developed by Bendat [61] and made it applicable to both narrow band and broad band signals. His method is based on simple weighted sum of Rayleigh and Gaussian distributions. In Lalanne method stress histogram N(S) is calculated using Eq. 3.50.

$$N(S) = \frac{1}{RMS} . \frac{\sqrt{1-\gamma^2}}{\sqrt{2\pi}} . e^{\frac{-S^2}{2RMS^2(1-\gamma^2)}} + \frac{S.\gamma}{2RMS} . \left[1 + erf\left(\frac{S.\gamma}{RMS\sqrt{2(1-\gamma^2)}}\right)\right] \qquad (3.50)$$

Where

$$erf(x) = \frac{2}{\sqrt{\pi}} \int_0^x e^{-t^2}\, dt \qquad (3.51)$$

3.5.4 Dirlik Method

Later Dirlik [67] in 1985 proposed a solution to compute PDF directly based on closed form empirical expression. The expression for PDF is only a function of four spectral moments m_0, m_1, m_2 and m_4. Dirlik's PDF equation is given in Eq. (3.52) [67].

$$P(S) = \frac{\frac{D_1}{Q} e^{\frac{-Z}{Q}} + \frac{D_2 Z}{R^2} e^{\frac{-Z^2}{2R^2}} + D_3\, Z\, e^{\frac{-Z^2}{2}}}{2\sqrt{m_0}} \qquad (3.52)$$

$$D_1 = \frac{2(x_m - \gamma^2)}{(1+\gamma^2)} \qquad (3.53)$$

$$D_2 = \frac{(1-\gamma-D_1-D_1^2)}{(1-R)} \tag{3.54}$$

$$D_3 = 1-D_1-D_2 \tag{3.55}$$

$$Z = \frac{S}{2\sqrt{m_0}} \tag{3.56}$$

$$Q = \frac{1.25(\gamma-D_3-D_2\ R)}{D_1} D_1 \tag{3.57}$$

$$R = \frac{(\gamma-x_m-D_1^2)}{1-\gamma-D_1-D_1^2} \tag{3.58}$$

$$\gamma = \frac{m_2}{\sqrt{m_0 m_4}} \tag{3.59}$$

$$x_m = \frac{m_1}{m_0}\sqrt{\frac{m_2}{m_4}} \tag{3.60}$$

Using the PDF calculated from the above equation Dirlik calculated the stress histogram directly using Eq. (3.48). Dirlik's method is the most general form and can be used for both narrow band and broad band signals.

Chapter 4

Proposed method

4.1 Introduction

Based on the discussions in chapter 2, E^2S^2 method developed by Dong et al [38] is very effective in predicting fatigue life of welded joints. Chapter 3 elaborated on methods to predict fatigue life under random loading using vibration fatigue techniques. This chapter explains the proposed method in this study, which combines E^2S^2 method and vibration fatigue technique to predict fatigue of welded joints under random loading.

4.2 Current Challenge

As discussed in section 2.4, in E^2S^2 method two important input quantities that are required for fatigue life prediction of welded joints are the force normal to the weld and bending moment parallel to the weld. Membrane stress and bending stress along the weld toe are calculated using these forces and moments based on Eq. (2.9). The structural stress σ_s is calculated by summing the membrane stress and bending stress.

When a welded joint is subjected to dynamic loading, force response and moment response are required over the entire period of time for calculating fatigue life of the joint. Consider a welded joint subjected to a sinusoidal dynamic bending load, with a specific frequency. It will generate a response force f_y and response moment m_x which will also be sinusoidal in nature. There might be a phase shift between the two responses as illustrated in the Fig 4.1. If only the amplitude f_{ya} of the force signal and the amplitude m_{xa} of the moment signal are used for calculating structural stress, it will lead to errors in the results because of the phase shift.

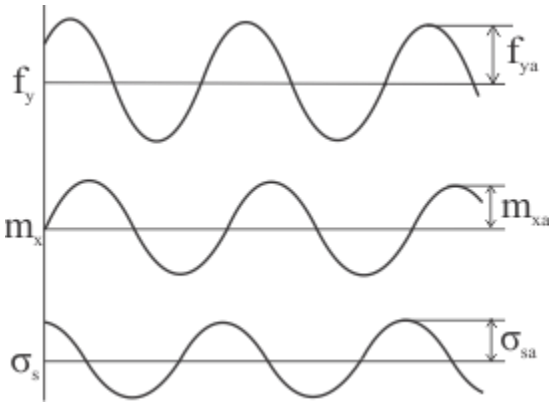

Fig 4.1 Structural stress in time domain

$$\sigma_{sa} \neq \frac{f_{ya}}{t} + \frac{6m_{xa}}{t^2} \tag{4.1}$$

For analysing structure subjected to random loading, PSD based method is found to be very efficient .When a welded joint is analysed using PSD based method ,response in terms of force PSD and moment PSD at the weld toe can be obtained at each frequency. By definition of PSD only amplitude of signal is preserved, phase information is lost. If structural stress PSD is calculated directly using response force and moment PSDs, it is equivalent to summing the membrane stress amplitude and bending stress amplitudes.

This will ignore the phase shift between the two signals, leading to inaccuracies in the results.

This creates challenge in combining E^2S^2 method and PSD based method for computing fatigue life of welded joints subjected to random loading. To overcome this difficulty a method is proposed in this thesis and is explained in the following sections.

4.3 Harmonic scale and PSD scale

Two types of scale are used in the proposed method, namely harmonic scale and PSD scale. Theoretical basics and relationship between the two scales are discussed in this section. Assume a plate with a hole subjected to a force. This will induce a stress say σ_a at the hole and σ_b at a distance Δ from the hole as shown in Fig 4.2. If the analysis is linear, the two stresses can be linearly related using a simple scale as shown in Eq. (4.2).

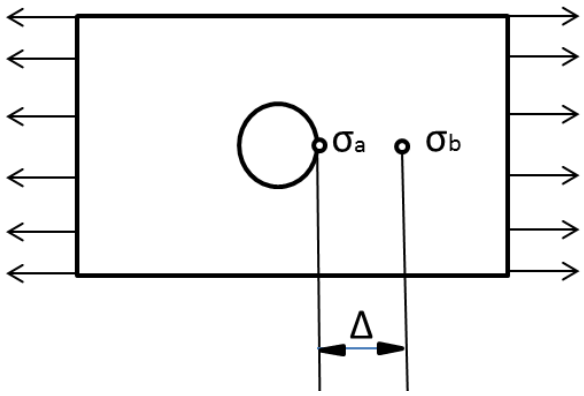

Fig 4.2 Linear Scale

$$\text{Scale} = \frac{\sigma_a}{\sigma_b} \tag{4.2}$$

If the system is linear and the deflection shape remains same, stress σ_a can be calculated using, stress σ_b and the linear scale for any load values. The scale is similar to geometric stress concentration factor, but stress measured at a fixed distance Δ is used instead of nominal stress.

4.3.1 Harmonic Scale

In a dynamic environment when a structure is subjected to dynamic loads, depending on the frequency of excitation the structure deflects in a specific form. The form it takes during an operating frequency is called operating deflection shape [68]. From section 3.3.2 the operating deflection shape can be calculated using modal superposition technique based on Eq. (3.33).

The scalar multiplier y called the modal co-ordinates dictates the operating deflection shape, it varies depending on the frequency of excitation. To demonstrate the variation of operating deflection shape over the excitation frequency a simple cantilever beam with properties shown in table 4.1 is used.

Length (mm)	Width (mm)	Height (mm)	Young's Modulus (M Pa)	Poison's Ratio	Density Tons/mm3
100	10	5	210000	0.3	2.085 E-4

Table 4.1 Properties of the cantilever beam

A two node linear beam element is used for representing the beam. One end of the beam is constrained in all directions. Element size of 1mm is used for the current model.

Modal analysis is first conducted on the model to understand its mode shape and natural frequencies. The first 5 modes and natural frequencies of the model are shown in table 4.2 and Fig 4.3.

Mode	Natural Frequency (Hz)	Shape
1	2.6	First Bending along Z
2	5.1	First Bending along Y
3	15.8	Second Bending along Z
4	30.5	Second Bending along Y
5	36.3	First Axial along X

Table 4.2 Natural frequencies and mode shapes of the cantilever beam

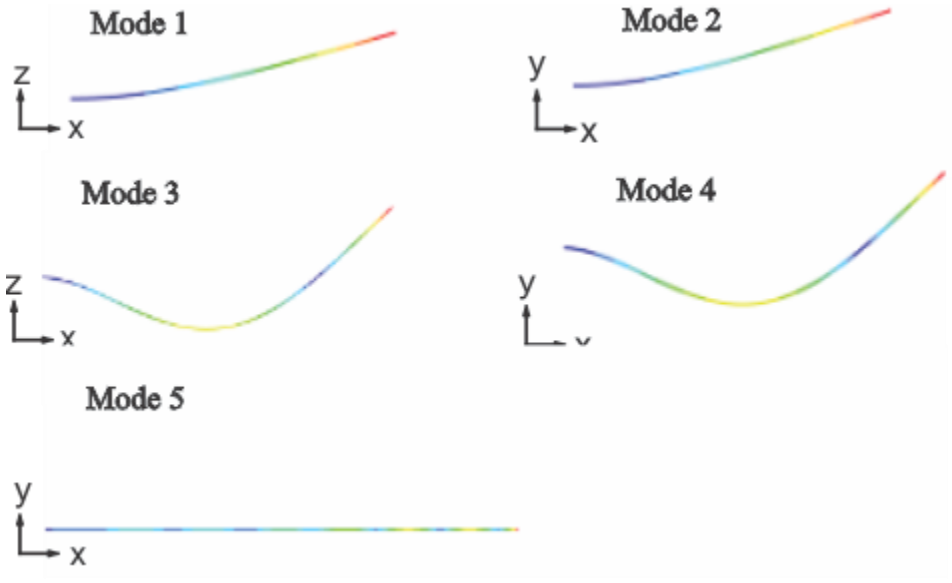

Fig 4.3 Mode shapes of the cantilever beam

Next the model is subjected to a harmonic base displacement of 1mm in Z-direction from 0-100 Hz. The generalized displacement or scalar multiplier y_n is plotted for the first five modes. Since the loading is in the Z-direction, only the first and the third modes which are the first and second bending modes along Z-axis participate in the analysis. Modes 2, 4 and 5 are orthogonal to applied excitation, so they do not contribute to this analysis.

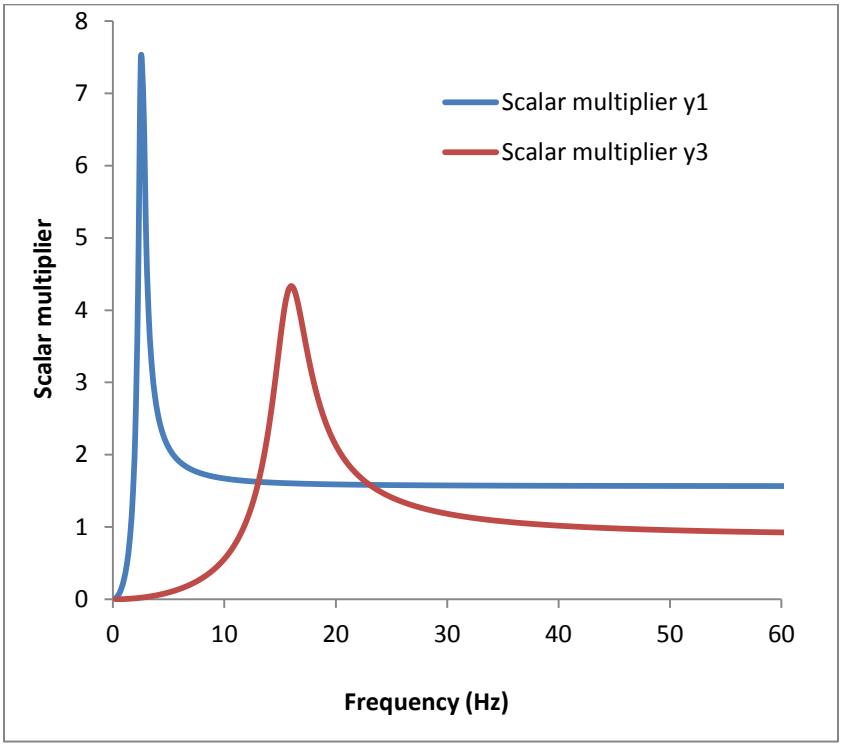

Fig 4.4 Scalar multiplier of the cantilever beam model

Around the first natural frequency the scalar multiplier y1 is very high, which indicate that the mode shape one will dominate the operating deflection shape. As the frequency gets closer to the third natural frequency, y_3 becomes higher than y1. Around the third natural frequency both Mode1 and Mode3 govern the operating deflection shape. This confirms that the operating deflection shape is a function of excitation frequency.

Since the operating deflection shape changes over frequency, a scale which relates the, stresses at the two nodes also varies over excitation frequency. The scale used in frequency response analysis is referred as harmonic scale in this thesis.

To calculate the harmonic scale for this model two nodes, Node-a is at a distance of 45mm from the fixed end and Node-b at a distance of 3mm from Node-a are selected as shown in Fig 4.5. These two nodes are selected since the variation of stress at this location is higher, which helps in understanding the harmonic scale better.

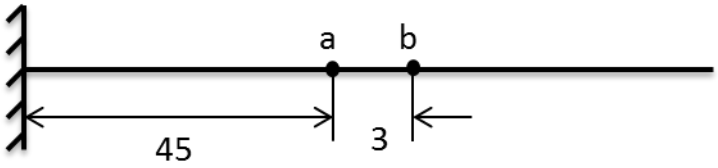

Fig 4.5 Nodal reference cantilever beam

Ratio of stress along x-axis between the two nodes is calculated at each frequency and plotted in a graph, Fig 4.6. As we can see from the graph the harmonic scale varies from .69 to 1.55, which proves harmonic scale is a function of excitation frequency.

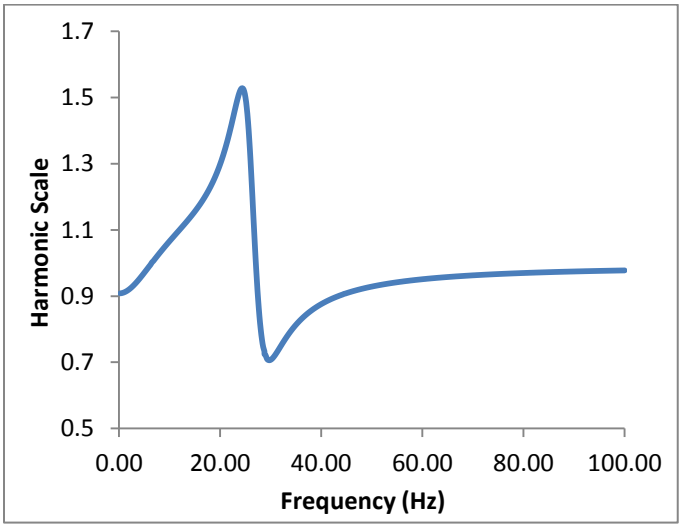

Fig 4.6 Harmonic scale of the cantilever beam

4.3.2 PSD Scale

Similar to harmonic scale, PSD scale is the ratio of stress PSD's between two nodes at a given frequency. In order to calculate PSD scale the same beam model is subjected to an equivalent base displacement PSD from 0-100 Hz. The PSD scale between Node-a and Node-b is plotted over the excitation frequency in Fig 4.7., as expected the PSD scale also varies over the excitation frequency.

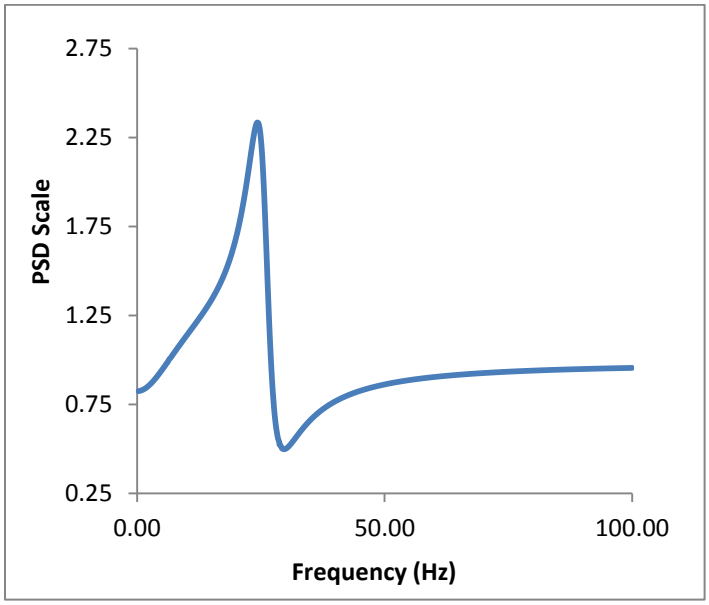

Fig 4.7 PSD scale of the cantilever beam

4.3.3 Relation between Harmonic Scale and PSD Scale

Now the relationship between PSD scale and Harmonic scale is explored. By definition of PSD, area of a strip under the PSD curve is equal to the RMS of the sine wave at that frequency [49]. Based on the RMS value approximate amplitude of the signal can be calculated at a given frequency using Eq. (3.12) [49].

Harmonic scale for a given frequency is given by

$$\text{Harmonic Scale} = \frac{\sigma_a}{\sigma_b} \tag{4.3}$$

$$= \frac{\sqrt{2.PSD_a.\Delta f}}{\sqrt{2.PSD_b.\Delta f}} \tag{4.4}$$

$$\text{Harmonic Scale} = \sqrt{PSD\ scale} \tag{4.5}$$

$$\text{PSD Scale} = (Harmonic\ scale)^2 \tag{4.6}$$

To verify this relationship, harmonic scale obtained from the beam model is squared and plotted along with the PSD scale obtained directly from FEA. From the graph shown below they match perfectly, which verifies this relationship.

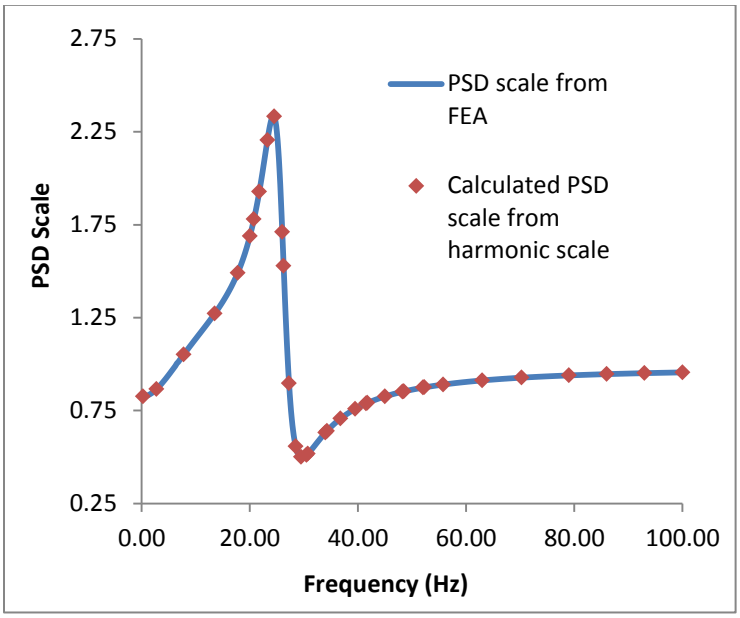

Fig 4.8 FEA PSD Scale vs. Calculated PSD Scale

The following conclusions can be derived based on the results from this section

1. Operating deflection shape is a function of excitation frequency.

2. In a dynamic analysis when a scale is derived between two nodes it is a function of excitation frequency.
3. PSD scale can be calculated from harmonic scale, if the boundary conditions and loading direction remain the same. PSD scale is equal to the square of harmonic scale at a given frequency.

4.4 The proposed method

The objective of the proposed method is to calculate structural stress PSD at the weld toe, using harmonic scale and PSD scale. The proposed method is illustrated using a flowchart shown in Fig 4.9.

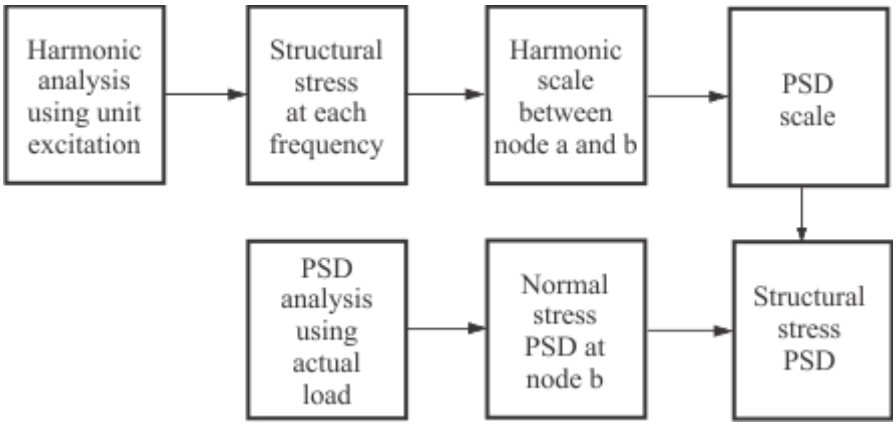

Fig 4.9 Process flow of the proposed method

In the proposed method, first a harmonic analysis is conducted using a unit excitation in the direction of actual load in study. From the analysis forces and moments at the weld

toe shown in Fig 4.10 is obtained in frequency domain. This response includes both amplitude and phase angle. At each frequency a time history of forces and moments can be recreated using this amplitude and phase angle. Using this data structural stress can be accurately calculated. The exact procedure is discussed in section 4.5.1.

Now harmonic scale at each frequency can be established between the structural stress σ_{sa} at weld toe Node-a and normal stress σ_b at Node-b, which is at a distance of Δ from the weld toe. Based on the relationship obtained in section 4.3.3, the harmonic scale is squared to obtain PSD scale at each frequency.

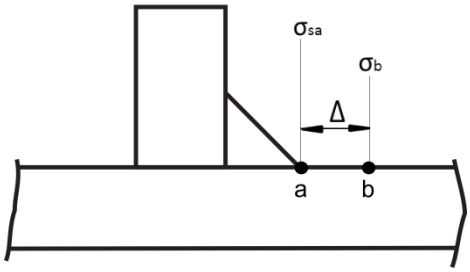

Fig 4.10 Structural stress at weld toe and normal stress at node b

Next frequency based PSD analysis is conducted on the model using the actual random load PSD. The normal stress response PSD at Node-b can be obtained from this analysis. Using the PSD scale and the stress PSD at Node-b, structural stress PSD at the weld can be calculated.

Fatigue life of welded joint using structural stress PSD can be obtained using the four methods discussed in section 3.5. For this research Design Life [50] software is used for calculating the fatigue life from the structural stress PSD.

Chapter 5

Numerical investigations and Results

5.1 Weld fatigue of a T-joint using the proposed method

In order to validate the proposed frequency domain method, fatigue life of a T-joint is analysed using the proposed method and compared with the life estimated using a transient dynamic analysis. Bus structure consists of three main joint configurations, namely T-joint, K-joint and X-joint. Among them T-joint is the most commonly used joint configuration. A T-Joint is a geometry configuration where a structural tube is welded perpendicular to another tube or welded to a plate. For this analysis a tube to plate welded configuration is used. For this study a rectangular tube 700mm long is attached to 10mm thick plate, the dimensions of plate and the tube are shown in Fig 5.1. The material properties and the tube section properties used for this study are shown in Table 5.1

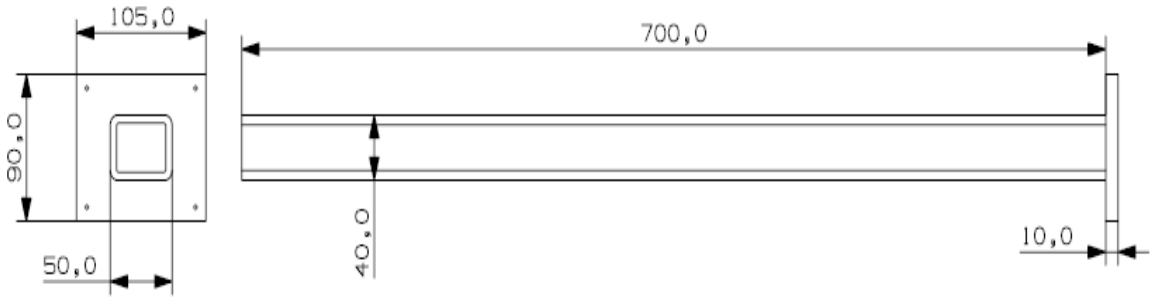

Fig 5.1 T -Joint Geometry

Width (mm)	Height (mm)	Thickness (mm)	Young's Modulus (MPa)	Poison's Ratio	Density Tons/mm3
50	40	2	202000	0.3	$7.85 X10^{-6}$

Table 5.1 Properties of T-Joint

A finite element (FE) model of the T-joint was developed using CAD geometry. Plate was modelled using four node shell elements. Since transient dynamic analysis was conducted later to calculate the fatigue in time domain, the number of degree of freedom of the FE model was set at an optimal level. Frist 75 mm of the tube section was modelled using four node shell elements, the rest of the tube was modelled using two node beam elements. Beam elements and shell elements were connected using rigid elements. The fillet weld connecting the plate and tube was modeled as per the recommendation given by Dong et al [33].

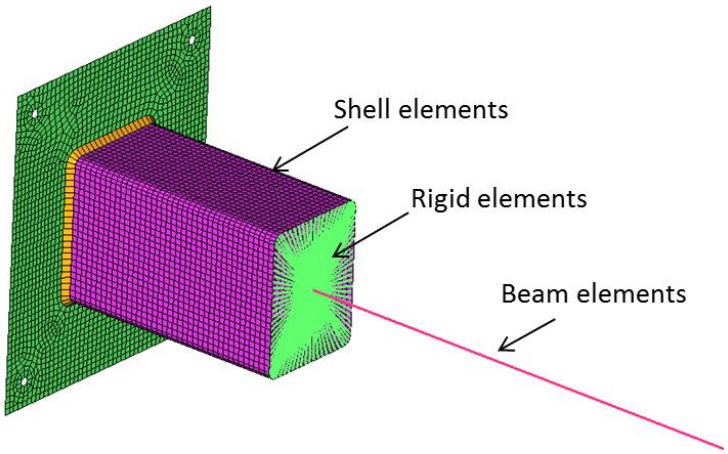

Fig 5.2 Finite Element Model of T- Joint

5.1.1 Modal analysis of T-joint

To validate this simplified model, another Finite Element Model was constructed, with the tube completely represented by four node shell elements. A modal analysis was conducted on the models, by constraining the holes in the plate. Natural frequency of the two models are listed in table 5.1, they compare very closely which validates the simplified model.

Mode	Natural Frequency (Hz)	
	Full Model	Reduced Model
1	17.2	17.3
2	20.4	20.6
3	353	352
4	418	417
5	428	428

Table 5.2 T- Joint natural frequency comparison

5.1.2 Static analysis of T-joint

The proposed method is based on the fact that the structure should behave linearly. To confirm the structural stress calculation procedure discussed in Section 2.4 is linear with load, static analysis was conducted on the model with four force magnitudes (25N, 50N, 75N and 100N) applied to the free end of the T-joint. Structural stress along weld toe shown in Fig 5.3, was calculated using the VBA-Excel tool from Section 2.4.

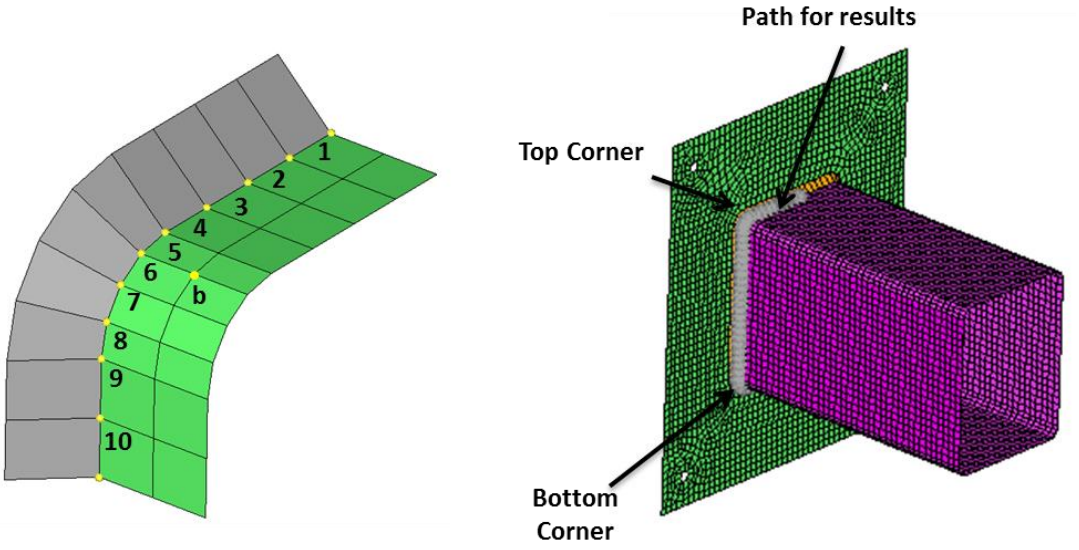

Fig 5.3 Node numbering along the weld Toe.

Structural stress calculated along weld toe for 25N load is shown in Fig 5.4. As we can see from the graph the top side of the beam is in tension and the bottom side of the beam is in compression. Maximum structural stress occurs at the corners of the tube as marked in Fig 5.3. This is the location where most of the failures were reported during fatigue test of the bus structure [20, 21] and T-joint tests [22]

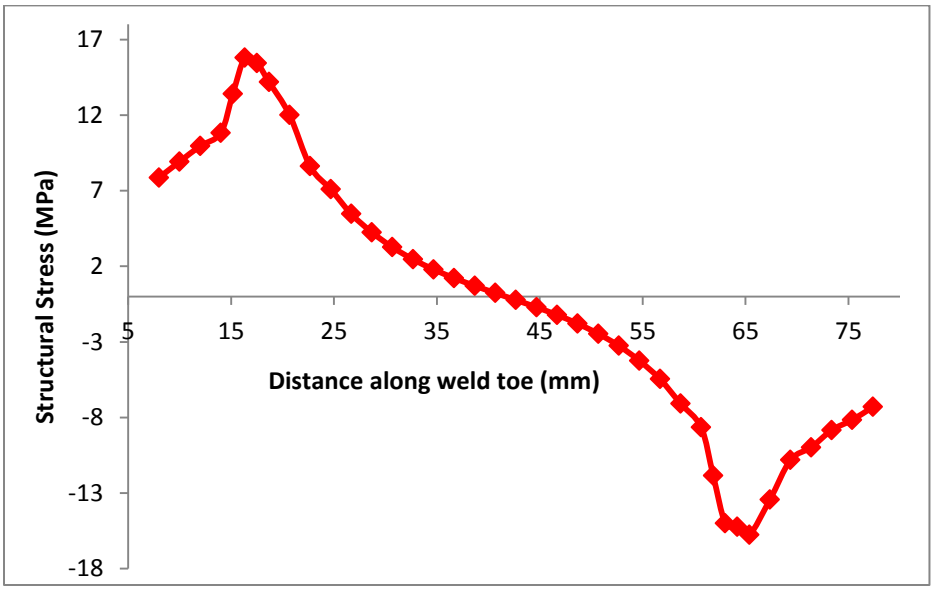

Fig 5.4 T-joint structural stress along weld toe

Stress levels are equal in both the top and the bottom corner, only the sign changes. For reporting simplicity, only the stress at the top corner of the joint is used for this study. Five nodes (node 5, 6, 7, 8 and 9) shown in Fig 5.3 are selected at the top corner along the weld toe, structural stress are reported for all the four loading condition. Structural stress is plotted against the applied force and shown in Fig 5.5. It is clear from the graph structural stress calculation is purely linear.

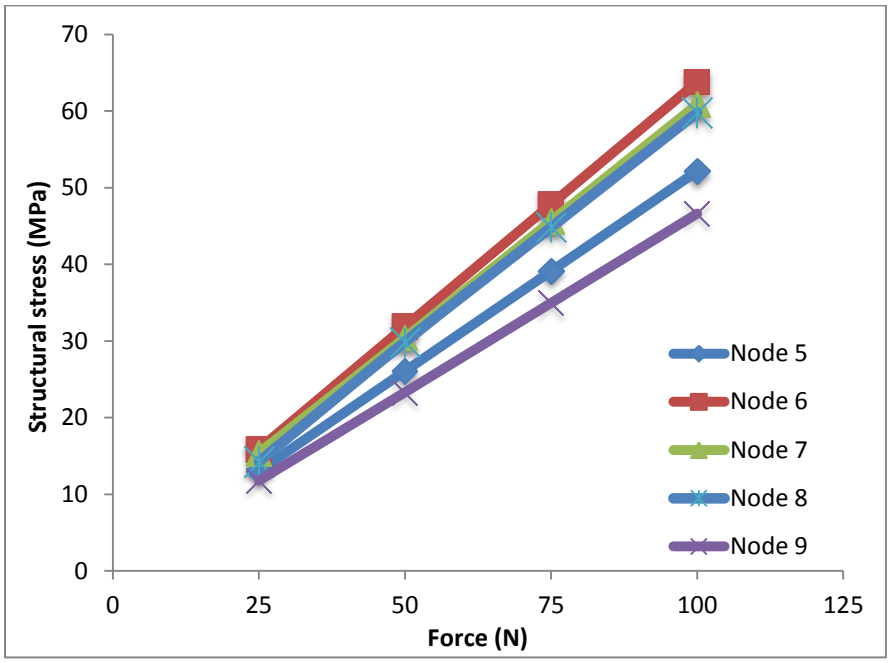

Fig 5.5 T-joint structural stress vs. applied force

5.1.3 Mesh Convergence study

In finite element method Gauss integration scheme is used for calculating the stiffness matrix [69]. In order to converge the results to accurate solution in Gauss integration scheme, order of the element is increased in p-method and number of elements is increased in h-method. In this research h-method is used. In this method, mesh convergence study is conducted by reducing the element size of the model and measuring the stress at each mesh size. If the stress change between the two mesh sizes is smaller than a pre-specified small value, then the mesh is said to have converged and results is closer to the accurate solution. Initially the structural stress method by Dong et al [38] was claimed to insensitive to mesh size. But later it was revised and the mesh size is claimed to be insensitive if value of the mesh size is around the thickness of the parts in study [9]. To verify

this, three finite element model of the T- joint were developed with element sizes equal to 0.5 x thickness , 1 x thickness and 1.5 x thickness. Structural stress is calculated at the top corner of the tube for all three mesh sizes. A graph is plotted with structural stress along Y-axis and distance along X-axis as shown in Fig 5.6. From the graph it is clear that mesh has converged for all the three mesh sizes. For this research model with mesh size of 1x thickness was used form here on.

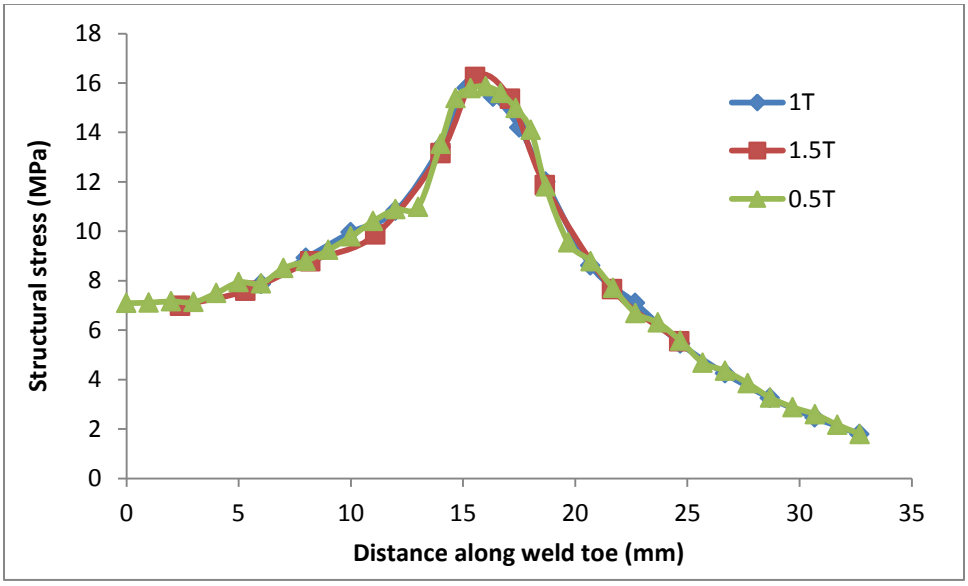

Fig 5.6 Structural stress for different mesh size

5.1.4 Harmonic Scale of T-joint

First step in the proposed method is the calculation of harmonic scale. In order to calculate the harmonic scale, T-joint FE model in study is subjected to a harmonic base displacement of 1mm in Y-direction from 0-60 Hz. Frequency of 0-60 Hz is selected, since it is the frequency range encountered on a bus due to road excitation [2].

To understand the operating deflection shape of the T-joint at the frequency range, the generalised displacement y is plotted against frequency as shown in Fig 5.7. Only y_2 is shown in the graph, all other values y_1, y_3, y_4 and y_5 are very low and closer to zero. From the graph it is evident that only mode shape-2 dominate the operating deflection shape of the structure.

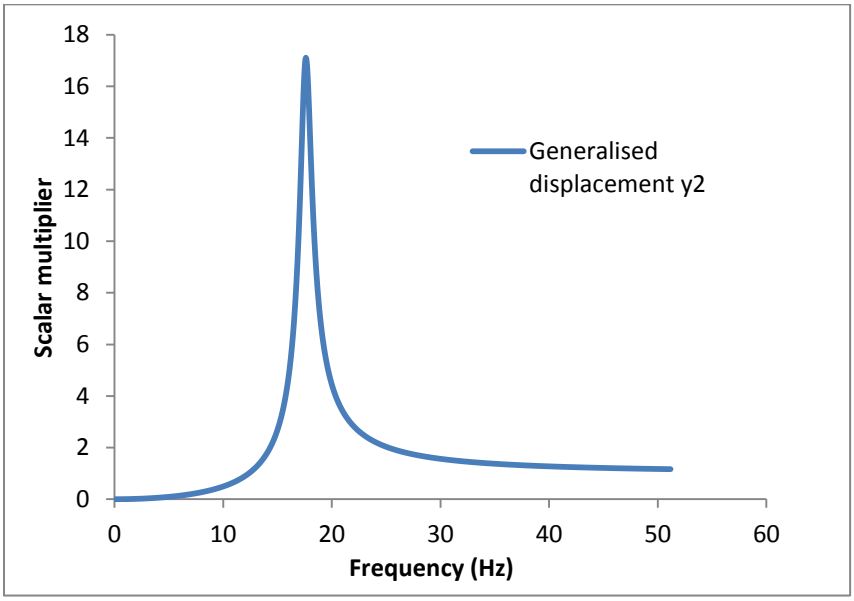

Fig 5.7 Generalised displacement of the T-Joint

From the static analysis the maximum structural stress is experienced at the top corner at Node-6. Structural stress was not calculated just based on the nodal force and moments at Node-6. From Eq. 2.10 the distributed quantities line force and line moments are influenced by adjacent nodal force and nodal moments. For static analysis calculation was simpler so the structural stress was calculated along the weld toe. But for harmonic analysis it would be tedious to calculate the results for the entire weld toe. So only 10 nodes at the top corner (Node 1-10) as shown in Fig 5.3, five nodes at either side of Node-6 is included in this calculation procedure.

From the results of the harmonic analysis three quantities namely the nodal force normal to the weld, nodal moment parallel to the weld at weld toe and normal stress at the adjacent Node-b shown in Fig 5.3 can be obtained. Results of the analysis will in frequency domain, represented using two graph amplitude A vs frequency and phase angle φ vs frequency. Time history data for each response quantities at each frequency can be calculated using Eq. (5.1).

$$Response\ in\ time\ domain\ = Acos(\omega t + \varphi) \tag{5.1}$$

Substituting nodal force amplitude and phase angle into Eq. (5.1) for a given frequency nodal force history response can be calculated. Similarly nodal moment time history for a given frequency can be calculated. Using this data structural stress time history for a given frequency can be calculated using the method discussed in section 2.5.

Now normal stress response time history at Node-b can be calculated using Eq. (5.1) for a given frequency. Using the structured stress and normal stress at Node-b, harmonic scale is calculated for the given frequency. The procedure is repeated and harmonic scale for each frequency is calculated between the structural stress at Node-a and normal stress at Node-b using Eq. (5.2).

$$(Harmonic\ Scale)_f \quad = (\ \sigma_{s6}/\sigma_{sb}\ )_f \tag{5.2}$$

In this analysis mostly Mode-2 govern the operating deflection shape participation of other modes was very minimal. Due to this harmonic scale is almost constant it varies only between 1.9 to 2.

Amplitude of the calculated structural stress at Node-1 and normal stress at Node-b are plotted against frequency and shown in Fig 5.8.

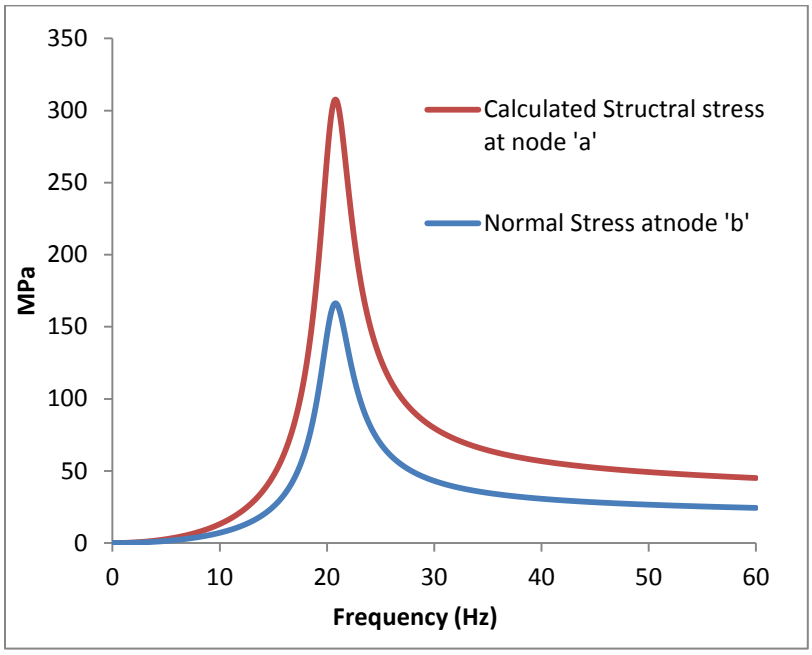

Fig 5.8 T-Joint Harmonic response

5.1.5 PSD Analysis

The next stage in the proposed method is to calculate the normal PSD stress response at Node-b using the actual random PSD signal. Once harmonic scale is calculated, they can be used for any number of loading, as long the direction of excitation and the boundary conditions are the same. For this analysis two displacement PSD's are assumed, the first PSD skewed towards the lower frequencies (load case1) as shown in Fig 5.9(a).The pro-file is similar actual test data, due to copyrights issues couldn't able to use the actual test data. The second one is the white noise (load case2) as shown in Fig 5.9(b).

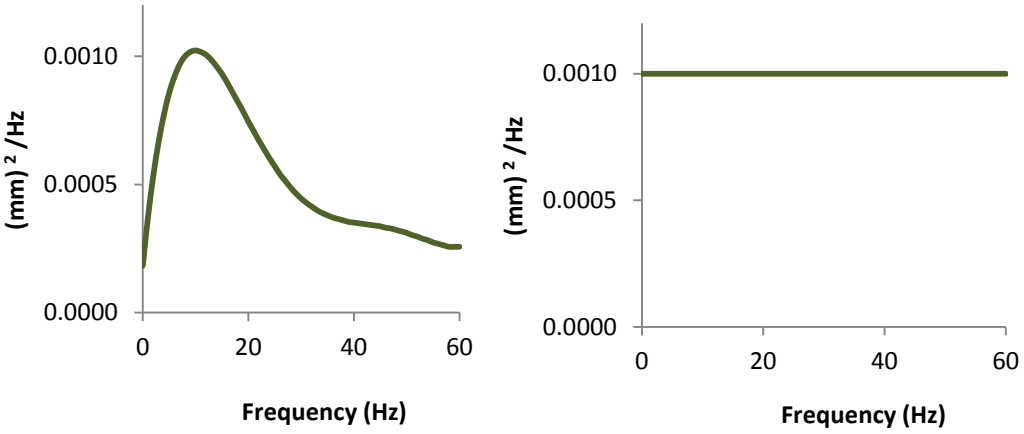

(a) (b)

Fig 5.9 Excitation- displacement PSD's

The T-joint was excited at the base using these displacement PSD's in the Y-direction. Normal stress PSD response at Node b was extracted from this FE analysis. Using the PSD scale calculated using harmonic scale, structural stress PSD at Node-a was calculated. For the two load cases response stress PSD's are plotted against frequency and is given in Fig 5.10.

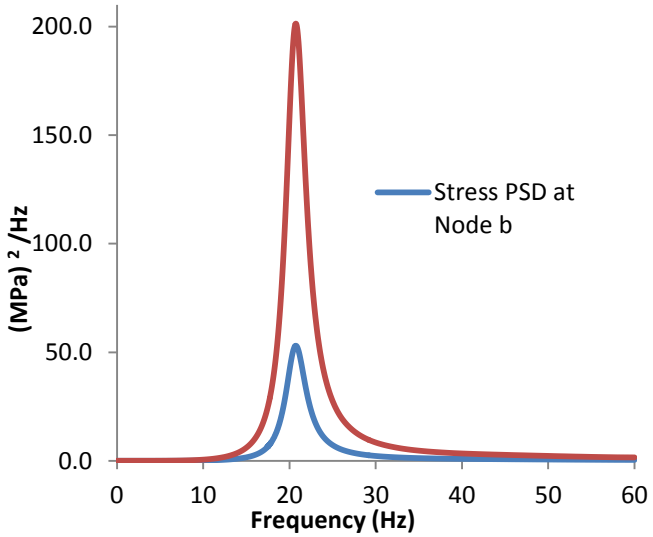

Fig 5.10 PSD stress response for load case 1

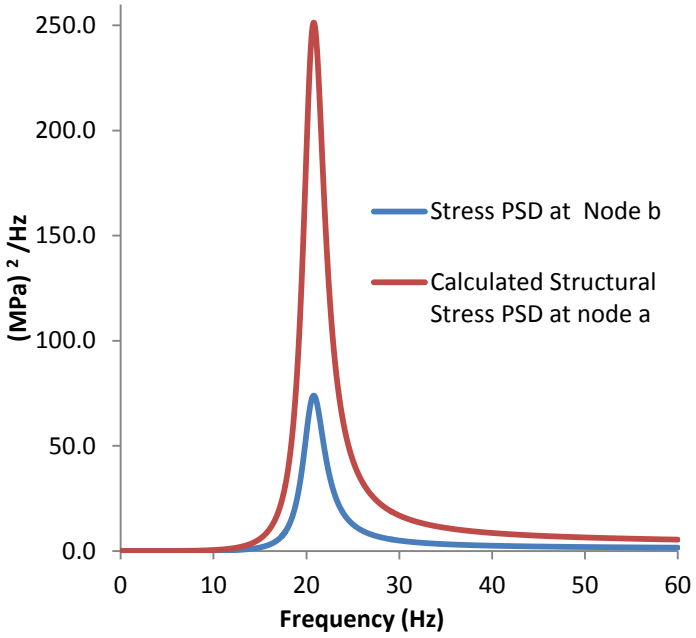

Fig 5.11 PSD stress response for load case 2

5.1.6 T-joint fatigue life using vibration fatigue technique

Once structural stress PSD at weld toe is calculated, fatigue life can be calculated using vibration fatigue technique discussed in Section 3.5. To help in the calculation process Design Life [50] fatigue software was used in this research. In this software series of calculation procedures that are important for fatigue calculations are grouped and automated in form of glyphs. The process flow used for obtaining fatigue life from structural stress PSD is shown in Fig 5.12.

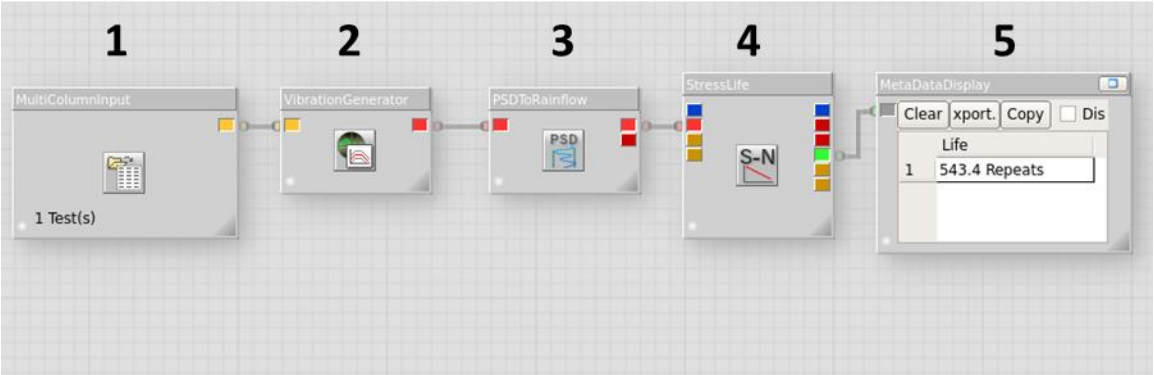

Fig 5.12 Process flow for analyzing vibration fatigue

Structural stress PSD calculated from Section 5.1.2 is stored in a coma separated values (CSV) file format. The first glyph is the input glyph it reads the CSV file and sends it to the second glyph called vibration generator, where the input is converted into a PSD histogram. The next glyph is the PSD to rainflow glyph, most of the important calculation procedures like calculating spectral moments, calculating stress PDF and finally calculating stress histogram are accomplished in this glyph. Stress PDF in this glyph can be calculated using any of the four process namely Narrow band process, Steinberg, Lalanne and Dirlik method. In the fourth stress life glyph damage and fatigue life is calculated using the stress histogram and fatigue properties of weld from Table 2.1.

Using this procedure fatigue life of T-joint is calculated for the two PSD load cases. The calculated mean life using all four methods is shown in the table 5.3.

Load case	Mean Life from Vibration fatigue analysis (Repeats)			
	Narrow Band	Steinberg	Lalanne	Dirlik
1	409	346	518	543
2	397	332	447	478

Table 5.3 Fatigue life proposed method

As expected Narrow band and Steinberg solution is giving conservative life estimates in comparison to Lalanne and Dirlik methods.

5.1.7 Fatigue life of T-joint using transient dynamic analysis

In order to conduct transient analysis, the first two displacement PSD's are converted to time domain. PSD is converted to time domain using inverse Fourier transform and random phase angles [48]. The process flow for this transform is shown in Fig 5.13.

Glyph 1 is the input PSD displacement histogram. This PSD signal is transformed to time signal using glyph 2 TS generator and glyph 3 custom Fourier. All the calculation procedure like inverse Fourier transform and adding the random phase angle is achieved using these two glyphs. The output is the displacement in time domain and is plotted using XY display glyph 4.

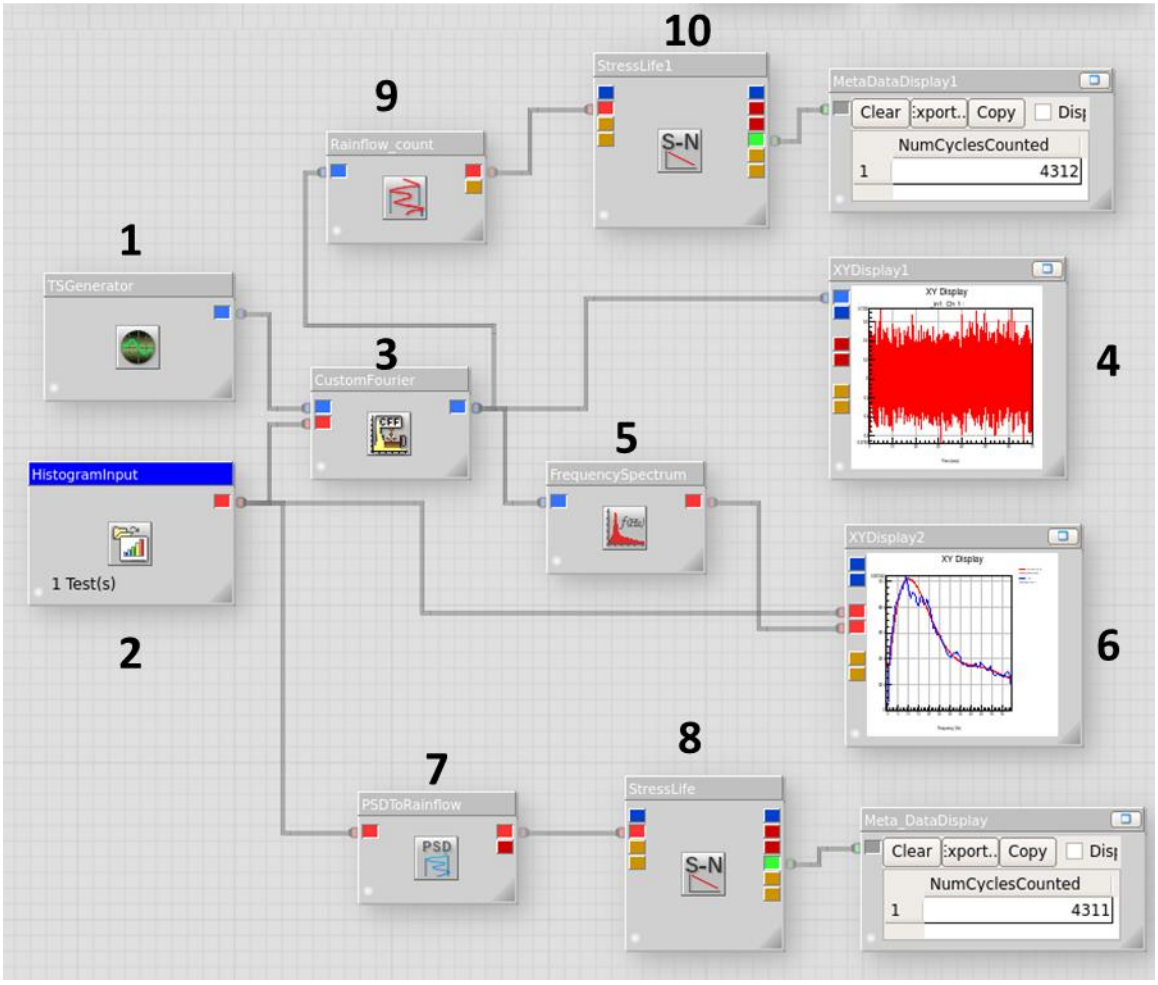

Fig 5.13 Process flow PSD to time series.

To verify the accuracy of the transformation process two checks are made. First the output time signal from custom Fourier glyph 3 is transformed back to PSD signal using glyph 5, this PSD is plotted over the original PSD from the input glyph 1 using glyph 6. If they match closer to each other the transformation process is said to be accurate.

The second important check is done by comparing the damage levels between the two signals. Using the same procedure discussed in Section 5.1.3, cycles to failure is calculated for the input PSD signal, using glyph 7 and 8. Next cycles to failure is calculated for the calculated time series signal using glyph 9 rainflow count and glyph 10 stresslife cy-

cle. If the cycles to failure match for both the signal, it implies the damage content of the original PSD signal is preserved.

Using this process the displacement time signal is generated for PSD1 and PSD2 using a sampling rate of 800 per sec. The process flow shown in Fig 5.13., already contain the result for PSD1 transformation. As we can see it passes both the checks, both PSD signals compare well as shown in glyph 6. Cycles to failure for both the input PSD signal and the transformed time signal matches very closely confirming the accuracy of the transformation process. The transformed time signal for PSD1 is shown in Fig 5.14. Similarly the PSD 2 is transformed and accuracy is verified.

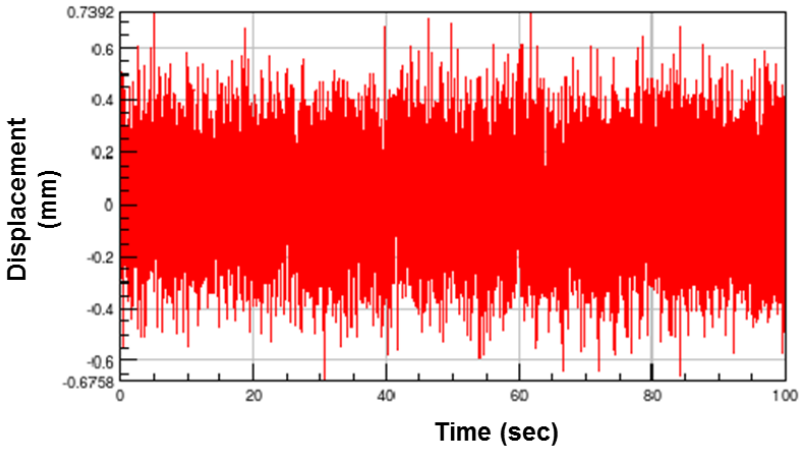

Fig 5.14 Load case1 displacement time series

Using this time history signal a mode based transient dynamic analysis is conducted on the T-joint. In order to capture all the peaks a time step of .001 sec is used for this analysis. Nodal force and nodal moment response at ten nodes discussed in section 5.1.3 is obtained as a discrete time series data. Line force and line moments are calculated at all these discrete points. Membrane stress and bending stress are then calculated based on the line force and line moments. Summing the membrane stress and bending stress at

each data point yields structural stress time history directly. This method is straight forward, but the computation time is very high. Time it took to run the simulation for 100 sec data using 2 CPU and 32 GB ram is tabulated in the table 5.4. As we can see there is massive difference in run times required for the simulation.

Load case	Run time (Hours)	
	PSD-response	Transient analysis
1	3.8	44.5
2	3.57	47.2

Table 5.4 Analysis run times

In order to compare the fatigue life against the proposed method, structural stress in time domain signal is converted to stress PSD using glyph2 which is frequency spectrum glyph. Once the structural stress is transformed to PSD glyph, the process flow shown in Fig 5.11 is same as the one discussed in section 5.1.3.

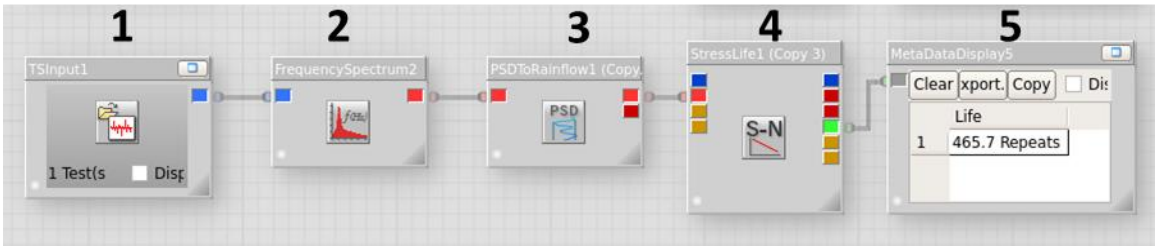

Fig 5.15 Process flow for fatigue analysis based on transient analysis

Using this process flow fatigue analysis is calculated using the four methods similar to Section 5.1.3. The results are shown in Table 5.5

Load case	Mean Life from Transient Analysis (Repeats)			
	Narrow Band	Steinberg	Lalanne	Dirlik
1	455	385	461	465
2	426	360	433	438

Table 5.5 Fatigue life predicted by different methods

The following conclusions can be derived based on the analysis in this section.

1. Fatigue life estimated based on the proposed method and the fatigue life calculated using the structural stress from transient analysis compare closely. This validates the proposed method.
2. Fatigue life obtained from Narrow band and Steinberg solution is conservative in comparison to Lalanne and Dirlik as expected. Since the Narrow band process assumes every peak has a valley which will result in conservative results as discussed in section 3.5.1. Steinberg solution is an extension of narrowband process (section 3.5.2), this will also yield conservative results.
3. Based on the analysis run times PSD based method is much faster. For this model the time required for transient dynamic analysis was almost 12 times compared to the PSD analysis. For larger models it would not be feasible to conduct the transient dynamic analysis.

5.2 Geometry based weld fatigue improvement technique

Most of the structural member in a tubular welded assembly can be simplified into a fixed beam or a cantilever beam model. T-Joint in this study can be simplified into a cantilever beam model. From the previous analysis the higher stresses are noticed at the welded joint which is located at the fixed end of the beam assembly. There are two main reasons for this behaviour. The first reason is, it is a cantilever beam as we can see from the bending moment diagram shown in Fig 5.16 maximum moment occurs at the fixed end of the beam which causes higher bending stress at the fixed end. The second reason for the increase in stress is caused by the stress concentration due to the macro geometry of the T-joint construction and stress concentration due to the micro geometry of the welds. The same principle also applies to the fixed beams where the bending moments are higher towards the fixed ends.

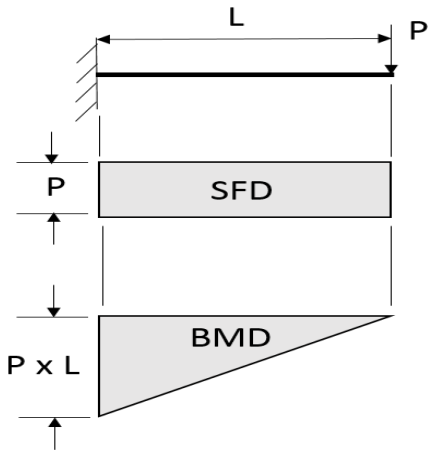

Fig 5.16 Shear force and bending moment diagram of cantilever beam

The higher stress close to the fixed ends can be reduced by increasing the section modulus of the beam. Section modulus of the rectangular tube can be altered by changing the thickness of tube or by changing the width and height of the tube. A correctly designed gusset can increase the section modulus closer to the fixed ends which will reduce the bending stress locally. In this study, the effects of changes in thickness and gusset geometry on fatigue life is analysed.

5.2.1 Effect of thickness changes

Thickness of the rectangular tube in the T-joint is changed and the structural stress at the welded joint is calculated using the procedure discussed in section 2.5. Initial reference thickness of 2mm is used for the study in the previous sections. Three more thicknesses of 3mm, 4mm and 5mm is used for this study. Structural stress distribution along the path shown in Fig 5.3 is calculated and plotted in Fig 5.17 below.

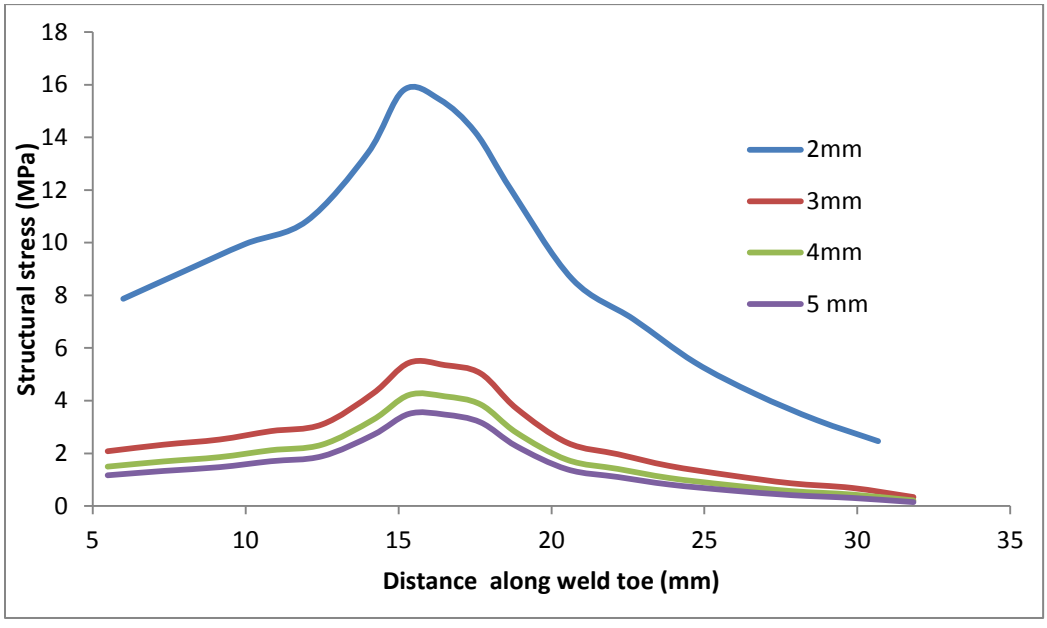

Fig 5.17 Structural stress for different tube thicknesses

From Eq. (2.9) there are two components in structural stress calculation, the first component is the membrane stress which changes linearly with change in thickness. The second component is the bending stress where the change is in the order of Inverse Square of thickness. To understand the effect of thickness change a graph is plotted with thickness along X-axis and inverse of thickness squared along Y-axis and shown in Fig 5.18. As we can see from the graph at lower thickness the value of 1/t^2 rapidly reduces with increase in thickness and at higher thickness the change is minimal. This is the main reason why the structural stress reduces rapidly between thicknesses 2mm and 3mm and only minimal changes between thicknesses 4mm and 5mm.

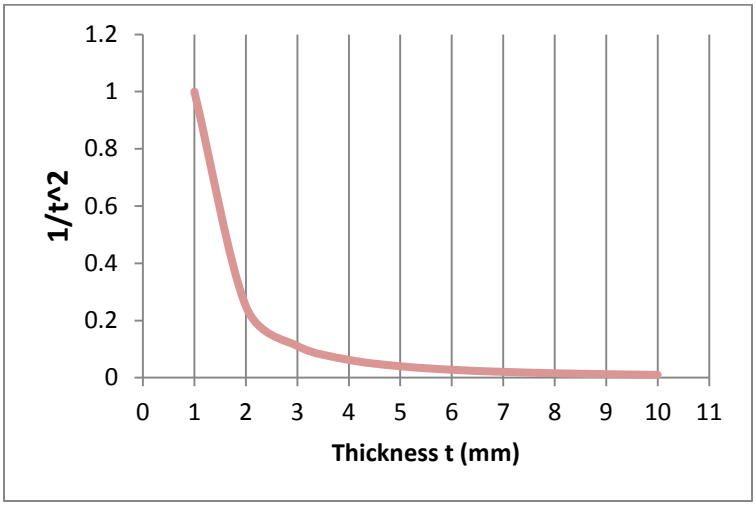

Fig 5.18 Plot of function 1/t^2

To understand the change in dynamic characteristics due to thickness change, a modal analysis is conducted on the models and the natural frequencies are reported in the Table 5.6. Due to the increase in thickness, the natural frequencies change. By changing the frequencies, a structure can be designed to operate outside resonant frequencies there by reducing the damage significantly.

Frequency (Hz)				
Mode No.	Thickness			
	2 mm	3 mm	4 mm	5 mm
1	17.3	20	21.8	23
2	20.6	23.9	26.1	27.7
3	352	342	332	323
4	417	405	395	385

Table 5.6 Effect of thickness change on natural frequency

In order to calculate the harmonic scale and to find the dominant modes that participate in the analysis a mode based harmonic response analysis is conducted on the models using the same method discussed in section 5.1.4. To understand the operating deflection shape, generalised displacement or scalar multiplier is plotted for different models and shown in Fig 5.19.

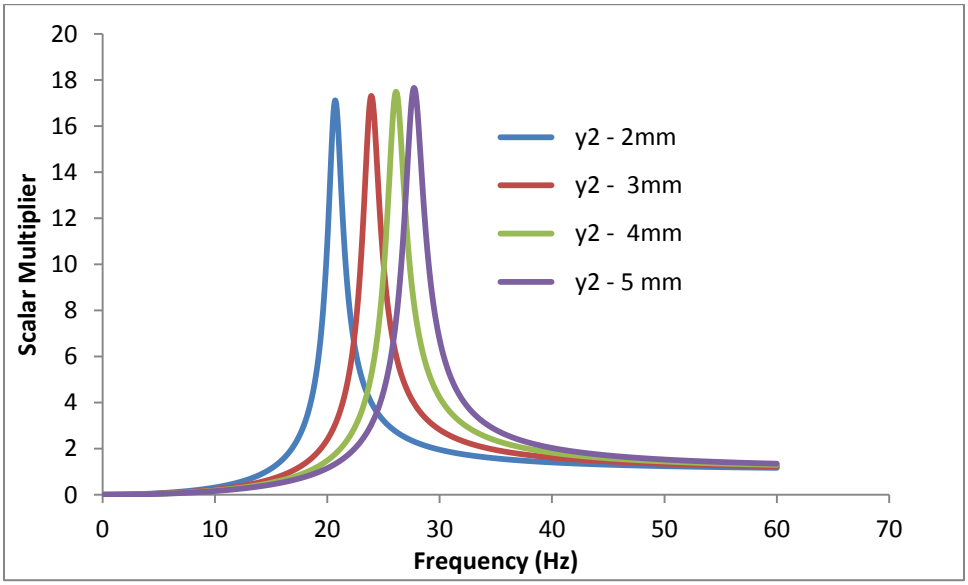

Fig 5.19 Generalised displacement of the T-Joint for different thicknesses

Similar to the previous study with 2mm thick tube, only mode 2 participates in the analysis due to the same reason discussed in section 5.1.4. The only change noticed due to the

increase in thickness, is the shift in natural frequencies. Since the road operating frequencies are from 0-60 Hz (section 4.5.5), the shift in natural frequency due to thickness change could not avoid resonance in this model.

Since only mode 2 participates in the operating deflection shape, harmonic scale is same for all four models. In the later section, fatigue life is calculated for these models using the PSD load and compared.

5.2.2 Effect of Gusset geometry

Traditionally gussets are added locally to stiffen the joints. Even though they are commonly used, only a few literatures are available on the shape of the gussets and its application. In this study, gussets with different shapes are numerically analysed and its effects on fatigue life of welded joints are explored.

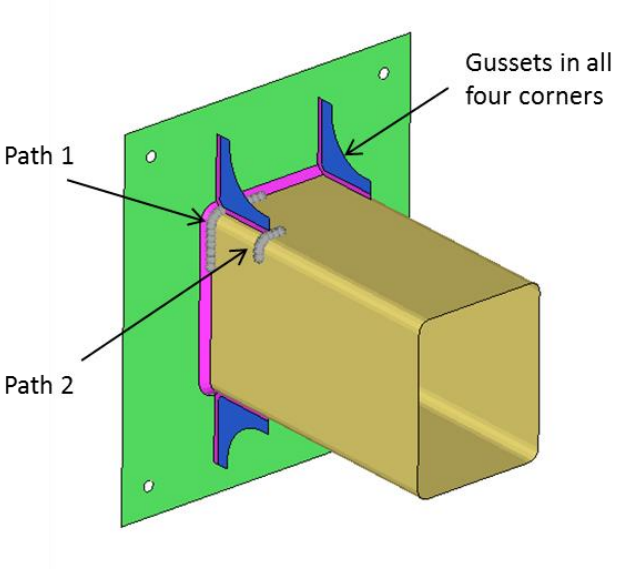

Fig 5.20 T-Joint geometry with gussets

Gussets are added to the four corners of the T-joint as shown in Fig 5.20. Similar to the thickness effects study, a static analysis is conducted on the model using four different gusset geometries as shown in Fig 5.21.

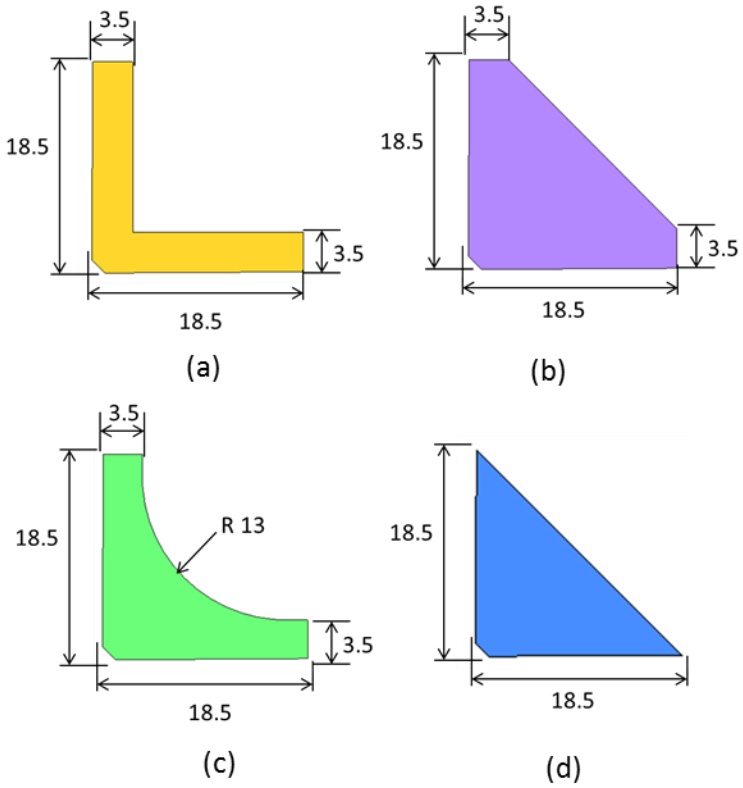

Fig 5.21 Gusset geometries (a) Gusset 1 (b) Gusset 2 (c) Gusset 3 (d) Gusset 4

Results are reported along path 1 and path 2 as shown in Fig 5.20. Path 1 captures the high stresses at the corner of the tube. Fatigue failures in welded joints often occurs at start and stop of the welds. In this model weld starts at the ends of the gussets, by E^2S^2 method at these locations structural stress has to be calculated normal to the welds. This is the reason for reporting structural stress along path 2.

As we can see from the graph shown in Fig 5.22, structural stress is reduced significantly due to the addition of gussets along path1. But higher stresses are observed along path 2 shown in Fig 5.23, where the weld starts. Still the structural stress with the gussets is lesser than the model without gusset.

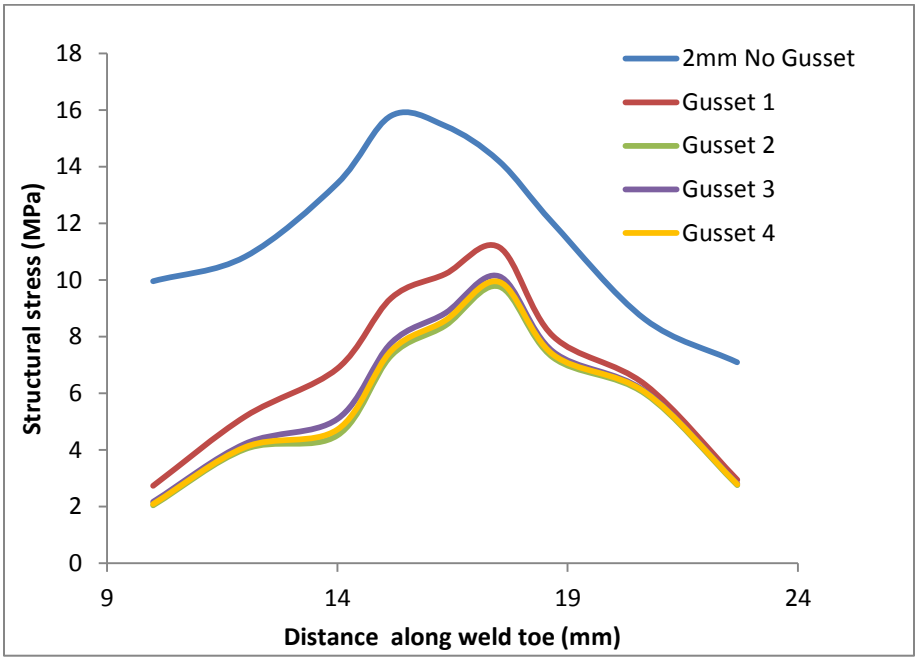

Fig 5.22 Variation of structural stress along path 1 - different gussets

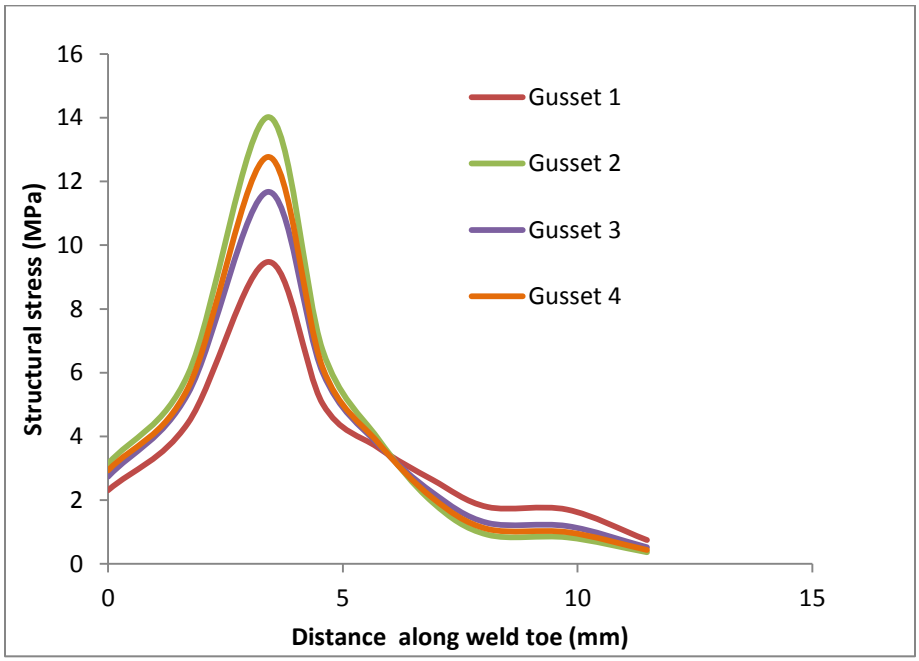

Fig 5.23 Variation of structural stress along path 2 - different gussets

By comparing structural stress along path2, gusset 1 performs better but the stress along path 1 and on the gusset itself is relatively high. This study is a comparative study where relatively lower load is used, but for higher loads the stress concentration on gusset1 will be problematic.

Structural stress distribution of models with gussets 2 and 4 along path 2, are relatively higher than the model with gusset 3. Hence the model with gusset 3 is preferred over the other models. Literature [70]also suggests this shape as a better choice for welded applications.

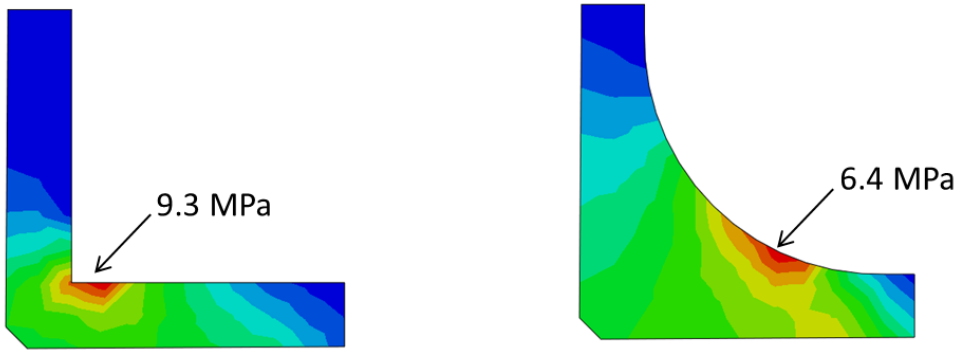

Fig 5.24 Maximum stress on gusset 1, gusset 3

In order to further improve the shape of gusset 3, shape optimisation is conducted using a commercially available FEA optimisation solver called Optistruct [71]. This software has multiple optimisation capabilities like topology, topography, shape, size …etc. For this study a mesh based shape optimisation technique is used and the finite element mesh is morphed to generate design variables. For this study four design variables shown in Fig 5.25 (a, b, c and d) are selected. Since structural stress cannot be directly calculated without post processing the results, nodal stress around the welds which are linearly related to structural stress are used as constraints for this optimisation study. The objective was set to reduce the mass of the gusset. Stress constraint was slowly adjusted and a maximum of 12.5 % reduction in stress is achieved. When the constrained was further increased the solution fails to converge.

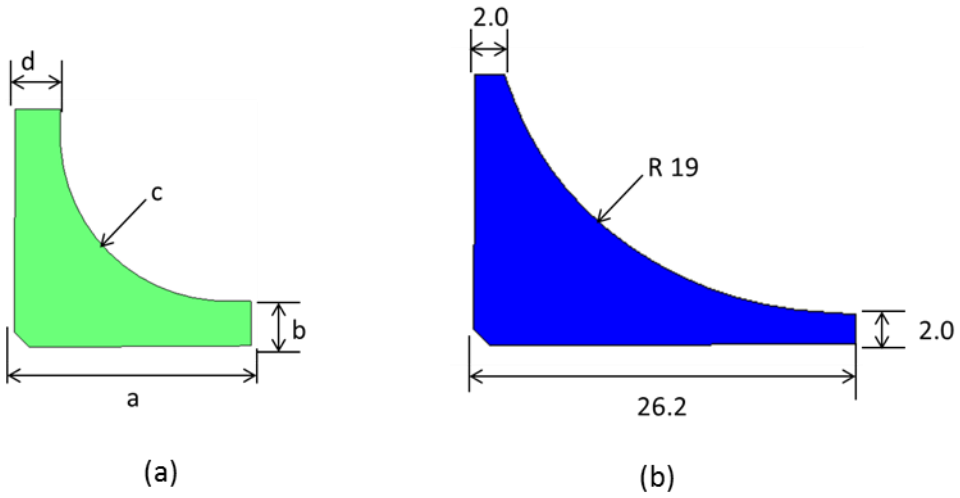

Fig 5.25 (a) Design variables for optimisation (b) Optimised gusset geometry

The optimised shape is shown in Fig 5.25 (b) and when compared to the original gusset geometry design variables a, c are increased and variables b, d are reduced.

In order to calculate the structural stress on the new optimised design static analysis is re-peated and structural stress is plotted along path1 and path2 and shown in Fig 5.26 and 5.27. As we can see from the graph structural stress is reduced by around 12% in both these locations.

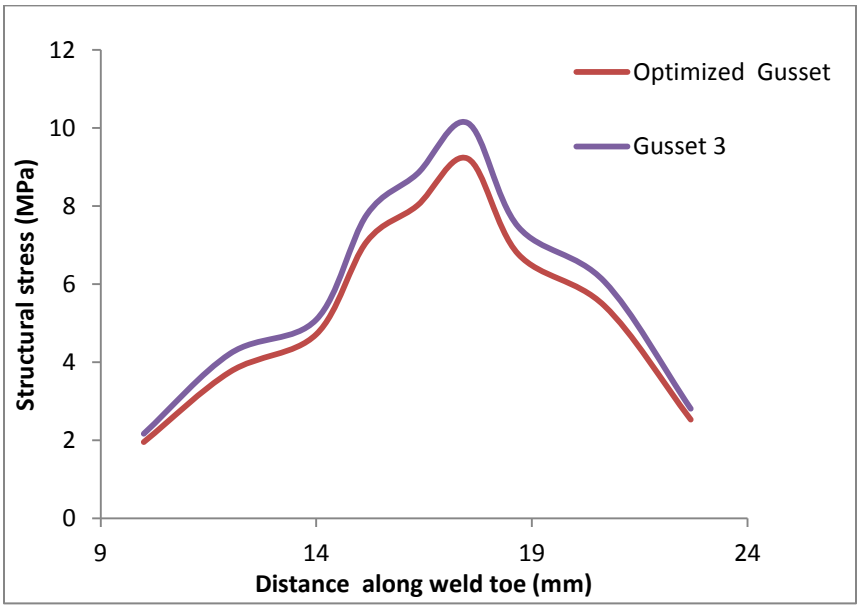

Fig 5.26 Variation of structural stress along path 1 – gusset 3 and optimised gusset

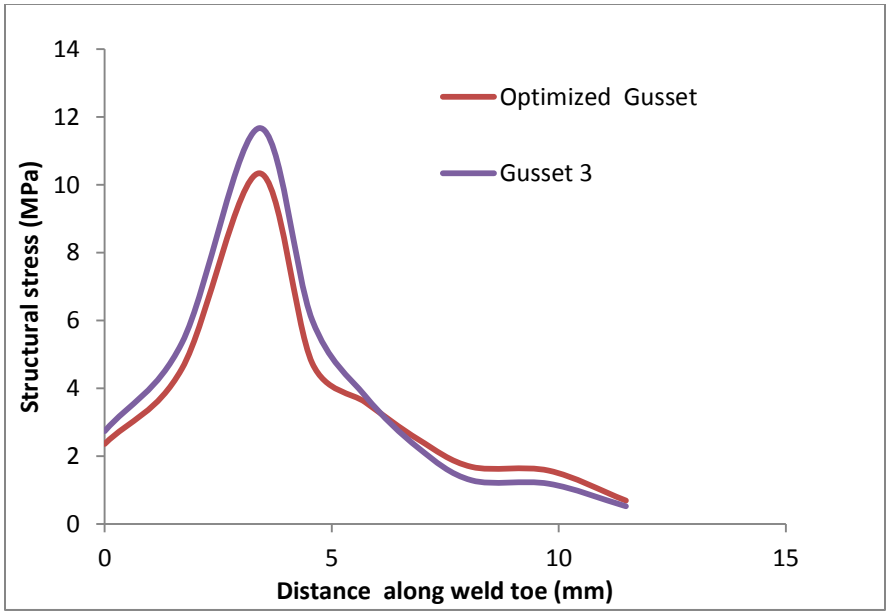

Fig 5.27 Variation of structural stress along path 2 – gusset 3 and optimised gusset

5.2.3 Effect of Geometry changes on fatigue life

In the previous section, effects of structural stress due to geometry changes were analysed. In this section, effects of fatigue life on geometric changes due to random loads are explored. For this study three models are used, 3 mm thick tube, 4 mm thick tube and 2 mm thick tube with optimised gusset. These models are randomly loaded using the white noise PSD shown in Fig 5.9 (b). This PSD is selected since the load is constant across all frequencies. This eliminates the chance of fatigue life variations due to natural frequency shift, which makes the comparison between different models easier.

Using the proposed method, structural stress PSD for all these models are calculated and plotted in Fig 5.28 along with the 2 mm thick baseline model. As we can see from the graph, there is a major reduction in PSD due to thickness change from 2 mm to 3 mm thick tube. But the change in PSD between 3 mm and 4 mm model is minimal which is following the similar trend as the structural stress from the static analysis discussed previously. PSD is reduced between 2 mm tube without gusset and the model with optimised gusset, but the reduction is not as significant compared to the thickness change from 2 mm to 3 mm.

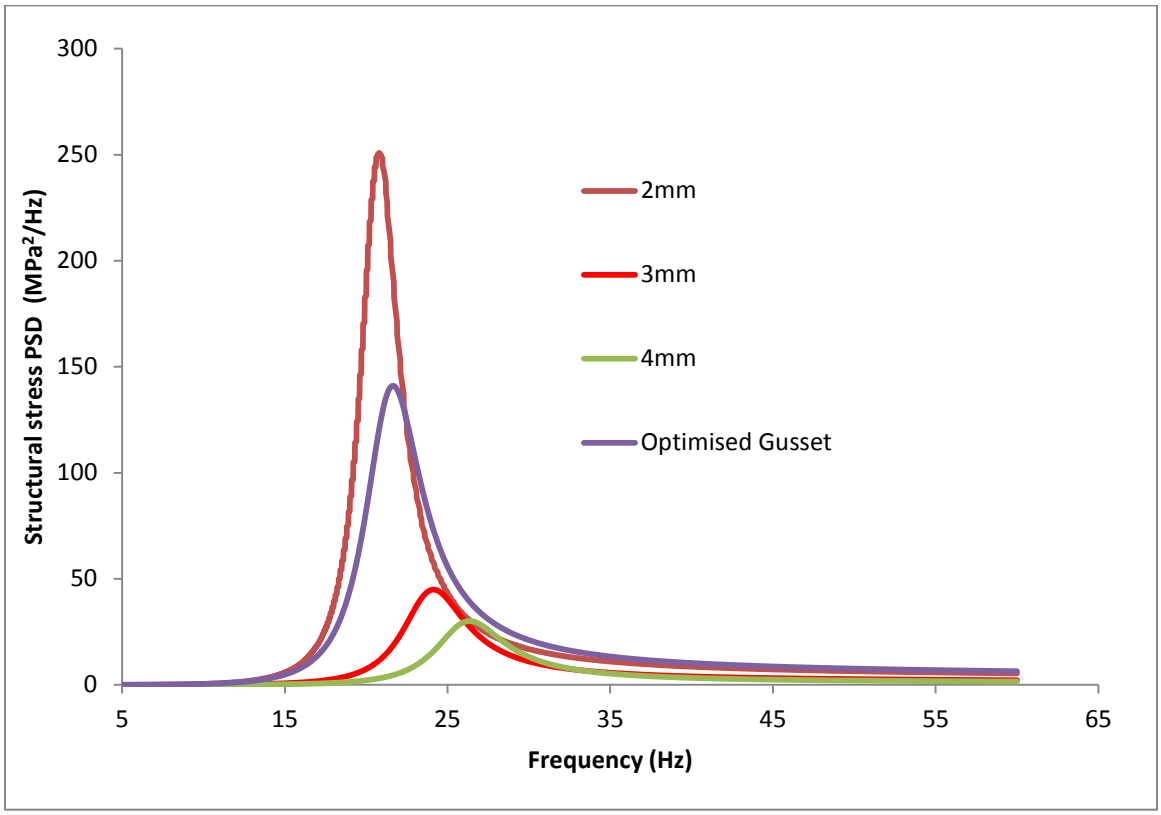

Fig 5.28 Variation of structural stress PSD

Using these structural stress PSD's mean fatigue life are estimated using the same procedure discussed in section 5.1.6. Results are shown in Table 5.7 along with the respective masses. Fatigue life also follows the same trend, with thickness reduction fatigue life increases significantly. The optimised gusset design increases the fatigue life almost 2.5 times in comparison to the baseline design.

When weight is compared there is a significant increase with increase in thickness. But weight increase is very minimal with the addition of gussets to the baseline model.

Variations	Mean fatigue life Dirlik's Method (Repeats)	Mass of the assembly (kg)	% of weight increase
2mm Tube	543	2.6	
2mm Tube with optimized gusset	1360	3.5	2%
3mm Tube	3538	4.4	34%
4mm Tube	5685	2.65	69%

Table 5.7 Estimated mean fatigue lives

The following conclusions can be derived based on the analysis in this section.

1. Based on the study it is found that, for bending dominant tubular welded joint problems structural stress is very sensitive to thickness changes, more specifically at lower thickness ranges. But the change in structural stress at higher thickness is not as significant as the lower thickness ranges. The main reason for this behaviour is bending part of the structural stress is inversely proportional to the square of thickness.
2. Addition of gusset closer to the fixed end tends to reduce the structural stress. Among the different gusset shapes study, gusset 3 which is an L-shaped plate with a fillet performed better with respect to stress reduction.
3. To further improve the geometry of the gusset 3, shape optimisation is performed on the model. The optimised design reduced the structural stress further by another 12 %. Gusset 3 provides a better profile for stress reduction, but it can be further improved depending on the space availability using shape optimisation.

4. Effects of fatigue life on the geometric changes are explored. It is observed that the fatigue life is significantly increased by increasing the thickness of the tube. The downside of increasing the thickness is that, it adds significant weight to the structure which is a big drawback for vehicle design.
5. The addition of gusset increases the fatigue life but not as substantial as the thickness change. The biggest advantage of adding gussets is that, it only accounts for a very little increase in weight.
6. Depending on the design requirements, it's a trade-off between thickness alterations and addition of gussets to the structure, in order to improve the fatigue life.

5.3 Fatigue evaluation of rack assembly

The objective of the thesis is to develop a method to validate the fatigue life of a bus welded rack assembly under random loading. During road test [2] accelerometers were installed at different locations of a bus structure, to measure the acceleration time history at each location. In order to obtain loading for rack fatigue analysis, an accelerometer can be installed at the base where the rack connects to the vehicle structure. In order to apply analyse the rack assembly base displacement time history is required. Acceleration measured from the road test has to be converted to displacement time history.

The base acceleration cannot be directly integrated twice to obtain base displacement, because this time integration amplifies the low frequency components and the errors present in the signal [72]. High pass filters can be used to remove the errors without compromis-

ing on the crucial information from the signal, it is an iterative and experience based method. There are other available methods like adding higher order polynomials to remove drift from the signal [72].

Base displacement time history can also be obtained using multi body dynamic simulation [73, 74] on whole vehicle over the virtual test tracks. Both removing the drift from the signal and multi body dynamics are vast topic and couldn't be covered within the scope of this thesis. However one of these techniques can be employed to obtain base displacement time histories. For this study base displacement PSD1 form Section 5.1.2 is used as the loading for the rack.

A commonly used rack configuration is selected for this thesis. The rack in study consists of four hollow rectangular tubes joined in T-joint configuration as shown in the Fig 5.29. The rack is designed to carry 250lb load bolted to the rack at three mounting location. ASTM A500 material with the following material properties including Young's modulus 30e6 PSI and Poisson's ratio 0.3 were used for the rack.

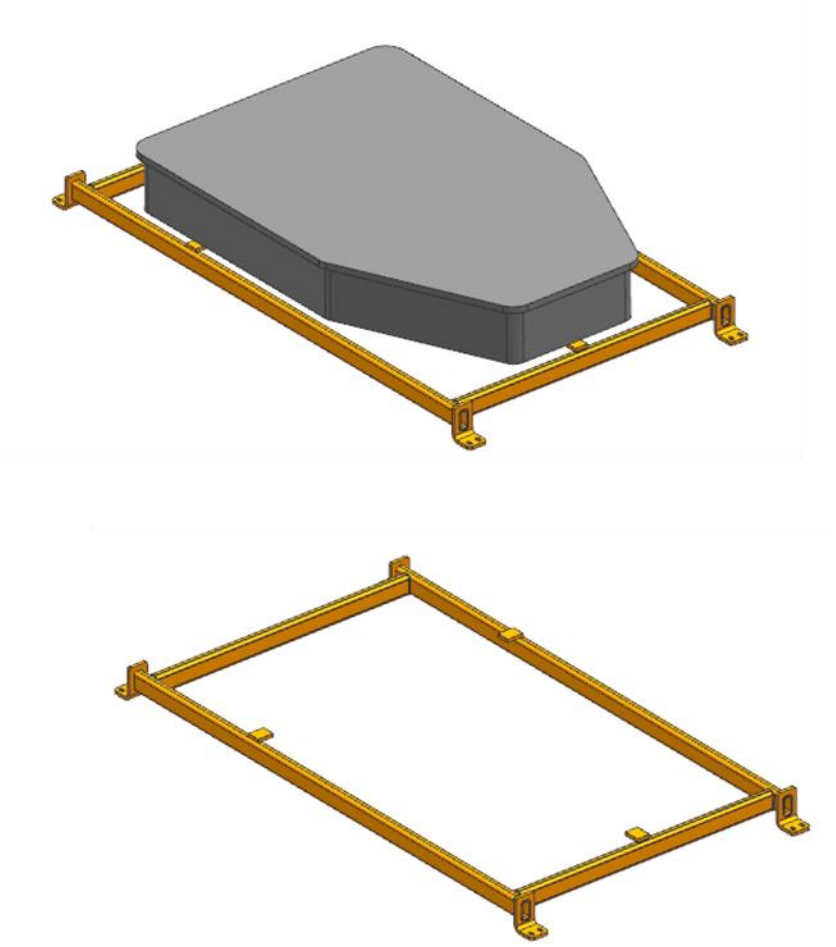

Fig 5.29 CAD Geometry of welded rack assembly

Finite Element Model of the rack is developed using Hypermesh [41] pre-processing software. The joint where higher stress is expected is modelled using four node shell elements and welds modelled using shell elements by following the guidelines described in Section 2.4. The remaining portion of the rack is modelled using two node linear beam elements. The 250lb mass is attached to the three mounting location using rigid links.

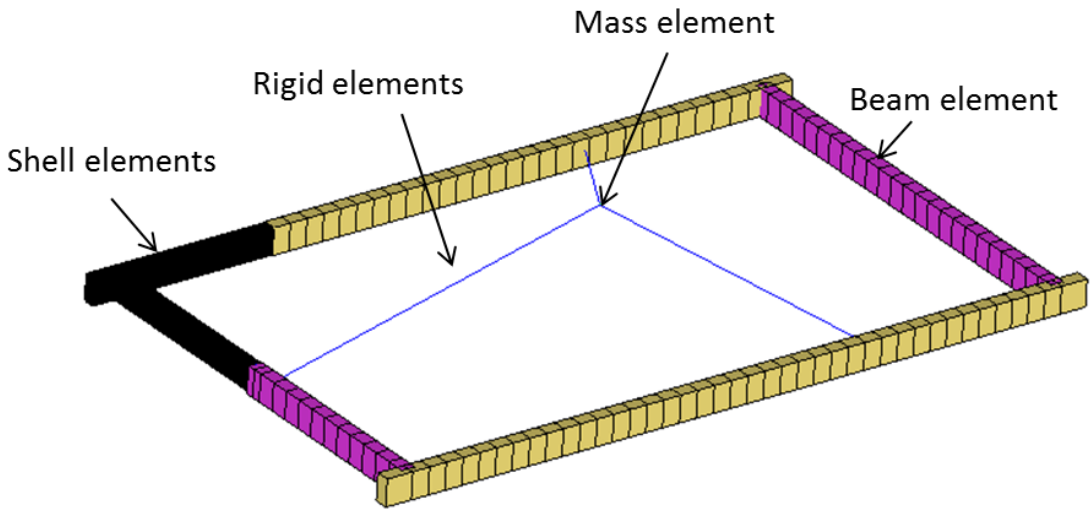

Fig 5.30 Finite element model of the Rack

In order to locate the node with the highest stress a static analysis is conducted on the model with gravity as load. As expected similar to previous analysis, the corner of the tube experiences maximum stress as shown in Fig 5.31.

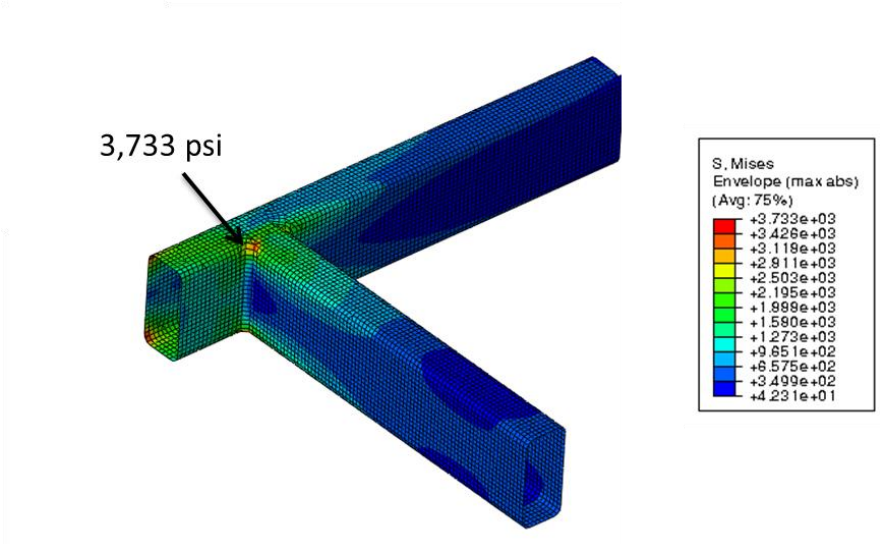

Fig 5.31 Von mises stress distribution of the rack

Structural stress is calculated along the weld toe shown in Fig 5.32 using the VBA-Excel tool from Section 2.4. The plot of stress over the distance along the weld toe is shown in Fig 5.33. The joint experiences the maximum structural stress near the top corner at node 105.

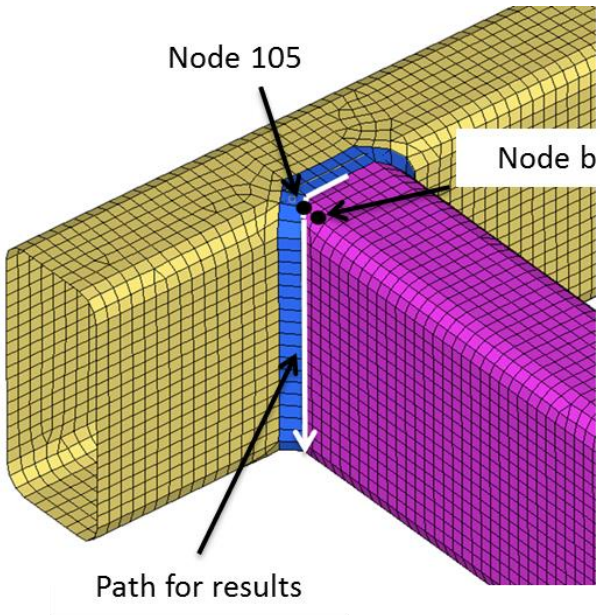

Fig 5.32 Path for stress results and critical node reference of the rack

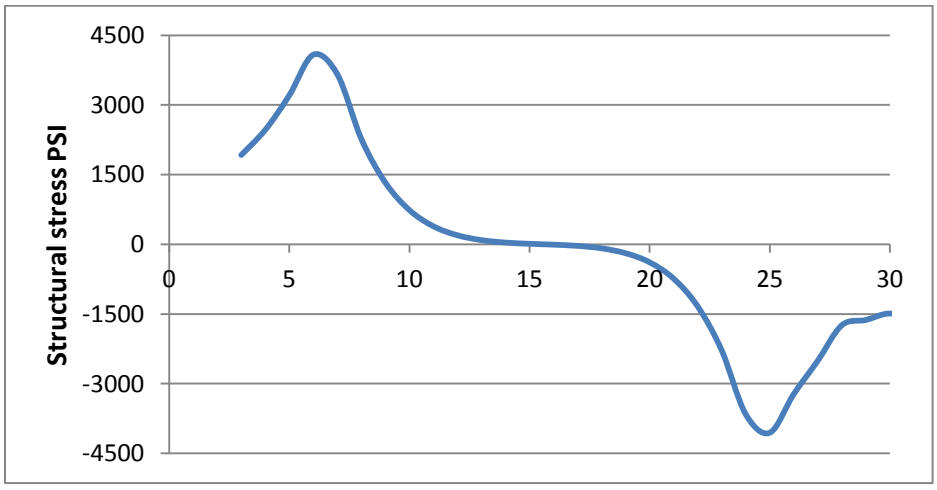

Fig 5.33 Structural stress along the weld toe

A modal analysis is conducted on the rack to understand its natural frequencies. Natural frequencies are listed in the Table 5.8.

As the loading is from 0-60Hz based on PSD1 shown in Section 5.1.2 only Mode-1 is going to participate in the operating deflection shape of the structure. The operating frequency of 0-60 Hz is selected since it was the frequency measured during the road operating test [2].

Mode	Frequency (Hz)
1	51.2
2	80.5
3	83.47
4	88
5	125.24

Table 5.8 Natural frequencies of the rack assembly

Next the proposed method is applied to the rack model. To calculate the harmonic scale for the proposed method, a harmonic analysis is conducted on the model using unit (1 mm) base displacement in Z-direction as discussed in Section 4.4. Based on static analysis, structural stress is maximum at node 105. Minimum life is expected at node 105. Harmonic scale is calculated between 105 and its adjacent node b shown in Fig 4.29.

Next the model is subjected to base displacement PSD using PSD1 from Section 5.1.2. As per proposed method, normal stress PSD at adjacent Node b is obtained from the PSD dynamic analysis.

Using the PSD scale calculated using harmonic scale, structural stress PSD at Node 105 is calculated. The response is shown in Fig 5.34.

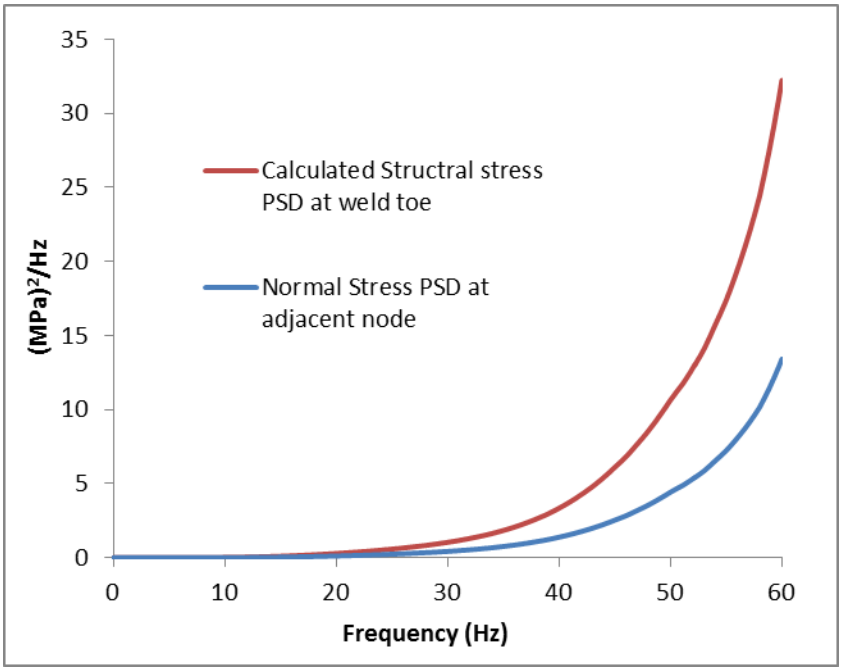

Fig 5.34 Rack PSD stress response

Using this response structural stress PSD life of the joint is calculated using the design life work flow process shown in Fig 5.12 discussed in section 5.1.6. The mean estimated life of the rack calculated by Dirlik's method is 14,220 repeats.

Load Case	Mean Life
1	14,220 repeats

Table 5.9 Estimated fatigue life of rack using proposed method

Chapter 6

Concluding remarks and Future work

Fatigue failure of the welded joints is one of the major structural problems faced by bus manufacturers. A computational model is proposed in this study which combines the E^2S^2 method for weld fatigue and PSD based analysis for random vibration.

First E^2S^2 weld fatigue computational method was studied in detail. Two models from literature was recreated and the understanding of the method was verified using these models.

In PSD based analysis the phase information of the response signal is lost. This makes it challenging to adopt E^2S^2 method with PSD based fatigue analysis. This challenge was overcome in the proposed method by two types of scale namely harmonic scale and PSD scale. Based on the study it is found both the scales are a function of excitation frequency. A Finite Element based cantilever beam analysis was conducted and harmonic scale and PSD scale where calculated. The results clearly showed the variation of scales over the excitation frequency. An analytical relationship was derived between the two scales,

PSD scale was found to be the square of harmonic scale. This relationship was verified by the cantilever beam FE model.

T-joint is one of the commonly used, weld joint configurations in a bus structure. Fatigue life of one of the T-joint is calculated using the proposed method, which is based on vibration fatigue technique.

To verify the proposed method a transient dynamic analysis is conducted on the T-joint using a base displacement time signal obtained by transforming the base displacement PSD signal. The time required to run this transient dynamic analysis was almost 12 times higher in comparison with the PSD analysis.

The structural stress was directly calculated in the transient analysis, since both amplitude and phase information is preserved in this analysis. Using this structural stress fatigue life was calculated using time domain fatigue technique.

Life estimated from the transient analysis and the proposed methods were compared and they were closer, this verifies the proposed method to validate T-joint. Using this proposed method a welded rack assembly was analysed and fatigue life is calculated.

The effect of geometry changes on fatigue life is studied. It is found that fatigue life increases significantly with the increase in thickness of the tube. The change in fatigue life is very high due to thickness increase in lower thickness ranges compared to higher thickness ranges. It is mainly due to the fact that the bending part of the structural stress is inversely proportional to the square of thickness. The major drawback of increasing tube thickness is the addition of considerable weight to the structure.

Adding gussets to the joints reduces the structural stress at the welded joints, thereby increasing the fatigue life. Among the different gusset shapes studied, L-shaped gusset with a fillet proves to be a better geometry. An optimisation study is conducted on the gusset geometry and the optimised gusset reduces the structural stress by another 12 %. The main advantages of adding gussets is that, it increases the fatigue life at the cost of very little weight addition to the structure.

Depending on the design requirements to improve the fatigue life and considering weight as one of the important attribute to the vehicle structure, one of the suggested geometry changes can be adopted.

6.1 Limitations of the current study

- The proposed method is only suited for loads with zero mean, since it is one of the basic requirement for PSD based dynamic analysis.
- In the current study only unidirectional random loads are considered. The idea is to calculate fatigue damage individually for each direction and finally sum up the damages to calculate the overall damage of the structure. However PSD based analysis does not consider the load sequencing effects.
- This study only considers the effect of single random excitation. But when the structure is larger and excited by multiple loads, cross correlation between the loads has to be evaluated. It might have significant effect on stress calculations.

- In the present study the proposed method was validated only using another computational model (transient dynamic analysis). No physical test is conducted yet to validate the proposed method.

6.2 Future work

To minimize some of the limitations discussed in the previous section, the following work can be conducted in the future to validate and improve the current method.

- Major drawback of using PSD based analysis for fatigue life calculations is that, the mean of the input signal is considered to be zero. But in a vehicle structure, gravity load is always present which acts as the mean load on the structure. The proposed method in the current state cannot handle this mean load, however it can be slightly modified to accommodate for the mean correction. In order to do so, first a static analysis can be conducted on the model in study, using gravity as load. The stress measured at the critical location is the mean stress of the model. Then using the proposed method, stress histogram at the critical location can be calculated. This stress histogram can be corrected with the calculated mean stress. Using Goodman or Gerber equations and S-N curve fatigue life can be estimated. Using this process, the mean stress generated due to gravity loads can be accounted in the proposed method.
- In order to apply this proposed method to vehicle application, it is important to obtain a proper load data. Ideally, acceleration in the time domain can be meas-

ured at a given location on a test vehicle. But acceleration cannot be directly used in the simulation, since double integration to get displacements will cause significant drift in the signal as discussed in the section 5.3. Another major challenge is that, multiple tests have to be conducted on the test vehicle in order to collect a reasonable acceleration time signal, which is quite expensive. To overcome these challenges, a numerical model of the full vehicle can be developed using multi-body dynamics [73] tools and can be calibrated to the test data. From this model, load displacement time histories can be calculated at any location on the vehicle model. Using the displacement time history, displacement PSD can be calculated using ncode design life [50] . From this method, PSD displacement can be obtained which is free from the drift, discussed earlier.

- The proposed method is applicable to welded assemblies subjected to unidirectional random loads. It can be only applied to welded sub-structures which has larger mass. But to apply the proposed method to larger applications like full vehicle, it has to be improved. There are four random excitation sources at the four wheels. These excitations may be related to each other or may be completely independent of each other. A PSD signal contains only the amplitude information of the signal. Without phase information, relating two load signals will be challenging. To overcome this, cross-correlation matrix can be introduced which relates any PSD signals. Using the PSD signal and cross- correlation matrix larger structures can be analyzed and fatigue life can be calculated using the proposed method. Further study is required to validate this process.

- Both the T-joint and the rack can be manufactured and tested using a single axis or a multiple axis shaker tables by applying the PSD displacements used in the current study. If the fatigue life compares closely proposed computational model is validated again and it improves the confidence level further.
- A FEA post-processor can be developed to automate all the calculation procedures in the proposed method, using TCL/TK programming tools in HyperView [41] post-processor or Python scripting language in Abaqus [45] post-processor. This will speed up the fatigue life calculation process. This will also help in setting up the constraints directly for running optimisation problems.
- Effect of thickness change on structural stress is studied in this research. The reason for large stress reduction in lower thickness ranges compared to higher thickness ranges is analytically proven. In order to verify this, a simple physical test can be conducted on the T-joint. Since, structural stress is linear with the applied load it will also be linear with respect to stress measured at any location closer to the welds. A strain gauge can be installed on a test specimen with different thicknesses and statically loaded. If the measured stress shows similar behaviour it verifies the numerical study.

Bibliography

[1] "Standard Bus Procurement Guidelines," APTA (American Public Transit Association) .www.apta.com.

[2] "Road Operating test of a New Flyer 40 ft Xcelsior Bus," New flyer Industries Internal test report.

[3] O. Doerk, W. Fricke and C. Weissenborn, "Comparison of different calculation methods for structural stresses at welded joints," *International journal of fatigue*, vol. 25, no. 5, pp. 359-369, 2003.

[4] "Design of steel structures—Part 1-9 Fatigue, British standards.," European Committee for Standardisation, 2005.

[5] "Code of practice for Fatigue Design and assessment of steel structure BS

7608:1993," British Standard, 1993.

[6] P.Dong, "A robust structural stress method for fatigue analysis of ship structures," in *ASME 22nd International Conference on Offshore Mechanics and Arctic Engineerin*, 2003.

[7] T. Partanen and E. Niemi, "Hot Spot stress approach to fatigue strength analysis of welded components: Fatigue test data for steel plate thickness up to 10mm. Fatigue Fract. Engng Mater.Struct. Vol.19,No. 6,pp. 709-722,1996.," *Fatigue & Fracture of Engineering Materials & Structures,* vol. 19, no. 6, pp. 709-722, 1996.

[8] D. Radaj, C. Sonsino and W. Fricke, Fatigue assessment of welded joints by local approaches. 2nd ed., Woodhead Publishing, 2006.

[9] P. Dong, M. Prager and D. Osage, "The Design master S-N curve in ASME Div 2 rewrite and its validations," *Welding in the world,* vol. 51, 2007.

[10] P. Dong and H. Kyuba, "Equilibrium-equivalent structural stress approach to fatigue analysis of a rectangular hollow section joint," *International Journal of Fatigue,* vol.

27, no. 1, p. 85–94, 2005.

[11] P. Dong, R. Potukutchi, H. Agrawal and P. Perumalswami , "Fatigue Analysis of Steel MIG Welds in Automotive Structures,," *SAE International DOI: 10.4271/2004-01-0627*, 2004.

[12] M. Kim and S. M. Kim , "A comparative study for the fatigue assessment of a shipstructure by use of Hotspot stress and structural stress approaches," *Ocean Engineering,* vol. 36, p. 1067–1072, 2009.

[13] W. Fricke, "Review fatigue analysis of welded joints: state of development.," *Marine structures,* vol. 16, pp. 185-200, 2003.

[14] S. C. F. W. Radaj D., "Recent developments in local concepts of fatigue assessment of welded joints. 31(2009) 2-11.," *International journal of fatigue,* vol. 31, no. 1, pp. 2-11, 2009.

[15] W. Fricke, "Guideline for the Fatigue Assessment by Notch Stress Analysis for Welded Structures," International Institute of Welding, 2010.

[16] J. Martinsson, "Fatigue Assement of Complex Welded Steel Structures ISBN 91-2783-968-6," Department of Lightweight structures, Department of Aeronautical and Vehicle Engineering Royal Institute of Technology, Stockholm.

[17] A.Hobbacher, "Recommendations for fatigue design of welded joints and components. IIW Doc XIII-2151r1-07/XV-1254r1-07," International Institute of Welding, 2007.

[18] D. Radaj, "Review of fatigue strength assessment of non-welded and welded structures based on local parameters," *International journal of fatigue*, vol. 18, no. 3, pp. 153-170, 1996.

[19] "International Institute of Welding," [Online]. Available: http://www.iiwelding.org/.

[20] "Design life Validation Test of a New Flyer 40-ft Xcelsior Coach," New flyer Industries Internal test report.

[21] "Design life Validation Test of a New Flyer 40-ft Xcelsior Coach," New flyer Industries Internal test report.

[22] "T-Joint Testing of Structural Steel Weldments TR11-60," New Flyer Industries Internal test report.

[23] K. Easterling and . K. Easterling, Introduction to the physical metallurgy of welding, 2nd edition,, Elsevier Ltd, 1992.

[24] K. Sindo, Welding Metallurgy, 2nd edition, ISBN: 978-0-471-43491-7: Wiley Inter Science publication, 2002.

[25] I. Ralph and F. Ali, "Metal Fatigue in Engineering Second Edition," John Wiley & Sons ISBN: 978-0-471-51059-8.

[26] C.-P. F. a. P.-H. C. T-L Teng, " Effect of weld geometry and residual stresses on fatigue in butt-welded joints,," *International Journal of pressure Vessel and piping,* vol. 79, no. 7, pp. 467-482, 2002.

[27] L. Karlsson, "Residual stresses due to welding of a nozzle to a pressure vessel," Division of Solid Mechanics, Lund University, Sweden, 2005.

[28] Veli-Matti Lihavainen and Gary Marquis, "Estimation of Fatigue Life Improvement

for Ultrasonic Impact treated Welded Joints," Lappeenranta University of Technology,Finland., Lappeenranta.

[29] G. Sigurdsson and I. Lotsberg , "Hot spot Stress S-N Curve for fatigue analysis of plated structures," *Journal of offshore me-chanics and artic engineeringDOI: 10.1115/1.2355512*, pp. 330-336, 2006.

[30] E. Mecozzi, M. Lecca, C. Sorrentino and M. Large, "Fatigue behaviour of high-strength steel-welded joints in offshore and marine systems (FATHOMS)," European Commission, 2010.

[31] Mikael Fermér, Magnus Adréasson and Bjorn Frödin, "Fatigue life prediction of MAG-Welded Thin-Sheet Structures. SAE Technical paper series 982311.," 1998.

[32] G. Savaidis and M. Vormwald, "Hot spot stress evaluation of fatigue in welded structural connections supported by finite element analysis. International journal of fatigue," *International journal of fatigue*, vol. 22, no. 2, pp. 85-91, 2000.

[33] E. Niemi, W. Fricke and S. Maddox, Designer’s guide to structural hot-spot stress

approach(IIW-1430-00), Woodhead Publishing ISBN 978-1-84569-124-0, 2006.

[34] C. Sonsino, "Multiaxial fatigue of welded joints under in-phase and out-of-phase local strains and stresses," *International journal of fatigue,* vol. 17, pp. 55-70, 1994.

[35] D. Taylor, N. Barrett and G. Lucano, "Some new methods for predicting fatigue in welded joints," *International Journal of Fatigue,* vol. 24, no. 5, pp. 509-519, 2002.

[36] Z.-G. Xiao and K. Yamada, "A method of determining geometric stress for fatigue strength evaluation of steel welded joints," *International Journal of fatigue,* vol. 26, no. 12, pp. 1277-1293, 2004.

[37] Z.-G. X. a. K. Yamada, " A method of determining geometric stress for fatigue strength evaluation of steel welded joints," *International journal of fatigue,* vol. 26, no. 12, pp. 1277-1293, 2004.

[38] P.Dong, "A Structural stress definition and numerical implementation for fatigue analysis of welded joints.," *International journal of fatigue,* vol. 33, no. 10, p. 865–876, 2001.

[39] H. Neuber, "Über die Berücksichtigung der Spannungskonzentration beiFestigkeitsberechnungen," *Konstruktion,* no. 20, p. 245–51, 1968.

[40] T. Seeger , V. Kottgen and R. Olivier , "Fatigue analysis of welded connections based on local English translation in IIW-doc.XIII-1408-91/XV-802-92, .," International Institute of Welding.

[41] "Hyperworks®, Release 10.0, Help System, Hypermesh Guide," Altair, Inc..

[42] S. Rao, Mechanical Vibrations, Addison Wesley publications ISBN 0-201-50156-2.

[43] N. Bishop, "Vibration fatigue analysis in the finite element environment," in . *An Invited Paper presented to the XVI ENCUENTRO DEL GRUPO ESPAÑOL DE FRACTURA*, Torremolinos, Spain, 1999.

[44] J. Tukey and J. Cooley, "An algorithm for the machine calculation of complex Fourier series,," Durham, 1964.

[45] "Abaqus®, release 6.13, Help System, Random response analysis, section 2.5.8, Abaqus theory guide".

[46] R. J. Ditolla, " Random vibration analysis by the power spectrum and response spectrum methods - Ph.D Thesis," University of Arizona, 1986.

[47] N. W. M. Bishop, "The use of frequency domain parameters to predict structural fatigue. Dissertation submitted for the Degree of Doctor of Philosophy," 1988.

[48] Neil Bishop, Finite element based fatigue calculations, NAFEMS, 2000.

[49] A. Halfpenny , "A frequency domain approach for fatigue life estimation from Finite Element Analysis," Dublin, 1999.

[50] [Online]. Available: http://www.ncode.com/en/products/ncode-designlife.

[51] T. Irvine, "Power spectral density units, Vibrationdata," [Online]. [Accessed 1998].

[52] "ANSYS®, Release 12.0, Help System, Structural Analysis Guide," ANSYS, Inc.

[53] Z.-F. Fu and J. He, Modal Analysis, Butterworth-Heinemann, 2001.

[54] H. Boyer, Ed., Altlas of Fatigue Curves, Ohio: American Society for Metals, 1997.

[55] " Standard Practice for Statistical Analysis of Linear or Linearized Stress-Life (S-N) and Strain-Life (ε-N) Fatigue Data," ASTM International, West Conshohocken, PA,

2004.

[56] "Standard method of statistical fatigue testing JSME S002-1981," Japan Society of Mechanical Engineers, 1981.

[57] M. Miner, "Cumulative damage in fatigue," *Journal of Applied Mechanics,* vol. 67, pp. 159-164, 1945.

[58] F. Kihm and A. Halfpenny, "Rainflow cycle counting and acoustic fatigue analysis techniques for random loading," in *RASD 10th International conference*, Southampton, 2010.

[59] M. M. a. E. T., "Fatigue of metals subjected to varying stress," *Presented to the JapanSociety of Mechanical Engineers,* 1968.

[60] Standard Practices for Cycle Counting in Fatigue Analysis ASTM E1049-85(2011)e1, ASTM International, West Conshohocken, PA , 2011.

[61] J. Bendat, "Probability functions for random responses," NASA report on contract.

[62] . N. W. M. Bishop and F. Sherratt, "Fatigue life prediction from power spectral

density data. Part 1, traditional approaches and Part 2, recent developments," *Environmegntal Engineerin,* vol. 2, 1989.

[63] M. Light and P. Wirsching, "Fatigue under wide band random loading," *J Struct*, pp. 1593-1607.

[64] W. Dover and . J. Kam , "Fast fatigue assessment procedure for offshore structures under random stress history," *Proc. Instn. Civ. Engrs,* vol. Part 2, no. 85, pp. 689-700, 1988.

[65] D. Steinberg, "Vibration analysis for electronic equipment," Wiley-Interscience ISBN978-0471376859, 2000.

[66] C. Lalanne, Mechanical vibration and shock ISBN: 978-1-84821-126-1, John Wiley & Sons, Inc., 2009.

[67] T. Dirlik, "Application of computers to fatigue analysis," 1985 Dissertation submitted for the Degree of Doctor of Philosophy Department of Engineering University of Warwick.

[68] Mark H. Richardson, Vibrant Technology, Inc., , " Is It a Mode Shape, or an Operating Deflection Shape?," Sound & Vibration Magazine 30th Anniversary Issue, Jamestown, California, 1997.

[69] R. Taylor and O. Zienkiewicz, The Finite Element Method Sixth edition, Butterworth-Heinemann publications ISBN 0 7506 5055 9, 2008.

[70] Z. I. Syed, "Stress analysis of welded gusseted frames Graduate Theses and Dissertations. Paper 12186.," Iowa State University, 2011.

[71] [Online]. Available: http://www.altairhyperworks.com/Product,19,OptiStruct.aspx.

[72] M. A. a. M. Partl, " Calculation of displacements of measured accelerations, analysis of two accelerometers and application in road engineering," in *6th Swiss Transport Research Conference*, 2006.

[73] A. L. a. S. Kangde, "Virtual Road Approach for Vehicle Durability Simulations," *SAE International Journal of Passenger Cars- Mechanical Systems* , vol. 6, no. 2, pp. 876-881, 2013.

[74] C. Patel, . P. P. Gohil and . B. Borhade, "Modelling and vibration analysis of a road profile measuring system," *International Journal of Automotive and Mechanical Engineering (IJAME)*, vol. 1, pp. 13-28, 2010.

[75] A. H. a. F. Kihm, "Rainflow cycle counting and acoustic fatigue analysis techniques for random loading," in *RASD 10th International conference*, Southampton, 2010.